Zentime

Perioperative Precision Medicine

Volume 1, Number 2; Sept. 30, 2023

ISSN: 2957-5443
Editor-in-Chief: Lize Xiong
Published by ZENTIME PUBLISHING CORPORATION

Perioperative Precision Medicine
eISSN: 2957-5443

Zentime

Review Article https://doi.org/10.61189/550782gbbqxs

Roles of post-translational modifications of C-type lectin receptor-induced signaling cascades in innate immune responses against *Candida albicans*

Ping Li[1], Lindong Cheng[2], Chunhua Liao[3], Jianhua Xia[4], Li Tan[5]

[1]Graduate School, Wannan Medical College, Anhui 241000, China. [2]Graduate School, Hebei North University, Hebei 075000, China. [3]School of Anesthesiology, Naval Medical University, Shanghai 200433, China. [4]Department of Anesthesiology, Shanghai Pudong New District People's Hospital, Shanghai 200433, China. [5]Department of Anesthesiology, Chongqing University Cancer Hospital, Chongqing 400030, China.

Acknowledgement: This work was supported by Health Science and Technology Project of Health Commission of Pudong New District (PW2020A-26).

Declaration of conflict of interest: None.

Received July 18, 2023; Accepted September 11, 2023; Published September 30, 2023

Highlights

- Risk of invasive *candida* infection and its related mortality are increasing significantly in perioperative patients.
- C-type lectin receptors are the primary pattern-recognition receptors for fungi-induced host defense and innate immune activation.
- Protein post-translational modifications are one of the core factors in host innate immune regulation.
- Post-translational modifications sites on proteins are anticipated to serve as potential targets for modulating anti-fungal immunity.

Abstract

Candida albicans (*C. albicans*), a conditional pathogenic fungus, is widespread in nature and can live in symbiosis with organisms in small quantities. When the normal microflora is imbalanced, the epithelial barrier is disrupted or the immune system becomes dysfunctional, *C. albicans* can change from commensal to pathogenic pathogen, causing both superficial and life-threatening systemic infections with no effective treatment. The morbidity and mortality of invasive *Candida* infections in perioperative patients are high due to underlying chronic diseases, immune deficiencies, and pathophysiological disorders. C-type lectin receptors (CLRs) are the main pattern-recognition receptors for fungal activation of innate immunity and host defense. Upon binding to ligands, CLRs induce multiple signal transduction cascades followed by activation of nuclear factor kappa B through spleen tyrosine kinase - and caspase recruitment domain containing protein 9-dependent pathways. Analyzing the effects of regulatory CLR-induced signaling cascades on host immune cells is critical for understanding the molecular mechanism in regulating antifungal immunity. As one of the core factors in host innate immune regulation, protein post-translational modifications regulate the strength of immune effects by modulating protein conformation, stability, affinity, subcellular localization, etc. This makes the post-translational modification sites promising as potential targets for modulating antifungal immunity. This review primarily described the study progress of post-translational modifications in controlling CLR-induced signaling cascades throughout the process of innate immunity against *C. albicans*. We aim to provide better understanding of these mechanisms and aid in the identification and development of biomarkers and drug targets for invasive candidiasis.

Keywords: *Candida albicans*, innate immunity, protein post-translational modifications, C-type lectin receptors

Introduction

The normal human body has a highly sophisticated innate and adaptive immune system that is naturally resistant to most fungal infections, with over 99% of *Candida albicans* (*C. albicans*) being cleared within the first hour of entry into the human bloodstream [1]. However, fungal infections have become a major cause of human diseases due to the increasing number

Address correspondence to: Li Tan, Department of Anesthesiology, Chongqing University Cancer Hospital, No.181 Hanyu Road, Chongqing 400030, China. E-mail: tanlihh@163.com.

of immune-compromised population having acquired immune deficiency syndrome, chemotherapy for tumors, organ transplants, post-immunosuppressive therapy and advanced age [2]. Hundreds of millions of patients worldwide are infected with pathogenic fungi each year, resulting in at least 1.5 million deaths per year, similar to the number of deaths due to tuberculosis [3]. *C. albicans* is the most common fungal pathogen, accounting for more than half of the invasive candidiasis [4].

In perioperative patients, various factors can increase the risk of *C. albicans* infection. First, operation compromise the immune function of body by inhibiting the activity of natural killer cells within hours of the surgery, and this inhibition can persist over time [5]. Natural killer cells are a significant component of innate immune system, play an important role in resistance to fungal infection, and kill fungi by releasing soluble cytotoxic molecules (perforin and granzyme) or activating apoptosis pathway [6, 7]. Second, perioperative pain induced by inflammatory factors can restrain immune function by interactions among the central nervous system, hypothalamic-pituitary-adrenal axis pathways, and immune system [8]. Third, critical patients undergoing surgery often need central venous indwelling catheter or peripheral venous indwelling catheter. Fungi can colonize in venous catheters, enter the blood, and cause bloodstream infections, threatening the safety of patients' lives [9, 10]. Last, longer hospitalization and intensive care unit stays undoubtedly increase the risk of infection. Fungal infection is a momentous factor for intensive care unit mortality [11].

Innate immunity plays a crucial role as the host's primary defense against invading pathogens, relying on intricate and dynamic interactions among various cellular and molecular components. Distinguishing between pathogens and self-components is a fundamental function of the innate immune system. Pattern recognition receptors (PRRs) recognize pathogen-associated molecular patterns. These PRRs are mainly expressed by myeloid macrophages including Toll-like receptors (TLRs), C-type lectin receptors (CLRs), nucleotide-binding oligomerization domain like receptors , retinoic acid-inducible gene 1-like receptors, and complement components and receptors [12]. All of these PRRs can mediate antifungal immunity, and CLRs are the most widely studied. The pathogen-associated molecular patterns mainly consist of *Candida* cell wall-associated glycans (mannans, glucans, chitin) [13].

CLRs are the main PRRs for fungi-induced activation of innate immunity and host defense [14]. The receptors dectin-1, dectin-2, dectin-3, and mincle bind to ligands, then recruit spleen tyrosine kinase (SYK) intracellularly, and are activated by an intermolecular auto-phosphorylation mechanism [15]. Activated SYK further activates dedicator of cytokinesis 2, phospholipase C-γ2, and protein kinase C-δ by phosphorylation, the latter phosphorylates caspase recruitment domain containing protein 9 (CARD9) and vesicles containing glucose transporter 1 (GLUT1). Phosphorylation of vesicles promotes GLUT1 translocation to the cytosol and thus increases glucose uptake by immune cells. SYK and CARD9 are transported from the cytosol to the cytoplasm via α-tubulin. Then, CARD9, B cell lymphoma 10, and mucosa-associated lymphoid tissue lymphoma translocation protein 1 together constitute the CBM complex. This complex ultimately leads to the activation of downstream nuclear factor kappa B (NF-κB) and mitogen-activated protein kinases [16]. These signaling pathways turn on a series of effector mechanisms, including the release of proinflammatory cytokines and phagocytosis, finally leading to fungus clearance [17].

Proteins, the essential components of living organisms, are the material basis of life and are involved in practically all cellular processes. To date, more than 50% of the proteins in human cells have been found to have different types of post-translational modifications (PTMs) [18]. PTMs can rapidly regulate various intracellular activities and expand the diversity of protein functions by affecting protein activity, stability, localization, and signal transduction under physiological and pathological conditions [19, 20], such as classical modifications including phosphorylation, ubiquitination, and methylation, as well as non-classical glycosylation, acetylation, malonylation, and succinylation [21]. During the anti-fungal process of innate immune cells, many proteins in the signaling pathway exhibit additional functions through PTMs, and these related enzymes involved in PTMs can indirectly and specifically regulate the anti-fungal ability of immune cells. Whether positively or negatively regulated, these modification-related enzymes have the potential to become targets for modulating the immune system. Therefore, this review focuses on how PTMs are involved in the innate immune response against *C. albicans*, primarily by regulating CLR-induced signaling cascades through ubiquitination, phosphorylation, acetylation, and glycosylation.

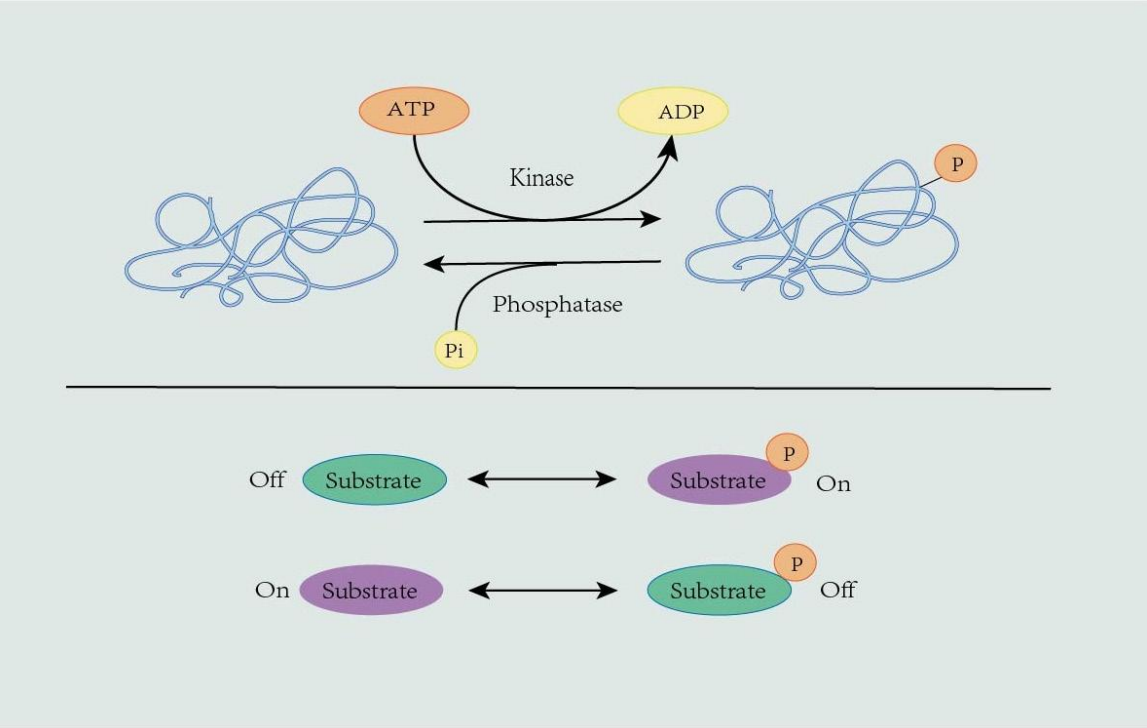

Figure 1. Phosphorylation and dephosphorylation. Phosphorylation and dephosphorylation are mediated by protein kinase and phosphatase, respectively. The phosphate group acts as a molecular switch that can be activated by phosphorylation or dephosphorylation of many substances.

Phosphorylation and dephosphorylation

In organisms, phosphorylation is the most widespread form of covalent modification in PTMs [22]. Phosphorylation plays an important regulatory role in the proper functioning of proteins by the transfer of the γ-position phosphate group of ATP or GTP to the amino acid residues of the substrate protein (mainly serine and threonine) catalyzed by phosphokinase, while the reverse process involves the removal of the corresponding phosphate group by protein kinase [23]. It is the opposing roles of these two enzymes and the energy consumption and production involved that make phosphorylation the preferred mode of regulation of many physiological activities in the body (e.g., transcriptional regulation, signal transduction, DNA damage repair) (**Figure 1**) [24].

Phosphorylation

EPH receptor B2 (EPHB2)

EPHB2 is a member of the EPH receptor family of receptor tyrosine kinase transmembrane glycoproteins. EPHB2 was recently found to directly recognize the fungal cell wall component β-glucan and to synergize with dectin-1 to activate downstream signaling. EPHB2 directly phosphorylates the downstream kinase SYK and promotes its activation. In EPHB2$^{-/-}$ macrophages, fungus-stimulated phosphorylation of SYK was almost completely lost. Ephb2-deficient mice were significantly more susceptible to *C. albicans*–induced infection than the WT mice [25]. EPHB2 also phosphorylates T-cell-activated Rho GTPase-activating protein at the Y310 site, and T-cell-activated Rho GTPase-activating protein acts as an adapter to regulate upstream EPHB2 and downstream CARD9 signaling [26]. In summary, EPHB2 regulates dectin-mediated immune signaling by modulating the phosphorylation of SYK and T-cell-activated Rho GTPase-activating protein during antifungal host defense.

SYK

SYK includes two N-terminal Src Homology 2 domains, one C-terminal kinase domain and two interdomain linkers [27]. These structural domains are bound together, leaving the Src Homology 2 domain in a stable inactivation state [28]. Phosphorylation is the most common method to activate SYK, and there are 10 autophosphorylation sites in SYK [29]. CLRs engagement promotes Src-dependent phosphorylation of its immunoreceptor tyrosine-based activation motif, recruits the SHP-2 tyrosine phosphatase, and activates SYK [30, 31]. This binding leads to conformational changes and unfolding of SYK, which is subsequently activated by SYK's own phosphorylation or by

phosphorylation of its upstream kinases [29]. SYK that acquires enzymatic activity activates its downstream substrate proteins through phosphorylation or even direct interaction, and transduces its downstream signaling cascade. Activated SYK phosphorylates dedicator of cytokinesis 2 at tyrosine 985 and tyrosine 1405, promoting the recruitment and activation of Rac GTPase, thereby increasing reactive oxygen species (ROS) production required for macrophage signaling activation and bactericidal activity [32].

Protein kinase C-δ (PKC-δ)

PKC-δ is activated under dectin-SYK signaling, mediates CARD9 phosphorylation at Thr231, and is involved in CBM complex assembly and classical NF-κB regulation. PKC-$\delta^{-/-}$ dendritic cells are defective in innate response to dectin-1, dectin-2, or mincle stimulation, while dendritic cells lacking PKC-α, PKC-β, or PKC-θ are immunocompetent. In addition, C. albicans significantly reduces the production of cytokines, such as tumor necrosis factor, interleukin (IL)-10, and IL-2, in PKC-$\delta^{-/-}$ cells compared to wild type. Similarly, RKC-$\delta^{-/-}$ mice are highly susceptible to fungal infections. Thus, PKC-δ is an important link between SYK activation and CARD9 signaling in CLR-mediated natural immunity and host protection [33]. On the other hand, PKC-δ promotes GLUT1 insertion into the cell membrane by phosphorylating vesicles bearing GLUT1, which promotes glucose uptake by neutrophils, thereby enhancing the neutrophil metabolic fitness [34].

Dephosphorylation

Steroid sulfatase (STS)

STS proteins are homologous protein phosphatases that share over-lapping functions, and are negative regulators of multiple signaling pathways [35]. For example, in T cells, STS phosphatase helps set the threshold for T cell activation by targeting Zap-70, an important kinase downstream of the T cell receptor [36]. In addition, STS-1 has been shown to control signaling downstream of glycoprotein VI-Fc receptor γ in platelets and Fcepsilon receptor in mast cells by targeting the ZAP-70 homolog SYK [37]. At 12 to 18 h after invasive *Candida* infection, the fungal burden in the kidneys of STS$^{-/-}$ mice began to decrease compared with that in wild-type mice, and a large number of leukocytes in STS$^{-/-}$ mice entered the kidneys to fight the infection, improving the survival rate of the mice. After stimulation of bone marrow-derived dendritic cells with fungal ligands, we observed no difference in other antifungal responses, such as cytokine or nitric oxide production, by STS$^{-/-}$BMDCs but enhanced ROS production. Although the signaling pathway from dectin to the initiation of the ROS response has not been fully elucidated, the involvement of SYK kinas has been identified [38]. Hyperphosphorylation of SYK in STS$^{-/-}$BMDCs was observed using a phosphor-specific antibody that recognizes the activation of SYK tyrosine phosphorylation. STS may be involved in antifungal immunity by regulating the level of SYK phosphorylation and activation, and thus ROS production [39].

Protein phosphatase 1 (PP1)

PP1 to CARD9 keeps CARD9 in a dephosphorylated and self-inhibited state, thereby inhibiting CBM complex formation and suppressing downstream NF-κB and JNK signaling. PP1 does not act directly on CARD9 but requires downstream mediation of kinase 3 (DOK3). DOK3 is a junctional molecule preferentially expressed in hematopoietic cells [40]. It acts as a specific regulator of downstream of several immune receptors, including TLR3, TLR4, and B-cell antigen receptor, during viral infection, endotoxin stimulation, and plasma cell differentiation [41-43]. In invasive fungal infections, DOK3 acts as an intermediate molecule that promotes the recruitment of PP1 to CARD9. Deletion of DOK3 enhances various antifungal effector functions of neutrophils, including phagocytosis, extracellular trap network, and pro-inflammatory cytokine production, through dephosphorylation of CARD9 by PP1, thereby increasing the fungicidal activity of neutrophils [44]. PKC-δ and PP1 keep CARD9 in a balanced activation state through phosphorylation and dephosphorylation to avoid excessive inflammatory immune response and immunosuppression (**Figure 2**).

Ubiquitination and Deubiquitination

Ubiquitin is a protein consisting of 76 amino acids and modify target proteins by mono-ubiquitination or polyubiquitination [45]. A single ubiquitin molecule is repeatedly attached to a ubiquitin lysine residue to form a ubiquitin chain. The ubiquitin molecule itself contains seven lysine residues, all of which can be ubiquitinated, and the N-terminus can also be attached to ubiquitin to form eight types of ubiquitin chains (K6, K11, K27, K29, K33, K48, K63 and MET1) [46]. Ubiquitination, an important PTM modality, is the process of ubiquitin binding to substrate molecules catalyzed by the ubiquitin-proteasome system. This process is facilitated by three enzymes: ubiquitin-activating enzyme, ubiquitin-conjugating enzyme (E2),

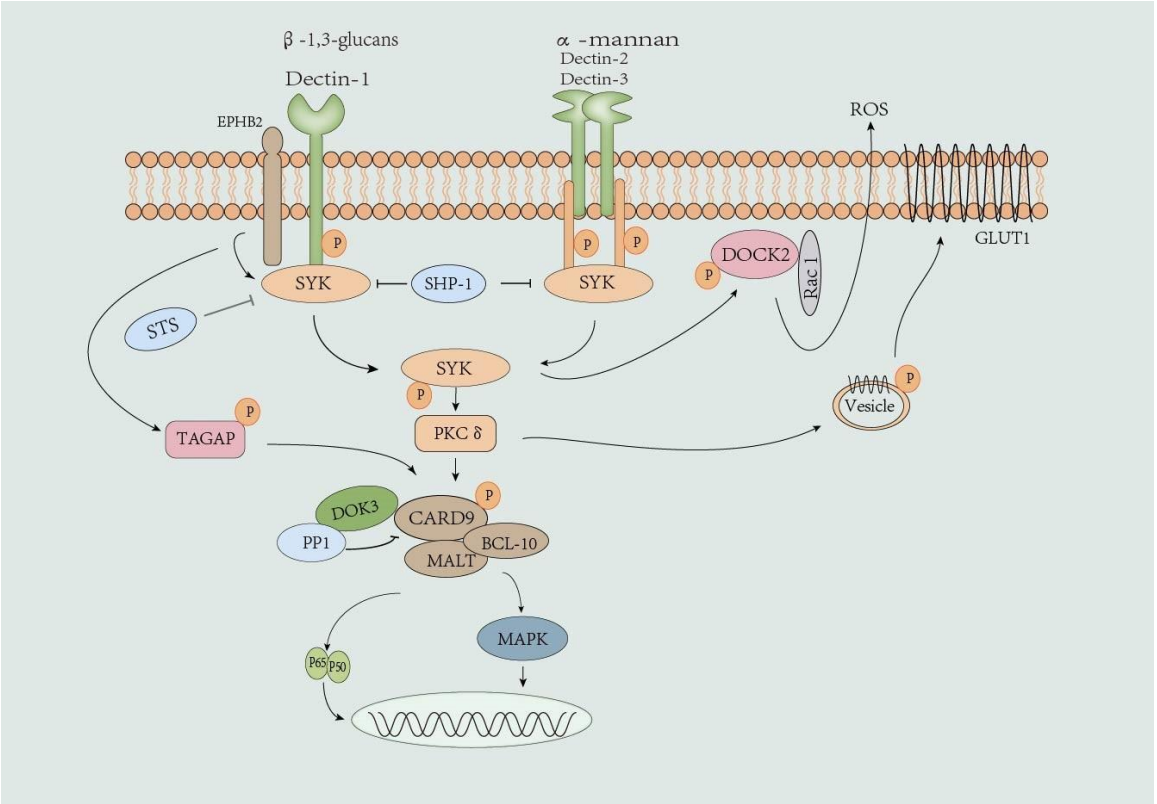

Figure 2. The role of phosphorylation and dephosphorylation in innate immunity against *C. albicans* infection. STS and SHP-1 inactivate SYK by mediating its dephosphorylation. Activated SYK stimulates DOCK2 phosphorylation and thus increases ROS production. PKC-δ activates CARD9 and vesicles containing GLUT1 by directly promoting its phosphorylation. Phosphorylation of vesicles promotes GLUT1 translocation to the cytosol and thus increases glucose uptake by immune cells. DOK3 mediates the recruitment of PP1 to CARD9, causing dephosphorylation and inactivation of CARD9. *C. albicans*, *Candida albicans*; EPHB2, EPH receptor B2; ROS, reactive oxygen species; STS, steroid sulfatase; SYK, spleen tyrosine kinase; DOCK2, dedicator of cytokinesis 2; GLUT1, glucose transporter 1; TAGAP, T-cell-activated Rho GTPase-activating protein; PKC-δ, protein kinase C-δ; CARD9, caspase recruitment domain containing protein 9; DOK3, downstream of kinase 3; PP1, protein phosphatase 1; MALT, mucosa-associated lymphoid tissue; MAPK, mitogen-activated protein kinases.

and ubiquitin ligase (E3). Ubiquitin-activating enzyme activates ubiquitin, E2 transfers ubiquitin to E3, and finally, E3 catalyzes the covalent attachment of ubiquitin to the target protein, or in some cases, E3 directly adds ubiquitin from E2 to the substrate [47]. Of these, E3 determines the specificity and precision of ubiquitin and substrate attachment, and the human genome has approximately more than 600 E3s, significantly more than 2 ubiquitin-activating enzymes and approximately 40 E2s. Thus, ubiquitination is more complex and functionally diverse than other protein modifications [48]. E3 ubiquitin ligases are divided into three families: the RING finger-type, HECT-type, and RING-between-RING [49]. At the same time, the human genome also has about 100 deubiquitinases, which are classified into 7 classes: USP, UCH, OUT, MJD, JAMM, MCPIP, and MINDY. These deubiquitinases are also highly specific and responsible for removing ubiquitin chains from proteins and other molecules (**Figure 3**) [50].

Ubiquitination

Casitas B-lineage lymphoma protein b (CBL-B)

CBL-B is one of three homologous proteins of the Cbl E3 ubiquitin ligase family that is ubiquitously expressed in all leukocyte subpopulations and negatively regulates the activation of signaling pathways, such as T-cell antigen receptor, B-cell antigen receptor, CD28, TLR4, high-affinity IgE receptor, and epidermal growth factor receptor [51-55]. During invasive *C. albicans* infection, CBL-B$^{-/-}$ mice were found to be highly resistant to disseminated candidiasis, with resistance characterized by reduced weight loss following infection, an absence of inflammatory damage, and enhanced survival. CBL-B$^{-/-}$ mice displayed enhanced fungal clearance within 24-48 hours of bloodstream infection, with a remarkable 10-fold reduction in fungal load observed in different peripheral organs when compared to control group [56]. CBL-B$^{-/-}$ bone marrow-derived myeloid mononuclear macrophages exhibited reduced ligand-mediated receptor internalization and degradation, increased dectin receptor expression, and

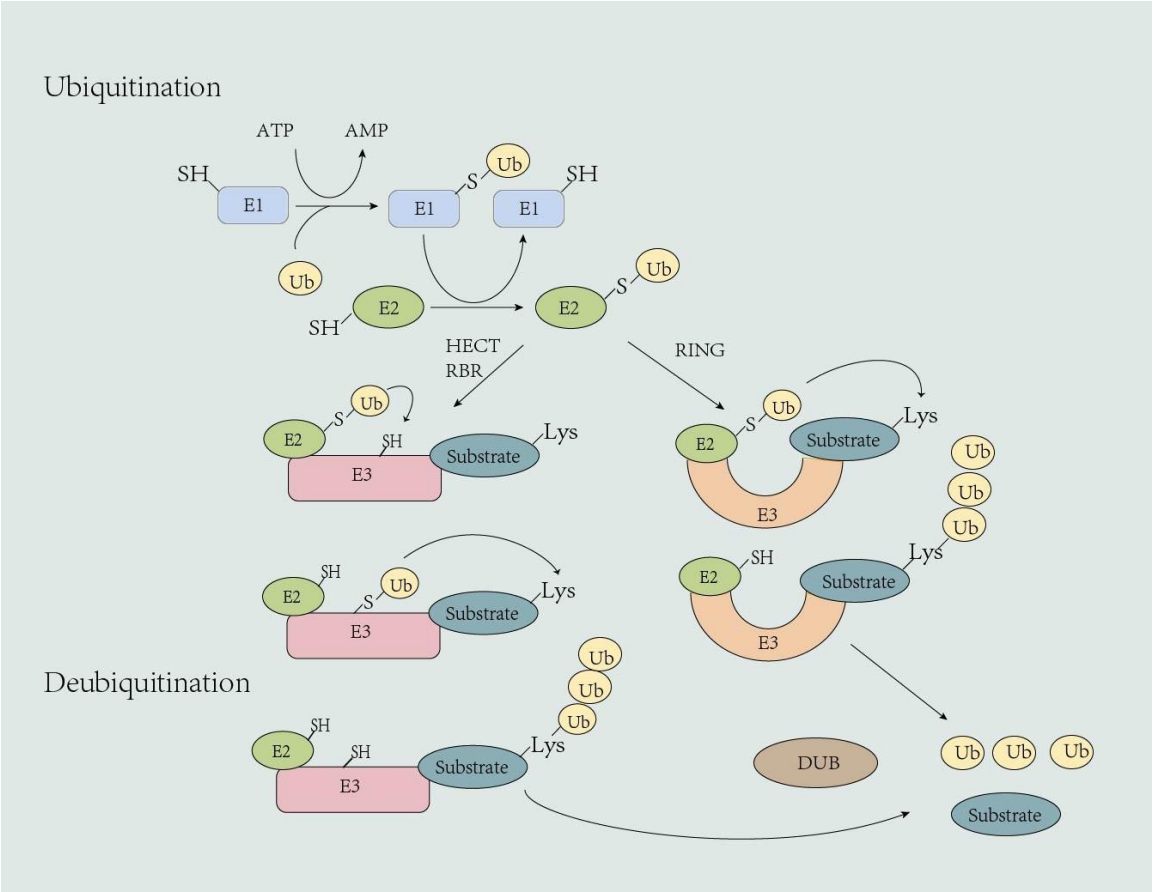

Figure 3. Ubiquitination and Deubiquitination. Ubiquitination is mainly mediated by E1, E2, E3. E1 first activates ubiquitin, then E2 transfers ubiquitin to E3, and finally E3 catalyzes the covalent binding of ubiquitin to the target protein, or E3 mediates the direct addition of ubiquitin from E2 to the substrate. De-ubiquitination is the removal process of ubiquitin from the substrate by deubiquitinating enzymes. E1, ubiquitin-activating enzyme; E2, ubiquitin-conjugating enzyme; E3, ubiquitin ligase; Ub, Ubiquitin; RBR, RING-between-RING; DUB, deubiquitinating enzyme.

elevated production of various pro-inflammatory factors and ROS compared to wild type macrophages [56]. This is because CBL-B can mediate the ubiquitination of these activated CLRs through the mutual binding of the junction protein Fc receptor γ and the tyrosine kinase SYK. Dectin-1 (K2, K27, and K34), dectin-2 (K10 and K12), and dectin-3 (K9) are the sites of ubiquitination of dectin-1, -2, -3, respectively [57, 58], and the ubiquitinated CLRs are sorted into lysosomes by the transport-essential endosomal sorting complex system for degradation, thereby negatively regulating the CLR-mediated innate immune response against fungal infections.

C- Casitas B-lineage lymphoma (C-CBL)

C-CBL, a CBL-B homologous family member, modulates intestinal inflammation by inhibiting fungal-induced non-classical NF-κB activation. Intestinal fungal-derived mannan activates C-CBL in dendritic cells via dectin-2 and dectin-3, thereby promoting C-CBL-mediated ubiquitination and degradation of RelB, a non-classical NF-κB family member. Meanwhile, the classical NF-κB family member p65 mediates the transcription of the anti-inflammatory cytokine IL-10 gene to suppress colitis, and RelB binds to p65 and inhibits p65-mediated production of IL-10. Thus, the lack of C-CBL in dendritic cells promotes mannan-induced activation of RelB, which binds to p65, thereby inhibiting p65-mediated IL-10 transcription, decreasing anti-inflammatory cytokines, exaggerating immunization, and making mice more susceptible to Dextran Sulfate Sodium Salt-induced colitis [59].

Tripartite motif containing 31 (TRIM31)

Up to now, nearly 80 TRIM family proteins have been identified in the human genome, many of which have been shown to have E3 ubiquitin ligase activity and are involved in various activities of the organism [60]. For example, TRIM31, a member of the TRIM/RBCC family and a RING finger E3 ubiquitin ligase, is involved in the regulation of viral and fungal infections, non-alcoholic fatty liver disease, hypertensive

nephropathy, ischemic brain injury, and other diseases [61-65]. TRIM31 also binds directly to nucleotide-binding oligomerization domain -like receptor thermal protein domain associated protein 3 (NLRP3), and K48-linked ubiquitination mediates protein degradation of NLRP3. TRIM31 can limit NLRP3 inflammasome activation under physiological conditions and is, therefore, expected to be a potential therapeutic target for NLRP3 inflammasome related diseases [66]. Recently, TRIM31 was found to be a key regulator of SYK activation. RIM31 interacts with SYK and catalyzes K27-linked polyubiquitination at the Lys375 and Lys517 sites of SYK. This process promotes translocation of SYK to the plasma membrane, enabling its binding to CLRs. Additionally, TRIM31 inhibits dephosphorylation of SYK by the phosphatase SHP-1, which in turn enhances SYK-mediated downstream signaling (CBM complex, inflammasome formation). In vitro TRIM31 deficient BMDCs and BMDMs significantly reduced the production of pro-inflammatory cytokines such as IL-6, tumor necrosis factor-α, IL-1β, IL-12, and IL-23. Similarly, TRIM31$^{-/-}$ mice were more susceptible to fungal infection, and demonstrated a more severe renal inflammatory response and lower survival rates than TRIM31$^{+/+}$ mice [62].

TRIM62

CARD9 is a central component of natural immune signaling against fungi mediated by CLRs, and when not activated, CARD9 is in a self-inhibited state. TRIM62 mediates polyubiquitination of CARD9 at the K27-linked at the Lys125 site of CARD9, disrupting the inhibitory state of CARD9 and enhancing the transduction of signaling pathways in which CARD9 is involved. Thus, similar with CARD9$^{-/-}$ mice, TRIM62$^{-/-}$ mice have an increased susceptibility to fungal infections [67]. Genetic sequencing of patients with inflammatory bowel disease showed that the protective CARD9 variants were not ubiquitinated by TRIM62 and suggested that the protective effect of C-terminal truncation might be mediated by the loss of TRIM62 interactions, thereby limiting the pro-inflammatory cytokine response. If the CARD9-TRIM62 interaction is blocked, the inflammatory response can be limited. The small-molecule inhibitors that block the CARD9-TRIM62 interaction have been developed and hold potential as therapeutic agents for the treatment of inflammatory bowel disease [68].

Neuronal precursor cell-expressed developmentally down-regulated 4 (NEDD4)

NEDD4 is a HECT type E3 ubiquitin ligase that has been shown to positively regulate T cell activation and proliferation [69]. Additionally, it has also been reported that Nedd4 is involved in anti-cellular bacterial clearance by promoting autophagy [70]. Nedd4$^{-/-}$ mice are highly susceptible to systemic *C. albicans* infection, which is associated with increased organ fungal load, defective inflammatory response, impaired recruitment of leukocytes to the kidney, and impaired granulocyte expression of ROS. The specific regulatory mechanism of Nedd4 is unclear. At a molecular level, Nedd4$^{-/-}$ macrophages showed reduced TGFβ-activated kinase 1 and NF-κB activity and normal SYK and PKC-δ activity during *C. albicans* infection. This indicates that NEDD4 regulates downstream of PKC-δ and upstream of TGFβ-activated kinase 1 to enhance immune cell killing against *C. albicans* [71].

Deubiquitination

Ubiquitin-proteasome system 15

The ubiquitin-specific proteases family comprises the largest number of deubiquitinating enzymes. During antifungal immunization, ubiquitin-specific protease15 removes TRIM62-mediated ubiquitination of CARD9 and inhibits the activation of CARD9, thereby inhibiting the formation of the CBM complex. Thus, the activation of CARD9 is co-regulated by ubiquitin-specific protease15 and TRIM62, so that the degree of activation is in a state of equilibrium [72].

Ovarian tumor deubiquitinase 1 (OTUD1)

OTUD1 is also an important regulator of CARD9. OTUD1 mainly removes K29, K33 and K63-linked polyubiquitination from CARD9 and promotes the formation of the CBM complex. OTUD1 deficiency reduces CARD9-mediated signaling, leading to reduced production of pro-inflammatory cytokines and chemokines. Meanwhile, OTUD1$^{-/-}$ mice have been found to have increased susceptibility to fungal infections [73]. In other studies, OTUD1 exerted tumor suppression by removing K63-linked ubiquitination on Yes-associated protein and inhibiting the degradation of P53 [74]. In addition, OTUD1 negatively regulated the RNA virus signaling pathway by targeting Smad ubiquitination regulatory factor 1 (Smurf1) (**Figure 4**) [75].

Acetylation and Deacetylation

Lysine acetylation is a conserved PTM, most commonly histone acetylation, and is usually regulated by acetyltransferase and deacetyl-

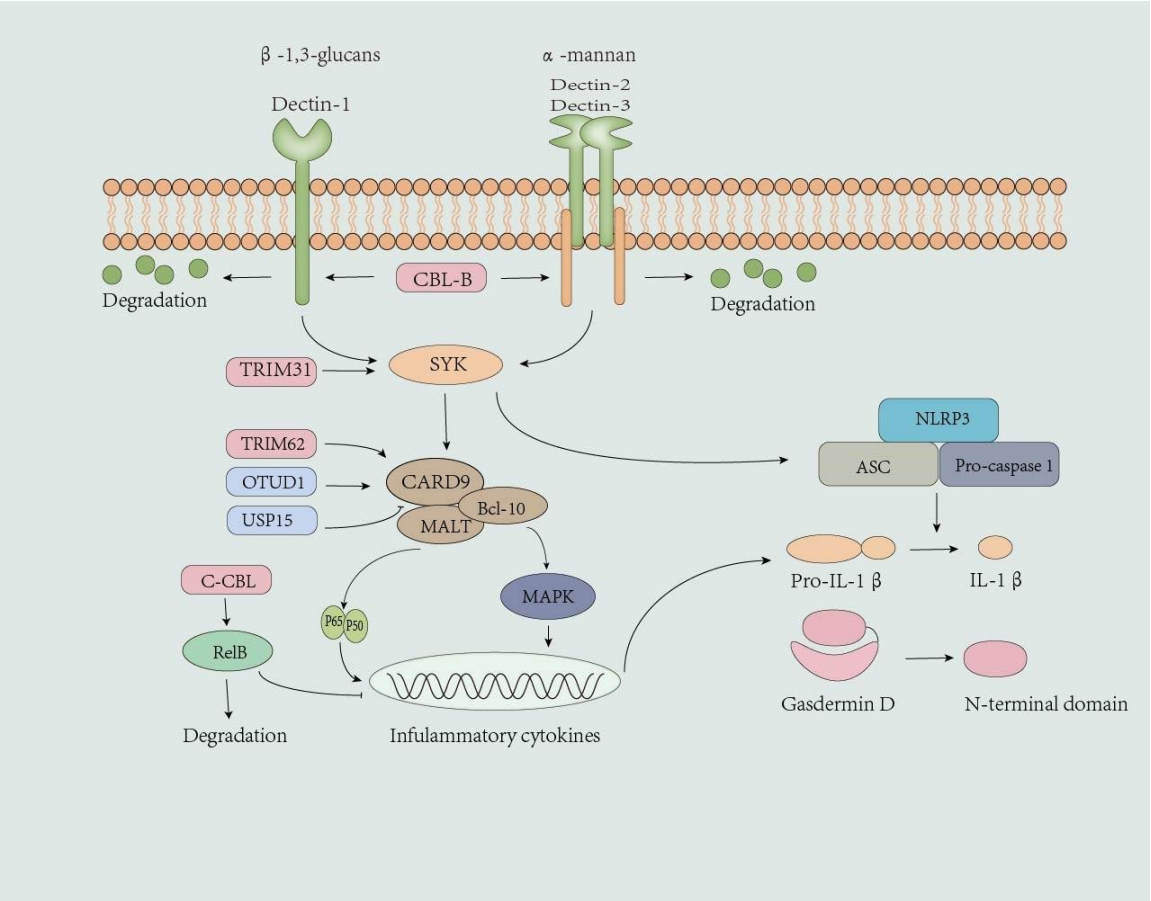

Figure 4. The role of ubiquitination and deubiquitination in innate immunity against *C. albicans* infection. Multiple E3 ubiquitin ligases are involved in the regulation of innate immunity against *C. albicans*. CBL-B and C-CBL promote the degradation of dectin-1, -2, -3 and RelB, respectively; TRIM31 facilitates SYK to immunoreceptor tyrosine-based activation motif translocation; TRIM62, OTUD1 and USP15 all act on CARD9 to maintain a balanced level of CARD9 activation through ubiquitination and deubiquitination. *C. albicans*, *Candida albicans*; CBL-B, casitas B-lineage lymphoma protein b; TRIM, tripartite motif containing; SYK, spleen tyrosine kinase; OTUD1, ovarian tumor deubiquitinase 1; CARD9, caspase recruitment domain containing protein 9; USP15, ubiquitin-specific protease 15; NLRP3, nucleotide-binding oligomerization domain -like receptor thermal protein domain associated protein 3; C-CBL, c-Casitas B-lineage lymphoma.

transferase [76]. Acetylation modifications usually occur in the structural domains of proteins, such as α-helix and β-fold, and the proteins with acetylation modifications are usually conserved, such as metabolism-related enzymes, ribosomes, and molecular chaperones [77]. With the continuous research on protein acetylation, studies have demonstrated that acetylation also plays an important regulatory role in the antifungal immune process [78, 79].

Acetylation

AP2A1 and α-tubulin N-acetyltransferase 1

AP2A1 and α-tubulin N-acetyltransferase 1 are recruited to α-tubulin via Myosin 1F (MYO1F), which promotes acetylation of α-tubulin. SYK and CARD9 molecules then activate downstream signaling pathways through acetylated tubules from the cell membrane into the cytoplasm. MYO1F is an unconventional myosin expressed mainly in mammalian immune cells. It plays a crucial role in regulating the migration of mast cells and neutrophils [80, 81], and modulating M1 polarization by stimulating intercellular adhesion of macrophages [82]. MYO1F also plays a key role in the activation of antifungal natural immune signaling and is required for dectin-induced acetylation of α-tubulin. Following systemic *Candida* infection, MYO1F-deficient mice were more severely infected relative to wild-type mice. Administration of AGK2 or AK-1, inhibitors of the deacetylase SIRT2, promoted dectin-activated signaling and proinflammatory gene expression, and produced a protective effect in mice with systemic *Candida* infection [78].

Deacetylation

Histone deacetylase 11 (HDAC11)

HDACs are enzymes that catalyze the removal

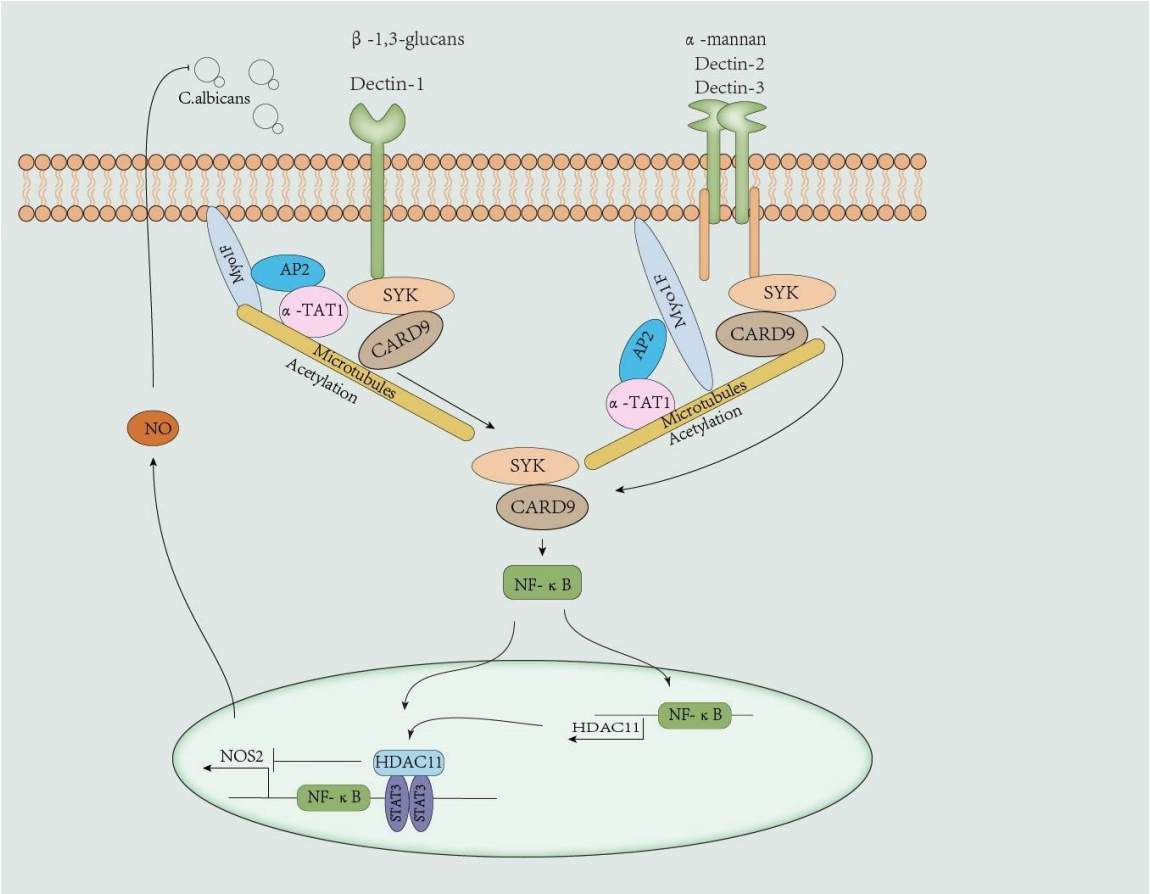

Figure 5. The role of acetylation and deacetylation in innate immunity against *C. albicans* infection. MYO1F mediates microtubule acetylation through recruitment of Tubulin and the AP2A1/αTAT complex, while SYK and CARD9 molecules activate downstream signaling pathways through acetylated microtubules from the cell membrane into the cytoplasm. The deacetylase HDAC11 promotes fungal immune escape by interacting with the transcription factor STAT3 and using STAT3 as a scaffold to bind to the iNOS gene promoter, inhibiting iNOS expression and reducing NO production. *C. albicans*, *Candida albicans*; AP, adaptor protein; SYK, spleen tyrosine kinase; αTAT1, α-tubulin N-acetyltransferase 1; CARD9, caspase recruitment domain containing protein 9; NF-κB, nuclear factor kappa B; HDAC11, histone deacetylase 11; STAT3, signal transducer and activator of transcription 3; iNOS, inducible nitric oxide synthase.

of acetyl functional groups from the lysine residues of both histone and nonhistone proteins [83]. Based on structure and function, HDACs are classified into four groups: class I HDACs (HDAC1, 2, 3 and 8), class II HDACs (HDAC4, 5, 6, 7, 9 and 10), class III HDACs (SIRT1–SIRT7) and class IV HDAC (HDAC11) [84]. As the only class IV HDAC, HDAC11 plays a critical role in a variety of cellular events, including cell proliferation and differentiation, metabolism, and tumorigenesis [85-87]. Loss of HDAC11 increases the acetylation of histone 3, 4 at the nitric oxide synthase 2 promoter, and leads to enhanced Nos2 transcription and corresponding inducible nitric oxide synthase levels in macrophages. The transcriptional repressor of Nos2, signal transducer and activator of transcription 3, interacts with HDAC11 and acts as a scaffolding protein to facilitate the binding of HDAC11 to the Nos2 promoter. Inhibition of signal transducer and activator of transcription 3 significantly reduced the aggregation of HDAC11 on the Nos2 promoter. Similarly, HDAC11 deletion reduced the abundance of signal transducer and activator of transcription 3 binding on the Nos2 promoter. Thus, fungal pathogens stimulate HDAC$^{-/-}$ mouse macrophages to produce more NO and ROS. HDAC11 inhibitor FT895 shows antifungal therapeutic effects in both *C. albicans* infected mice and human cells (**Figure 5**) [79].

Glycosylation

In the human immune system, all immunoglobulins and most complement components are glycosylated and depending on the glycosidic bond. There are two main types of glycosylation: O-linked glycosylation and N-linked glycosylation [88]. Through glycosyltransferases, sugars form glycosidic bonds with amino acid residues of various proteins to form glycoproteins, which play an important role in the regulation of protein folding and stabilization, cell growth, receptor activation, cell adhesion, and immune

Table 1. Summary of the targets and mechanisms of protein post-translational modifications in antifungal innate immunity

Enzymes	Substrate	Mechanism of Regulation	Biological Function
Phosphorylation			
EPHB2	SYK TAGAP (Tyr310)	Activation	Co-receptor; promoting SYK, TAGAP phosphorylation, and enhancing CLRs-mediated immune signaling [25, 26].
SYK	DOCK2 (Tyr985, 1405)	Activation	DOCK2 phosphorylation mediates ROS production [32].
	Vesicles with GLUT1	Transposition	Enhancing neutrophil metabolic fitness [34]
PKC-δ	CARD9 (Thr231)	Activation	Signaling between SYK and CARD9 [95].
Dephosphorylation			
STS	SYK	Inactivation	Inhibiting ROS production [39].
PP1	CARD9	Inhibited activation	Inhibiting the antifungal effect of PMN [44].
Ubiquitination			
CBL-B	Dectin-1 (Lys2, 27, 34) Dectin-2 (Lys10, 12) Dectin-3 (Lys9)	Degradation	Inhibiting dectin-1/2/3-mediated immune responses [57].
C-CBL	RelB	Degradation	Promoting IL-10 production, anti-inflammatory and immune balance[59].
TRIM31	SYK (Lys375, 517)	Transposition	Promoting the binding of SYK to CLRs and inhibiting the dephosphorylation of SYK by SHP-1 [62].
TRIM62	CARD9 (Lys125)	Activation	Dissolving the self-inhibited state of CARD9 and promoting CBM complex formation [67].
NEDD4	—	—	Enhancing the immune response [71].
De-ubiquitination			
USP15	CARD9	Inhibition	Inhibiting the activation of CARD9 [72].
OTUD1	CARD9	Activation	Promoting the formation of CBM complexes [75].
Acetylation			
αTAT1	α-tubulin	Transposition	SYK and CARD9 enter the cytoplasm and activate downstream signal pathways [78].
Deacetylation			
HDAC11	NOS2 promoter	Initiate transcription	Reducing NO, ROS generation [79].
Glycosylation			
JAGN1	—	—	Engaging in glycoprotein processing and protein transport in the endoplasmic reticulum and Golgi [91].

Note: EPHB2, erythropoietin-producing hepatocellular carcinoma receptor B2; SYK, spleen tyrosine kinase; TAGAP, T-cell-activated Rho GTPase-activating protein; CLRs, C-type lectin receptors; DOCK2, dedicator of cytokinesis 2; ROS, reactive oxygen species; GLUT1, glucose transporter 1; CARD9, caspase recruitment domain containing protein 9; PKC-δ, protein kinase C-δ; STS, steroid sulfatase; CBL-B, casitas B-lineage lymphoma protein b; C-CBL, c-casitas B-lineage lymphoma; TRIM, tripartite motif containing; NEDD4, neuronal precursor cell-expressed developmentally down-regulated 4; USP15, ubiquitin-specific protease 15; OTUD1, ovarian tumor deubiquitinase 1; αTAT1, α-tubulin N-acetyltransferase 1; HDAC11, histone deacetylase 11; JAGN1, jagunal homolog 1.

response [89, 90].

Jagunal homolog 1 (JAGN1)

The protein encoded by JAGN1 is an endoplasmic reticulum transmembrane protein that functions in the early secretory pathway and is required for neutrophil differentiation and survival. JAGN1 mutations can cause severe congenital neutropenia [91]. Following systemic *C. albicans* infection, JAGN1-deficient mice showed significant weight loss, enlarged mortality, and increased organ fungal burden. Deletion of JAGN1 alters glycoprotein processing and protein transport in the endoplasmic reticulum and Golgi by analysis of mass spectrometry data. In particular, altered glycosylation of the cell adhesion and migration molecules CD177, CD11b and CD18 was observed, as well as significant alterations in the glycosylation of neutrophil collagenase, matrix metalloproteinase-9, lactoferrin, lipocalin 2, binding bead protein,

and myeloid bacteriocin, which are associated with cytotoxic effector functions of neutrophils. Thus, deletion of JAGN1 leads to obvious glycosylation changes in key molecules involved in neutrophil migration and neutrophil cytotoxicity [92].

Discussion

Invasive *Candida* infections are a serious threat to human health, especially in perioperative immunocompromised patients. The main clinical treatment for invasive *Candida* infections is still the use of antifungal drugs. There are three main classes of antifungal drugs in common use, namely azoles, polyenes, and echinocandins [93]. These antifungal drugs usually target the ergosterol biosynthetic pathway, fungal cell membranes, or cell walls. However, the increasing toxicity and resistance of these drugs has led to unsatisfactory clinical outcomes, and the mortality rate of invasive *Candida* infections still exceeds 50% [94]. Therefore, it is necessary to explore novel therapeutic approaches to combat fungal infections.

The regression of any infection depends on the pathogenic capacity of the pathogenic bacteria and the ability of the immune system to kill it. In addition to developing new drugs to target *Candida* itself, it is possible to fight infection by modulating the immune system. Through the previous description of the regulatory role of the PTMs in the antifungal immune process, we have gained insights into the targets and mechanisms of action of the enzymes associated with PTMs in the antifungal immune process (**Table 1**). These substances play a very important role in the control of fungal infections. Therefore, modulating the progression of anti-fungal immunity through the regulation of PTMs could be a promising avenue for intervention.

In existing studies, systemic in vivo delivery of CBL-B siRNA into mice have protected them from lethal disseminated candidiasis and greatly reduced post-infection mortality and organ fungal burden. Administration of AGK2 or AK-1 inhibitors of the deacetylase SIRT2 promoted dectin-activated signaling and proinflammatory gene expression, and produced a protective effect on mice with systemic *Candida* infection [57, 79]. The above approaches interfere with enzymes and negatively regulate the immune process against *C. albicans*, by siRNA and inhibitors, thus enhancing the antibacterial capacity of the cells, as well as in mice. This suggests that the anti-inflammatory capacity of immune cells can be directly regulated by modulating the activity of these enzymes. This allows these enzymes to function as potential therapeutic targets, and the immunity of the host during invasive *Candida* infections can be enhanced by developing drugs that target these enzymes.

In conclusion, PTMs that modulate host innate immune response against *C. albicans* invasion hold great research value. However, clinical treatment for fungal infections still faces significant challenges, and more sustained and in-depth research is needed in the future.

References

[1] Lionakis MS, Lim JK, Lee CC, et al. Organ-specific innate immune responses in a mouse model of invasive candidiasis. J Innate Immun 2011;3:180-199.

[2] Bugli F, Massaro F, Buonocore F, et al. Design and Characterization of Myristoylated and Non-Myristoylated Peptides Effective against *Candida* spp. Clinical Isolates. Int J Mol Sci 2022;23:2164.

[3] Pianalto KM, Alspaugh JA. New Horizons in Antifungal Therapy. J Fungi (Basel) 2016;2(4):26.

[4] Pfaller MA, Diekema DJ. Epidemiology of invasive candidiasis: a persistent public health problem. Clin Microbiol Rev 2007;20:133-163.

[5] Page GG. Surgeryinduced immunosuppression and postoperative pain management. AACN Clin Issues 2005;16:302-309; quiz 416-418.

[6] Schmidt S, Condorelli A, Koltze A, et al. NK Cells and Their Role in Invasive Mold Infection. J Fungi (Basel) 2017;3(2):5.

[7] Schmidt S, Tramsen L, Lehrnbecher T. Natural Killer Cells in Antifungal Immunity. Front Immunol 2017;8:1623.

[8] Ben-Eliyahu S. The promotion of tumor metastasis by surgery and stress: immunological basis and implications for psychoneuroimmunology. Brain Behav Immun 2003;17 Suppl 1:S27-S36.

[9] Sato A, Nakamura I, Fujita H, et al. Peripheral venous catheter-related bloodstream infection is associated with severe complications and potential death: a retrospective observational study. BMC Infect Dis 2017;17:434.

[10] Tatsuno K, Ikeda M, Wakabayashi Y, et al. Clinical Features of Bloodstream Infections Associated with Peripheral Versus Central Venous Catheters. Infect Dis Ther 2019;8:343-352.

[11] Yang SP, Chen YY, Hsu HS, et al. A risk factor analysis of healthcare-associated fungal infections in an intensive care unit: a retrospective cohort study. BMC Infect Dis 2013;13:10.

[12] Leopold Wager CM, Hole CR, Wozniak KL, et al. Cryptococcus and Phagocytes: Complex Interactions that Influence Disease Outcome. Front Microbiol 2016;7:105.
[13] Costa-de-Oliveira S and Rodrigues AG. *Candida albicans* Antifungal Resistance and Tolerance in Bloodstream Infections: The Triad Yeast-Host-Antifungal. Microorganisms 2020;8(2):154.
[14] Lionakis MS, Drummond RA and Hohl TM. Immune responses to human fungal pathogens and therapeutic prospects. Nat Rev Immunol 2023;23:433-452.
[15] Borriello F, Zanoni I, Granucci F. Cellular and molecular mechanisms of antifungal innate immunity at epithelial barriers: The role of C-type lectin receptors. Eur J Immunol 2020;50:317-325.
[16] Roth S, Bergmann H, Jaeger M, et al. Vav Proteins Are Key Regulators of Card9 Signaling for Innate Antifungal Immunity. Cell Rep 2016;17:2572-2583.
[17] Hardison SE, Brown GD. C-type lectin receptors orchestrate antifungal immunity. Nat Immunol 2012;13:817-822.
[18] Wan L, Xu K, Chen Z, et al. Roles of Post-translational Modifications in Spinocerebellar Ataxias. Front Cell Neurosci 2018;12:290.
[19] Doyle HA, Mamula MJ. Post-translational protein modifications in antigen recognition and autoimmunity. Trends Immunol 2001;22:443-449.
[20] Karve TM, Cheema AK. Small changes huge impact: the role of protein posttranslational modifications in cellular homeostasis and disease. J Amino Acids 2011;2011:207691.
[21] Liu J, Qian C, Cao X. Post-Translational Modification Control of Innate Immunity. Immunity 2016;45:15-30.
[22] Incel A, Arribas Díez I, Wierzbicka C, et al. Selective Enrichment of Histidine Phosphorylated Peptides Using Molecularly Imprinted Polymers. Anal Chem 2021;93:3857-3866.
[23] Klement E, Medzihradszky KF. Extracellular Protein Phosphorylation, the Neglected Side of the Modification. Mol Cell Proteomics 2017;16:1-7.
[24] Kraeva N, Lestinova T, Ishemgulova A, et al. LmxM.22.0250-Encoded Dual Specificity Protein/Lipid Phosphatase Impairs Leishmania mexicana Virulence In Vitro. Pathogens 2019;8(4):241.
[25] Sun W, Wang H, Hu H, et al. Cutting Edge: EPHB2 Is a Coreceptor for Fungal Recognition and Phosphorylation of Syk in the Dectin-1 Signaling Pathway. J Immunol 2021;206:1419-1423.
[26] Chen J, He R, Sun W, et al. TAGAP instructs Th17 differentiation by bridging Dectin activation to EPHB2 signaling in innate antifungal response. Nat Commun 2020;11:1913.
[27] Long X, Yu Y, Perlaky L, et al. Stromal CYR61 Confers Resistance to Mitoxantrone via Spleen Tyrosine Kinase Activation in Human Acute Myeloid Leukaemia. Br J Haematol 2015;170:704-718.
[28] Jiang M, Liu R, Chen Y, et al. A combined experimental and computational study of Vam3, a derivative of resveratrol, and Syk interaction. Int J Mol Sci 2014;15:17188-17203.
[29] de Castro RO, Zhang J, Jamur MC, et al. Tyrosines in the carboxyl terminus regulate Syk kinase activity and function. J Biol Chem 2010;285:26674-26684.
[30] Lionakis MS, Levitz SM. Host Control of Fungal Infections: Lessons from Basic Studies and Human Cohorts. Annu Rev Immunol 2018;36:157-191.
[31] Deng Z, Ma S, Zhou H, et al. Tyrosine phosphatase SHP-2 mediates C-type lectin receptor-induced activation of the kinase Syk and anti-fungal TH17 responses. Nat Immunol 2015;16:642-652.
[32] Ma X, Tan X, Yu B, et al. DOCK2 regulates antifungal immunity by regulating RAC GTPase activity. Cell Mol Immunol 2022;19:602-618.
[33] Strasser D, Neumann K, Bergmann H, et al. Syk kinase-coupled C-type lectin receptors engage protein kinase C-delta to elicit Card9 adaptor-mediated innate immunity. Immunity 2012;36:32-42.
[34] Li DD, Jawale CV, Zhou C, et al. Fungal sensing enhances neutrophil metabolic fitness by regulating antifungal Glut1 activity. Cell Host Microbe 2022;30:530-544 e536.
[35] Carpino N, Naseem S, Frank DM, et al. Modulating Host Signaling Pathways to Promote Resistance to Infection by *Candida albicans*. Front Cell Infect Microbiol 2017;7:481.
[36] San Luis B, Sondgeroth B, Nassar N, et al. Sts-2 is a phosphatase that negatively regulates zeta-associated protein (ZAP)-70 and T cell receptor signaling pathways. J Biol Chem 2011;286:15943-15954.
[37] Reppschläger K, Gosselin J, Dangelmaier CA, et al. TULA-2 Protein Phosphatase Suppresses Activation of Syk through the GPVI Platelet Receptor for Collagen by Dephosphorylating Tyr(P)346, a Regulatory Site of Syk. J Biol Chem 2016;291:22427-22441.
[38] Kerrigan AM, Brown GD. Syk-coupled C-type lectins in immunity. Trends Immunol 2011;32:151-156.
[39] Frank D, Naseem S, Russo GL, et al. Phagocytes from Mice Lacking the Sts Phosphatases Have an Enhanced Antifungal

Response to *Candida albicans*. mBio 2018;9(4):e00782-18.
[40] Lemay S, Davidson D, Latour S, et al. Dok-3, a novel adapter molecule involved in the negative regulation of immunoreceptor signaling. Mol Cell Biol 2000;20:2743-2754.
[41] Kim SS, Lee KG, Chin CS, et al. DOK3 is required for IFN-β production by enabling TRAF3/TBK1 complex formation and IRF3 activation. J Immunol 2014;193:840-848.
[42] Peng Q, O'Loughlin JL, Humphrey MB. DOK3 negatively regulates LPS responses and endotoxin tolerance. PLoS One 2012;7:e39967.
[43] Ou X, Xu S, Li YF, et al. Adaptor protein DOK3 promotes plasma cell differentiation by regulating the expression of programmed cell death 1 ligands. Proc Natl Acad Sci U S A 2014;111:11431-11436.
[44] Loh JT, Xu S, Huo JX, et al. Dok3-protein phosphatase 1 interaction attenuates Card9 signaling and neutrophil-dependent antifungal immunity. J Clin Invest 2019;129:2717-2729.
[45] Liang W, Fang J, Zhou S, et al. The role of ubiquitin-specific peptidases in glioma progression. Biomed Pharmacother 2022;146:112585.
[46] Ebner P, Versteeg GA, Ikeda F. Ubiquitin enzymes in the regulation of immune responses. Crit Rev Biochem Mol Biol 2017;52:425-460.
[47] Varshavsky A. The Ubiquitin System, Autophagy, and Regulated Protein Degradation. Annu Rev Biochem 2017;86:123-128.
[48] Hutchins AP, Liu S, Diez D, et al. The repertoires of ubiquitinating and deubiquitinating enzymes in eukaryotic genomes. Mol Biol Evol 2013;30:1172-1187.
[49] Asmamaw MD, Liu Y, Zheng YC, et al. Skp2 in the ubiquitin-proteasome system: A comprehensive review. Med Res Rev 2020;40:1920-1949.
[50] Mevissen TET, Komander D. Mechanisms of Deubiquitinase Specificity and Regulation. Annu Rev Biochem 2017;86:159-192.
[51] Shamim M, Nanjappa SG, Singh A, et al. Cbl-b regulates antigen-induced TCR down-regulation and IFN-gamma production by effector CD8 T cells without affecting functional avidity. J Immunol 2007;179:7233-7243.
[52] Sohn HW, Gu H, Pierce SK. Cbl-b negatively regulates B cell antigen receptor signaling in mature B cells through ubiquitination of the tyrosine kinase Syk. J Exp Med 2003;197:1511-1524.
[53] Chiang YJ, Kole HK, Brown K, et al. Cbl-b regulates the CD28 dependence of T-cell activation. Nature 2000;403:216-220.
[54] Han C, Jin J, Xu S, et al. Integrin CD11b negatively regulates TLR-triggered inflammatory responses by activating Syk and promoting degradation of MyD88 and TRIF via Cbl-b. Nat Immunol 2010;11:734-742.
[55] Paolino M, Choidas A, Wallner S, et al. The E3 ligase Cbl-b and TAM receptors regulate cancer metastasis via natural killer cells. Nature 2014;507:508-512.
[56] Wirnsberger G, Zwolanek F, Asaoka T, et al. Inhibition of CBLB protects from lethal *Candida albicans* sepsis. Nat Med 2016;22:915-923.
[57] van de Veerdonk FL, Netea MG. CBLB ubiquitin ligase: a major regulator of antifungal immunity. Nat Med 2016;22:834-835.
[58] Zhu LL, Luo TM, Xu X, et al. E3 ubiquitin ligase Cbl-b negatively regulates C-type lectin receptor-mediated antifungal innate immunity. J Exp Med 2016;213:1555-1570.
[59] Duan JL, He HQ, Yu Y, et al. E3 ligase c-Cbl regulates intestinal inflammation through suppressing fungi-induced noncanonical NF-κB activation. Sci Adv 2021;7(19):eabe5171.
[60] Li Y, Wu H, Wu W, et al. Structural insights into the TRIM family of ubiquitin E3 ligases. Cell Res 2014;24:762-765.
[61] Liu B, Zhang M, Chu H, et al. The ubiquitin E3 ligase TRIM31 promotes aggregation and activation of the signaling adaptor MAVS through Lys63-linked polyubiquitination. Nat Immunol 2017;18:214-224.
[62] Wang X, Zhang H, Shao Z, et al. TRIM31 facilitates K27-linked polyubiquitination of SYK to regulate antifungal immunity. Signal Transduct Target Ther 2021;6:298.
[63] Xu M, Tan J, Dong W, et al. The E3 ubiquitin-protein ligase Trim31 alleviates non-alcoholic fatty liver disease by targeting Rhbdf2 in mouse hepatocytes. Nat Commun 2022;13:1052.
[64] Zhang J, Cao L, Wang X, et al. The E3 ubiquitin ligase TRIM31 plays a critical role in hypertensive nephropathy by promoting proteasomal degradation of MAP3K7 in the TGF-β1 signaling pathway. Cell Death Differ 2022;29:556-567.
[65] Zeng S, Zhao Z, Zheng S, et al. The E3 ubiquitin ligase TRIM31 is involved in cerebral ischemic injury by promoting degradation of TIGAR. Redox Biol 2021;45:102058.
[66] Song H, Liu B, Huai W, et al. The E3 ubiquitin ligase TRIM31 attenuates NLRP3 inflammasome activation by promoting proteasomal degradation of NLRP3. Nat Commun 2016;7:13727.
[67] Cao Z, Conway KL, Heath RJ, et al. Ubiquitin Ligase TRIM62 Regulates CARD9-Mediated Anti-fungal Immunity and Intestinal Inflammation. Immunity 2015;43:715-726.

[68] Leshchiner ES, Rush JS, Durney MA, et al. Small-molecule inhibitors directly target CARD9 and mimic its protective variant in inflammatory bowel disease. Proc Natl Acad Sci U S A 2017;114:11392-11397.
[69] Guo H, Qiao G, Ying H, et al. E3 ubiquitin ligase Cbl-b regulates Pten via Nedd4 in T cells independently of its ubiquitin ligase activity. Cell Rep 2012;1:472-482.
[70] Pei G, Buijze H, Liu H, et al. The E3 ubiquitin ligase NEDD4 enhances killing of membrane-perturbing intracellular bacteria by promoting autophagy. Autophagy 2017;13:2041-2055.
[71] Nuro-Gyina PK, Tang N, Guo H, et al. HECT E3 Ubiquitin Ligase Nedd4 Is Required for Antifungal Innate Immunity. J Immunol 2021;207:868-877.
[72] Xu W, Rush JS, Graham DB, et al. USP15 Deubiquitinates CARD9 to Downregulate C-Type Lectin Receptor-Mediated Signaling. Immunohorizons 2020;4:670-678.
[73] Chen X, Zhang H, Wang X, et al. OTUD1 Regulates Antifungal Innate Immunity through Deubiquitination of CARD9. J Immunol 2021;206:1832-1843.
[74] Piao S, Pei HZ, Huang B, et al. Ovarian tumor domain-containing protein 1 deubiquitinates and stabilizes p53. Cell Signal 2017;33:22-29.
[75] Zhang L, Liu J, Qian L, et al. Induction of OTUD1 by RNA viruses potently inhibits innate immune responses by promoting degradation of the MAVS/TRAF3/TRAF6 signalosome. PLoS Pathog 2018;14:e1007067.
[76] Ji Y, Chen Z, Cen Z, et al. A comprehensive mouse brain acetylome-the cellular-specific distribution of acetylated brain proteins. Front Cell Neurosci 2022;16:980815.
[77] Choudhary C, Weinert BT, Nishida Y, et al. The growing landscape of lysine acetylation links metabolism and cell signalling. Nat Rev Mol Cell Biol 2014;15:536-550.
[78] Sun W, Ma X, Wang H, et al. MYO1F regulates antifungal immunity by regulating acetylation of microtubules. Proc Natl Acad Sci U S A 2021;118(30):e2100230118.
[79] Wu H, Yin X, Zhao X, et al. HDAC11 negatively regulates antifungal immunity by inhibiting Nos2 expression via binding with transcriptional repressor STAT3. Redox Biol 2022;56:102461.
[80] Teixeira MM. Myo1f is critical for neutrophil migration in vivo. Blood 2018;131:1879-1880.
[81] Navinés-Ferrer A, Ainsua-Enrich E, Serrano-Candelas E, et al. Myo1f, an Unconventional Long-Tailed Myosin, Is a New Partner for the Adaptor 3BP2 Involved in Mast Cell Migration. Front Immunol 2019;10:1058.
[82] Piedra-Quintero ZL, Serrano C, Villegas-Sepúlveda N, et al. Myosin 1F Regulates M1-Polarization by Stimulating Intercellular Adhesion in Macrophages. Front Immunol 2018;9:3118.
[83] Shakespear MR, Halili MA, Irvine KM, et al. Histone deacetylases as regulators of inflammation and immunity. Trends Immunol 2011;32:335-343.
[84] Yanginlar C, Logie C. HDAC11 is a regulator of diverse immune functions. Biochim Biophys Acta Gene Regul Mech 2018;1861:54-59.
[85] Sun L, Marin de Evsikova C, Bian K, et al. Programming and Regulation of Metabolic Homeostasis by HDAC11. EBioMedicine 2018;33:157-168.
[86] Thole TM, Lodrini M, Fabian J, et al. Neuroblastoma cells depend on HDAC11 for mitotic cell cycle progression and survival. Cell Death Dis 2017;8:e2635.
[87] Byun SK, An TH, Son MJ, et al. HDAC11 Inhibits Myoblast Differentiation through Repression of MyoD-Dependent Transcription. Mol Cells 2017;40:667-676.
[88] Zhu H, Wang S, Liu D, et al. Identifying Sialylation Linkages at the Glycopeptide Level by Glycosyltransferase Labeling Assisted Mass Spectrometry (GLAMS). Anal Chem 2020;92:6297-6303.
[89] Ohtsubo K, Marth JD. Glycosylation in cellular mechanisms of health and disease. Cell 2006;126:855-867.
[90] Rudd PM, Elliott T, Cresswell P, et al. Glycosylation and the immune system. Science 2001;291:2370-2376.
[91] Boztug K, Järvinen PM, Salzer E, et al. JAGN1 deficiency causes aberrant myeloid cell homeostasis and congenital neutropenia. Nat Genet 2014;46:1021-1027.
[92] Wirnsberger G, Zwolanek F, Stadlmann J, et al. Jagunal homolog 1 is a critical regulator of neutrophil function in fungal host defense. Nat Genet 2014;46:1028-1033.
[93] Chang YL, Yu SJ, Heitman J, et al. New facets of antifungal therapy. Virulence 2017;8:222-236.
[94] Pfaller MA, Diekema DJ. Epidemiology of invasive mycoses in North America. Crit Rev Microbiol 2010;36:1-53.
[95] Li X, Cullere X, Nishi H, et al. PKC-δ activation in neutrophils promotes fungal clearance. J Leukoc Biol 2016;100:581-588.

Perioperative Precision Medicine
eISSN: 2957-5443

Zentime

Review Article https://doi.org/10.61189/663074tcakcn

Research progress of frontier image processing in medical endoscopes

Jinjing Wu[1,*], Yang Yuan[2,*], Long Liu[1], Haipo Cui[1], Tianying Xu[3], Miao Zhou[4], Zhanheng Chen[3], Bing Xu[3]

[1]School of Health Science and Engineering, University of Shanghai for Science and Technology, Shanghai 200093, China.[2]School of Computer Science and Artificial Intelligence, Changzhou University, Jiangsu 213164, China.[3]School of Anesthesiology, Second Military Medical University/Naval Medical University, Shanghai 200433, China. [4]Department of Anesthesiology, the Affiliated Cancer Hospital of Nanjing Medical University, Jiangsu Cancer Hospital, Jiangsu Institute of Cancer Research, Nanjing Medical University, Nanjing 210009, Jiangsu, China.
[*]The authors contribute equally.

Acknowledgements: This work was supported by the National Natural Science Foundation of China (62002297, 62073225, 61836005), the Science and Technology Commission of Shanghai Municipality (20XD1434400), the Talent Development Fund of Shanghai (2020075), Medical-Engineering Cross Fund of Shanghai Jiao Tong University (YG2022QN043), and the Guangxi Science and Technology Base and Talent Special Project (2021AC19394). The authors would like to thank all the guest editors and anonymous reviewers for their constructive comments.

Declaration of conflict of interest: None.

Received July 19, 2023; Accepted September 6, 2023; Published September 30, 2023

Highlights

- Medical endoscopic images can provide doctors with more accurate, visualized, and three-dimensional views of various internal tissues.
- Image processing techniques such as image denoising, image deblurring, image enhancement, and image segmentation can improve the imaging quality of endoscopes.

Abstract

In the modern medical diagnosis, digital medical images can provide physicians with a more accurate, visualized, and three-dimensional view of various tissues. These images assist in predicting, diagnosing, and treating diseases. However, medical images are highly susceptible to noise contamination from the influence of imaging equipment and the capture process, which poses a significant challenge in the analysis of medical images. This review summarizes the image processing technologies applied in endoscopy, such as image denoising, image deblurring, image enhancement, and image segmentation, involving traditional computational models and deep learning algorithms used in these technologies. Additionally, the clinical applications of these techniques are also discussed.

Keywords: Endoscopy, image denoising, image deblurring, image enhancement, image segmentation, artificial intelligence

Introduction

The development history of endoscopy is long and rich. In 1806, Philipp Bozzini developed the first endoscope, known as the “Lichtleiter,” which was successfully used for examinations of bladder, esophagus, and urethra. Subsequently, in 1954, Harold Hopkins from the United Kingdom invented fiber-optic endoscope, marking the inception of modern gastrointestinal endoscopy. In 1983, Welch-Allyn, a company based in the United States, introduced the world’s first electronic endoscope, which quickly found applications in clinical practice. Since then, electronic endoscopy has become a focal point of research, particularly with the dominance of the Japanese company Olympus in the electronic endoscope market. However, traditional endoscopes have limitations in image quality due to factors such as hardware

Address correspondence to: Haipo Cui, School of Health Science and Engineering, University of Shanghai for Science and Technology, NO.334, Jungong Road, Shanghai 200093, China. E-mail: h_b_cui@163.com, Tel: +86-21-55271290; **Bing Xu**, School of Anesthesiology, Second Military Medical University/Naval Medical University, No.800 Xiangyin Road, Shanghai 200433, China. E-mail: mzxubing1992@163.com, Tel: +86-21-81872030; **Zhanheng Chen**, School of Anesthesiology, Second Military Medical University/Naval Medical University, No.800 Xiangyin Road, Shanghai 200433, China. E-mail: chenzhanheng17@mails.ucas.ac.cn, Tel: +86 21 81872034.

constraints, which restrict their accuracy in disease diagnosis. To improve the quality of endoscopic images, modern endoscope researchers are dedicated to developing better techniques to enhance the applicability of endoscopy in detecting hard-to-detect lesions like adenomas. Image processing methods play a crucial role in endoscopy, encompassing research in areas such as image denoising, image deblurring, image enhancement, and image segmentation. These studies aim to make the images clearer and more visible, thus enhancing the applicability of endoscopy in the diagnosis of hard-to-detect lesions like adenomas.

With the advancement of artificial intelligence (AI) technology, image processing algorithms have also been continuously updated and iterated. The integration of endoscopy with AI has gained increasing attention. In recent years, deep learning has shown promising applications in the field of image processing, including image detection, image segmentation, and image restoration. Tola et al. proposed a convolutional neural network (CNN) for the detection of brain diseases such as inflammatory diseases, cerebrovascular diseases, and tumor diseases in magnetic resonance imaging (MRI) images [1]. Gupta et al. developed an effective computer-aided diagnosis system that includes four main processing steps: image preprocessing, lung image feature extraction, feature selection using bio-inspired evolutionary algorithms, and potential disease classification [2]. Xue et al. proposed two generative adversarial networks (GANs), namely Segmentor and Critic, for learning the transformation between brain MRI images and binary segmentation maps of brain tumors [3]. Schlegl et al. trained GANs using healthy patches in the retinal region to learn the data distribution of healthy tissues for anomaly detection in retinal images [4].

This paper provides a comprehensive overview of the research progress on the application of advanced image processing methods in endoscopy. In Section 2, a concise description of the process of literature search is provided. In Section 3, a brief introduction to deep learning methods is presented. In Section 4, the existing image processing techniques are outlined, including image denoising, image deblurring, image enhancement, and image segmentation. In Section 5, we summarize the content of this paper and discuss the current research challenges. In Section 6, future research directions are proposed.

Literature research

A literature search was conducted on PubMed, Web of Science, and Science Direct using the following search terms: “endoscope and deep learning,” “medical and image restoration,” “endoscope and image denoising,” “endoscope and image deblurring,” and “endoscope and image enhancement.” The search covered publications from 2009 to 2022. Initially, a total of 150 studies were identified. After screening for relevance, 31 studies were included. **Table 1** summarizes the key findings and main conclusions of the included literature.

Classical deep learning methods for image processing

Deep learning, a branch of machine learning, is an algorithm that utilizes artificial neural networks to automatically extract features from data. Unlike traditional machine learning methods that require manual feature extraction, deep learning algorithms perform both feature extraction and classification in an end-to-end manner, which makes deep learning particularly effective in various domains. The application scenarios of deep learning can be categorized into three major domains: (1) computer vision, such as image recognition and object detection; (2) natural language processing, including machine translation and text processing; (3) speech technology, such as speech recognition [5-13].

Convolutional neural networks (CNNs)

CNNs are widely based on deep learning models specifically designed for processing image and audio data. The core principle of CNNs is to extract local features of an image through convolutional operations and reduce the dimensionality of features through pooling operations. Classification or regression tasks are then performed through fully connected layers. The key components of CNN models include convolutional layers, pooling layers, and fully connected layers. The structure of a CNN is illustrated in **Figure 1**. The convolutional layer is the core of CNN, which extracts features from the input image through sliding convolutional kernels. The parameters of each convolutional kernel can be learned, so that the network can automatically extract features with different levels and abstractions. Pooling is a technique used to downsample the input image, reducing the number of pixels while retaining essential information. Its primary purpose is to decrease computational complexity. The two main types of pooling are max pooling and average pool-

Table 1. Summary of literature

Authors	Focus of study	Principal conclusions
Gopi et al. [14]	Denoising capsule endoscope images using double density dual tree complex wavelet transform.	The proposed method effectively reduces noise in capsule endoscopic images, improving their quality and enhancing diagnostic accuracy.
Patil et al. [15]	Denoising medical images using wavelet transform and singular value decomposition.	Wavelet transform and singular value decomposition effectively denoise medical images, preserving important features and improving image quality for enhanced diagnostic accuracy.
Qu et al. [16]	Real-time removal of stripe noise in endoscope images.	The article presents a real-time method for effectively removing stripe noise in endoscope images, improving image quality and facilitating accurate diagnosis.
Ning et al. [17]	Developing effective methods for removing noise in medical images, aiming to enhance image quality and improve the accuracy of medical diagnosis.	The research successfully investigates and proposes effective techniques for removing noise in medical images, leading to improved image quality and facilitating accurate medical diagnosis.
Magadalena et al. [18]	RGB-based compressed medical imaging using sparsity averaging reweighted analysis for wireless capsule endoscopy images.	The article proposes an RGB-based compressed medical imaging method for wireless capsule endoscopy images, utilizing sparsity averaging reweighted analysis. The approach effectively reduces data size while preserving image quality, enabling efficient transmission and storage of medical images.
Zhang et al. [19]	Deep CNN-based image denoising beyond Gaussian denoising.	The article introduces a CNN approach for image denoising, surpassing traditional Gaussian denoising methods. The proposed method achieves superior denoising performance by learning residual information, enhancing image quality, and preserving fine details.
Izadi et al. [20]	Blind image denoising using noise whiteness prior in the WhiteNNer method.	The article proposes the WhiteNNer method, which utilizes noise whiteness priors for blind image denoising. The approach effectively reduces noise and improves image quality without requiring prior knowledge of noise characteristics, making it suitable for various real-world denoising applications.
Zou et al. [21]	CNN-based blind denoising method for endoscopic images.	In this article, a novel CNN-based blind denoising method is proposed for the denoising of endoscopic images. The method demonstrates effective noise reduction and enhances image quality, leading to improved visibility of important structures and enabling more accurate diagnosis in endoscopy applications.
Ahmed et al. [23]	The denoising CNN can remove the noise on the image and improve the clarity and contrast by learning the noise distribution in the endoscope.	The study introduces an enhanced classification method using transfer learning and well-trained CNN models. It incorporates a noise removal stage as a pre-processing step, leading to improved performance on multiclass medical problems.
Peng et al. [25]	They present a frame work that can restore blurry frames by synthesizing image details from the nearby sharp frames.	The proposed synthesis-based approach successfully deblurs endoscopic videos, improving visual quality and enhancing image clarity, contributing to diagnostic and surgical applications.

Authors	Focus of study	Principal conclusions
Tchaka et al. [26]	The article focuses on chromaticity-based smoke removal in endoscopic images, aiming to effectively eliminate smoke artifacts and enhance image visibility for accurate diagnosis and better guiding surgical procedures.	Smoke artifacts in endoscopic images are effectively reduced using achromaticity-based approach, resulting in improved visibility and enhanced image quality for better diagnostic accuracy.
Wang et al. [27]	Reduction of bubble-like frames in wireless capsule endoscopy videos using an RSS filter.	The article demonstrates that employing an RSS filter effectively reduces bubble-like frames in wireless capsule endoscopy videos. The proposed method enhances the quality of the videos, improving visual clarity and facilitating accurate diagnosis.
Lin et al. [30]	Desmoking algorithm for endoscopic images using an improved U-Net model.	The article proposes an improved U-Net model for desmoking endoscopic images, effectively reducing smoke artifacts and improving image visibility. The method enhances the quality of images, facilitating accurate diagnosis in endoscopy.
Yang et al. [31]	Deep learning-based methods for deblurring and super-resolution reconstruction of endoscopic images.	The article presents deep learning-based techniques for deblurring and super-resolution reconstruction of endoscopic images, achieving improved image quality and enhanced visual details, and enabling better visualization and accurate diagnosis in endoscopy.
Hai et al. [32]	Image enhancement using Contrast Limited Adaptive Histogram Equalization for 3D images in stereoscopic endoscopy.	The article proposes using Contrast Limited Adaptive Histogram Equalization for enhancing 3D images in stereoscopic endoscopy. The method effectively improves image quality, enhances visual details, and enables better visualization of anatomical structures for accurate diagnosis.
Sato et al. [33]	Texture and color enhancement imaging for improving endoscopic image quality and enhancing visual details.	The article presents the Texture and color enhancement imaging method for endoscopic image enhancement, effectively improving image quality, enhancing texture and color, and facilitating better visualization of important details, leading to improved diagnostic capabilities in endoscopy.
Zhang et al. [34]	Improved weighted guided filtering for enhancing medical endoscope images.	The article proposes an improved weighted guided filtering method for enhancing medical endoscope images, effectively reducing noise, enhancing image details, and improving overall visual quality, leading to improved diagnostic capabilities in medical applications.
Wu et al. [35]	Quality enhancement of endoscopic images using Retinex and Pseudo-HDR synthesis algorithms.	The article presents Retinex and pseudo-HDR synthesis algorithms for enhancing the quality of endoscopic images, resulting in improved visual perception, enhanced details, and better image quality for accurate diagnosis and analysis in endoscopy.
An et al. [36]	Development of the EIEN, based on the Retinex theory, for endoscopic image enhancement.	The article introduces the EIEN, based on Retinex theory, for endoscopic image enhancement, effectively improving image quality, enhancing details, and providing better visual perception for improved diagnostic accuracy in endoscopy.
Shen et al. [37]	Content-aware specular reflection suppression in endoscopic images using adaptive image inpainting and neural network techniques.	The article presents a method for content-aware specular reflection suppression in endoscopic images using adaptive image inpainting and neural network, effectively removing reflections and enhancing image quality, and enabling better visualization and accurate diagnosis in endoscopy.

Authors	Focus of study	Principal conclusions
Gómez et al. [38]	Low-light image enhancement of high-speed endoscopic videos using a CNN.	The article presents a CNN-based method for low-light image enhancement of high-speed endoscopic videos, effectively improving visibility, enhancing details, and providing better image quality for accurate diagnosis in endoscopy.
Huang et al. [39]	Deep unsupervised endoscopic image enhancement through multi-image fusion.	The article demonstrates that deep unsupervised endoscopic image enhancement based on multi-image fusion can effectively improve the visual quality and enhance the details of endoscopic images without the need for manual annotations.
Li et al. [40]	Endoscopy image enhancement using adversarial training with generalized imaging defect models.	The article proposes an endoscopy image enhancement method based on adversarial training and generalized imaging defect models, effectively reducing image artifacts and improving the visual quality of endoscopic images.
Jha et al. [43]	Real-time polyp segmentation in video endoscopy using NanoNet, achieving accurate and efficient detection of polyps in capsule endoscopy and colonoscopy.	The article presents NanoNet, a real-time polyp segmentation method for video endoscopy, enabling accurate and efficient detection of polyps in capsule endoscopy and colonoscopy procedures.
Laves et al. [44]	Laryngeal endoscopic image dataset and CNN-based segmentation for improved analysis.	A comprehensive dataset of laryngeal endoscopic images was created for the study, and CNN-based semantic segmentation techniques were applied. The results demonstrated improved analysis and segmentation accuracy in laryngeal endoscopy.
Iwasa et al. [45]	Deep learning-based automatic segmentation of pancreatic tumors using contrast-enhanced endoscopic ultrasound video images.	Deep learning enables accurate segmentation of pancreatic tumors in contrast-enhanced endoscopic ultrasound videos, providing potential for improved diagnosis and treatment planning.

Note: CNN, convolutional neural network; RSS, recursive shadow suppression; EIEN, environmental information exchange network.

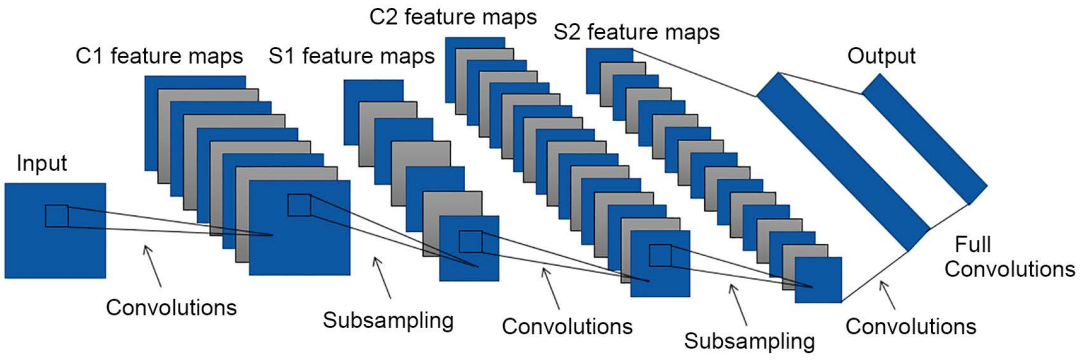

Figure 1. Structure of a CNN. CNN, convolutional neural network.

ing. The fully connected layer plays a role of classifier in the entire CNN. Before passing to fully connected layer, the outputs from previous layers need to be flattened.

Additionally, CNN models incorporate nonlinear activation functions, such as the rectified linear unit function, to introduce nonlinearity without changing the input shape, thereby enhancing the expressive power of the model. The training process of CNN models typically involves the use of a backpropagation algorithm to optimize the loss function and adjust the model parameters, enabling accurate classification or regression. Due to the local connectivity and weight-sharing properties of CNN models, they have shown excellent performance in image processing tasks and are commonly applied in image classification, object detection, and image segmentation.

Transfer learning

Transfer learning is a machine learning method

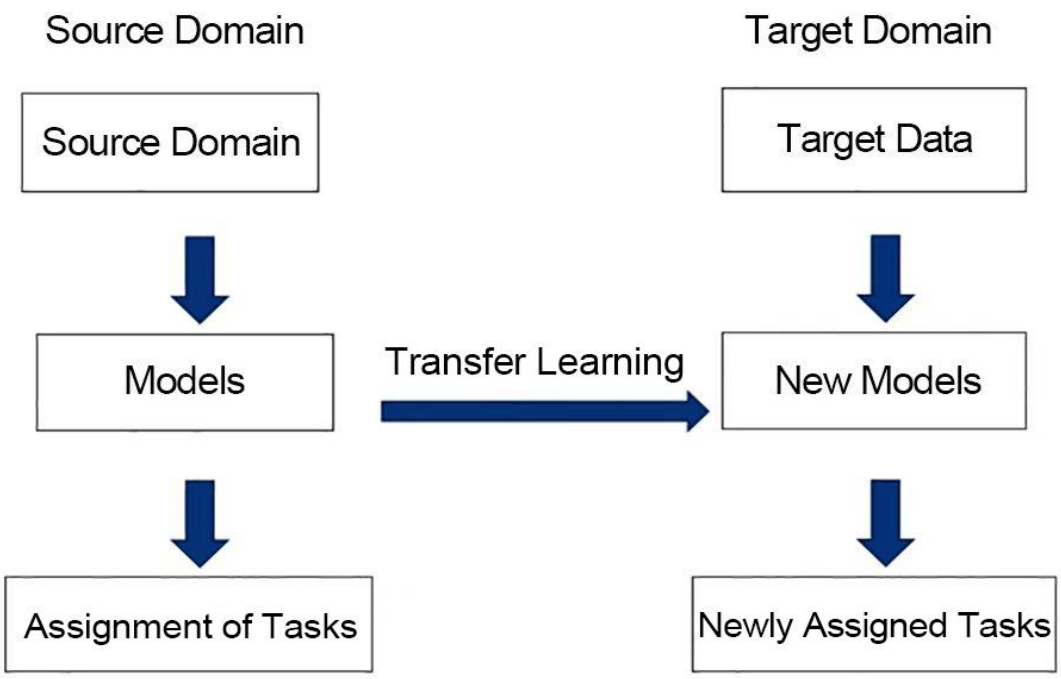

Figure 2. Flowchart of transfer learning.

that leverages knowledge and model parameters learned from one task to improve the performance of another related task. By employing transfer learning, the learning performance of the target task can be enhanced, especially when there is limited or insufficient labeled data available. This approach utilizes the knowledge and experience gained from the source task to aid the learning process of the target task. The core principle of transfer learning is based on the observation that there are shared underlying features and knowledge across different tasks and domains. These underlying features and knowledge can be acquired through pre-training models on the source task. By employing transfer learning, these learned features and knowledge can be applied to the target task, thereby accelerating the learning process and improving its performance.

Transfer learning consists of several key steps, including pre-training, feature extraction, and fine-tuning. This learning method has extensive applications in various domains such as object recognition, object detection, natural language processing, and medical image analysis. It addresses the challenge of limited data and constrained computational resources in the target task by utilizing the learned features and knowledge from the source task. Transfer learning has widespread applications across different fields and provides powerful tools and methods for addressing practical problems. The process flowchart is illustrated in **Figure 2**.

Data augmentation

In image processing, data augmentation is often an indispensable part aimed at improving image quality, increasing dataset diversity, and enhancing the generalization capability of the models. The principle of data augmentation involves applying a series of transformation operations to the original image, such as geometric transformations (translation, rotation, scaling), color transformations (brightness adjustment, contrast enhancement, color distortion), and adding image noise, so as to generate new training samples. By introducing these transformations, uncertainties and diversities present in the real world can be simulated, making the model more robust.

With the widespread application of deep learning, unsupervised data augmentation has emerged as a novel approach. It involves enhancing the training dataset by synthesizing data automatically. Unlike traditional data augmentation methods, unsupervised data augmentation does not rely on any external supervision signals. Instead, it utilizes the features and statistical properties of its data to generate new training samples. Data augmentation finds extensive applications in various domains, in-

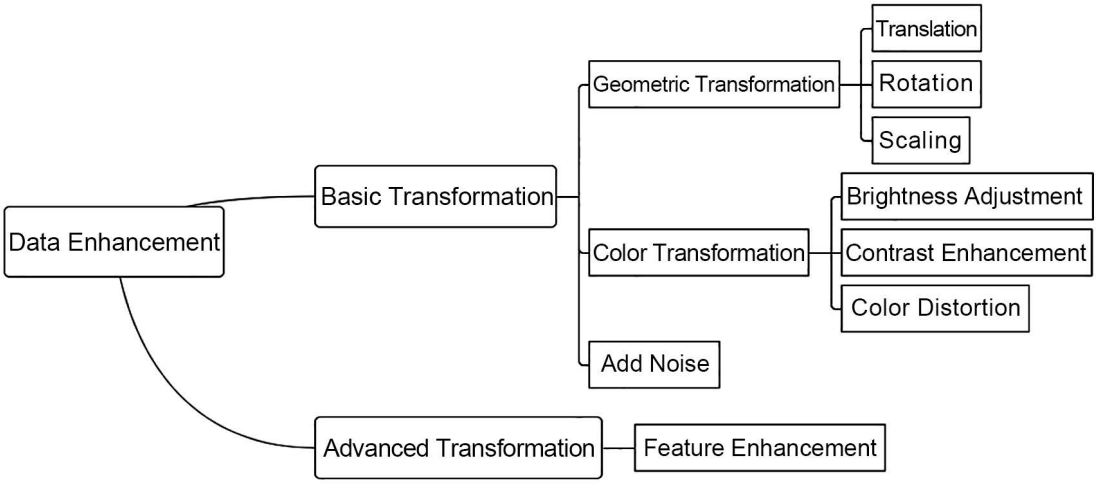

Figure 3. Data augmentation flowchart.

Table 2. High-quality images and corresponding image processing techniques

Characteristics of high-quality images	Corresponding image processing techniques
High resolution	Image sharpening and denoising
Good contrast	Histogram equalization and contrast enhancement
Rich details and textures	Local enhancement and texture enhancement
No blurring or motion blur	Image deblurring and motion blur correction
Uniform illumination	Image illumination equalization and background illumination correction
No noise or artifacts	Image denoising and artifact removal
Moving object detection	Moving object tracking and segmentation

cluding image classification, object detection, semantic segmentation, and anomaly detection, among others. The process flowchart of data augmentation is illustrated in **Figure 3**.

Image processing techniques in endoscopes

Medical image processing is an important branch of image processing that applies image processing techniques to the analysis and recognition of medical image data. Medical image data include computed tomography scans, MRI scans, X-rays, ultrasound images, and others. These image data contain rich information that can be utilized for disease diagnosis and treatment. Medical image processing techniques can enhance, segment, register, and classify these image data, extracting useful information to assist doctors in diagnosis and treatment decision-making. Medical image processing techniques can be applied in tumor detection, organ segmentation, lesion identification, surgical navigation, and more. The application of medical image processing techniques can improve diagnostic accuracy and treatment effectiveness while reducing healthcare resource waste and patient trauma. The characteristics and targeted image processing of high-quality medical images are illustrated in **Table 2**, as depicted in this academic paper.

Denoising of endoscopic images

After studying the principles of image noise, researchers discovered that the noise frequencies exhibit regular patterns. Based on the distribution characteristics and the nature of the images themselves, numerous traditional image denoising methods have emerged. One of the conventional approaches used in medical denoising is based on wavelet transform, which has also been applied in endoscopy. Gopi et al. proposed a method based on dual-tree complex wavelet transform using bivariate shrinkage to reduce noise in intestinal images [14]. In subsequent years, Patil et al. combined wavelet transform with singular value decomposition to further reduce noise [15]. The experimental results demonstrated that this approach outperformed the use of wavelet denoising alone, and the denoised images were advantageous for further processing tasks such as image segmentation and recognition. Furthermore, due to the use of small-sized sensors for imaging in endoscopy, images are often transmitted as high-speed serial signals or analog signals,

which can introduce striped noise. Qu et al. proposed a real-time denoising method for removing stripe noise, where the Fourier transform of each row of the noisy image was implemented on a field-programmable gate array [16]. This method can identify frequency domain and suppress the stripe noise spectrum. The designed endoscope was applied in urological systems, effectively meeting the clinical requirements for pathological diagnosis. Another common type of noise in endoscopic images is salt-and-pepper noise. Ning et al. employed traditional median filtering and adaptive median filtering methods to evaluate their denoising effectiveness based on the peak signal-to-noise ratio and the degree of noise degradation in the original images [17]. The study analyzed the influence of filtering noise density on the quality of denoised images. Their results demonstrated that both methods effectively eliminated salt-and-pepper noise in computed tomography and MRI images while preserving image edges and details.

Most traditional medical image processing methods are developed based on the characteristics of the images themselves, statistical features of the noise, and distribution patterns. Generally, these methods can be classified into two categories: spatial domain-based and transform domain-based approaches. Traditional filters often process the entire noisy image without considering the specific characteristics of the noise. As a result, they fail to properly handle local textures, leading to the blurring of image details. Therefore, researchers have been striving to develop denoising algorithms that can effectively preserve local detail features while maintaining good edge preservation.

In recent years, with the development of machine learning, there has been an emergence of model-based and learning-based methods for processing endoscopic images. Machine learning techniques can be categorized into dictionary learning methods and deep learning methods. Magdalena et al. proposed a medical image processing method based on RGB compression [18]. This approach uses sparsity averaging with reweighted analysis to convert the image into a low-dimensional sparse representation. Compression and decompression algorithms are then employed to compress and reconstruct images. This method shows potential applications in wireless capsule endoscope image transmission and storage. In addition to noise caused by devices, uneven illumination also affects physicians' observation and diagnosis of lesions. The emergence of CNNs has opened up new possibilities in image processing. However, there are few CNN-based blind image-denoising models. Zhang et al. proposed an endoscopic image denoising algorithm based on spatial U-Net [19]. This algorithm utilizes spatial attention mechanisms to extract and enhance important information in the image, reducing the influence of noise and artifacts. The U-Net structure can effectively restore the details and texture information of endoscopic images while avoiding excessive image smoothing. Izadi et al. introduced the deep image prior method, which uses a randomly initialized neural network and white Gaussian noise as input to denoise real images through thousands of iterations [20]. However, this method requires manual termination of the iteration process, making it computationally intensive. Zou et al. proposed a block-based blind denoising method [21]. They also designed a two-stage CNN model to process each block. The first stage extracts image features using convolution, and the second stage performs blind denoising on the extracted features. Compared to Lempitsky's experiments, this approach improves the deep image prior method by resolving the challenge of determining the iteration's terminate point in the absence of specific noise models and prior information [22]. Ahmed et al. used a CNN approach, where a denoising CNN learned the noise distribution in endoscopic images, thereby removing noise and enhancing clarity and contrast, and then the enhanced images were classified to aid physicians in disease diagnosis [23]. **Table 3** summarizes some common denoising methods.

Image deblurring

Capsule endoscopy is a type of endoscopy that is particularly prone to motion blur. Factors such as camera movement during the procedure and its relatively small field of view contribute to the reduced quality of capsule endoscopy images. Consequently, these images exhibit motion blur, overexposure, and underexposure, all of which hinder subsequent texture analysis and lesion identification. Traditional deblurring methods primarily focus on image blur models and utilize known blur kernels for deconvolution operations to obtain sharp images, resulting in predominantly non-blind deblurring methods. Single-image deblurring methods can estimate either a uniform blur kernel or a spatially varying blur kernel for image deconvolution. Cho et al. argued that applying image deconvolution to video deblurring is problematic since some deconvolution artifacts may be further amplified by temporal factors and

Table 3. Common image denoising methods

Method	Keywords	Advantages	Disadvantages	Effect comparison
BM3D	Image denoising, block matching	Suitable for different types of noise	High computational complexity and poor performance for signal-to-noise ratio images	Compared with other methods, it performs better under the Gaussian noise effect, but can be generally applied for other types of noise.
NLM	Image denoising, non-local means	Better preservation of image details and edge information, with a certain degree of versatility	High computational complexity and poor performance for images with high noise levels	It performs better with Gaussian noise and pretzel noise, but maintains an average performance for other types of noise.
CNN	Image denoising, CNN	Suitable for various types of noise; good denoising effect	Requires a large amount of annotated data and high computational complexity.	Compared to traditional methods, deep learning-based methods have better denoising performance.
DnCNN	Deep learning, CNN	Fast training speed, good denoising effect, suitable for different types of noise	Requires a large amount of data for training and may be over-fitted.	Better result enhancement compared to traditional methods.
FFDNet	Grayscale images, noise removal	Better adaptability to different types of noise and better noise removal effect	Training takes a long time and requires a large amount of noisy data for training.	Compared to DnCNN, it performs better in the processing of different types of noise.
WGAN	Deep learning, GANs	Capable of generating more realistic images	Longer training time	Compared with traditional methods, WGAN performs better in noise removal and can reduce image distortion.

Note: BM3D, block-matching 3D; NLM, non-local mean; CNN, convolutional neural network; GAN, generative adversarial network; DnCNN, denoising convulsive neural network; FFDNet, fast and flexible denoising convolutional neural network; WGAN, Wasserstein generative adversarial network.

exaggerated in the video [24]. In endoscopic surgery, physicians need to diagnose and treat patients by observing their organs or tissues through the endoscope. However, the vibrations or movements of the endoscope during the surgical process often result in video blur, which affects the observation and diagnosis. Therefore, Peng et al. proposed a framework that can restore blurry frames by synthesizing image details from neighboring sharp frames [25]. They also introduced a non-parametric grid-based motion model to align sharp frames with blurry frames. By directly comparing blurry patches with the nearest matching sharp patches in the endoscopic images, the effectiveness of the algorithm was demonstrated, outputting clearer endoscopic images. Additionally, during endoscopic examinations, the use of biopsy tools can introduce various disturbances to endoscopic images, such as haze, noise, oversaturation, illumination disruptions, and fogging caused by changes of body temperature. Therefore, image defogging is also necessary to improve the visibility. Tchak et al. proposed a chromatic-based defogging method that simulates the formation process of haze in images [26]. They combined an adaptive dark channel prior approach with histogram equalization to eliminate foggy artifacts, restore the image, and enhance contrast and brightness. This approach improves image quality in endoscopic surgery without using additional suction devices. Wang et al. presented a method using recursive shadow suppression filters to reduce bubble frames through detecting bubbles in capsule endoscopy videos, thereby enhancing the visualization of gastrointestinal lesions [27].

Traditional deblurring methods, mostly based on fixed blur kernels, are unable to remove non-uniform motion blur. Moreover, these traditional algorithms often require significant processing time, making them impractical for real-world applications. In recent years, CNNs have been widely utilized in various image restoration tasks due to their efficiency and high function approximation capabilities. Commonly used network architectures include CNNs and GANs. In 2017, Nah et al. introduced a multi-scale deblurring algorithm based on CNNs [28]. By downscaling the images from low-resolution to high-resolution, this research achieved the

Table 4. Common image deblurring methods

Method	Keywords	Advantages	Disadvantages	Effect comparison
Wiener filters	Statistic, filtering	Simple and computationally efficient	Not applicable to complex blur and noise, limited effect	Weak effect, poor effect on complex blurs
Total variation	Edge-holding, regularization	Preserves image detail, suitable for complex blurs	Insufficient smooth details and long processing time	Better retention of image details, but may result in overly strong smoothing effects
Multi-scale fuzzy processing	Image pyramids, multi-scale	Capable of handling different levels of blur, with adjustable effects	High computational complexity, may lead to over-enhancement	Better results, can adapt to different levels of blur
CNN-based approach	Deep learning, CNNs	Capable of learning complex image features to provide better image detail recovery	Requires a large number of annotated image pairs for training and longer training time	Good recovery of image details and textures
DebulrGAN	Deep learning, end-to-end training	Direct mapping from blurred images to clear images	Requires a large number of annotated image pairs for training and longer training time	Ability to recover a clear image directly from a blurred image

Note: CNN, convolutional neural network; GAN, generative adversarial network.

removal of various types of blurs. Building upon this work, Shi et al. proposed a gradient-guided GAN that employed the Res2net structure as the backbone, consisting of image and gradient branches [29]. They designed a lightweight pre-processing network to correct excessive blur and improve training efficiency. Their results demonstrated significant improvements in visual restoration with no noticeable artifacts or structural deformations. However, the computational cost of this network is high, leading to significant training overhead. Lin et al. also presented an end-to-end encoder-decoder network architecture to remove blood blur [30]. They incorporated residual learning and cascaded learning methods to alleviate the insufficient clarity and lack of details when reconstructing issue images affected by blood occlusion. The aim was to enhance the visualization quality of endoscopic images impacted by blood contamination, so as to improve the image reading experience of physicians, aiding in more accurate diagnosis. The Vector Quantized-Variational AutoEncoder (VQ-VAE) model was selected as the backbone network, and a GAN was employed to train a dataset for generating blood blur, effectively reducing the cost of dataset collection. Deblurring is often combined with super-resolution enhancement algorithms. Yang et al. proposed an end-to-end endoscopic image deblurring and super-resolution algorithm, which consists of three components: a deblurring network, a super-resolution network, and a feature fusion network [31]. This approach significantly reduces computational costs during neural network training, overcoming issues related to insufficient training data and slow processing speeds. It enables real-time deep imprinting of endoscopic imaging. Additionally, the deblurring algorithm improves image clarity, and the super-resolution algorithm enhances the restoration of image details, which is crucial for observing subtle lesions or structural features. **Table 4** summarizes some common deblurring methods.

Image enhancement

Medical image enhancement techniques play a crucial role in medical image processing and serve as important preprocessing step for identification and detection algorithms in medical image analysis. Traditional medical image enhancement algorithms can be mainly categorized into two types: spatial domain-based and frequency domain-based methods, with most studies focusing on spatial domain-based approaches. Hai et al. proposed an image enhancement method based on contrast limited adaptive histogram equalization for enhancing stereoscopic endoscopic 3D images [32]. This method involves dividing the image into nearly equal-sized non-overlapping regions to obtain histogram clip limits. Then, the histogram of each region is redistributed and equalized through histogram equalization. A reference image is determined by searching conditions, and global histogram matching is employed to

correct color discrepancies between the two stereoscopic views. This method effectively enhances image details, eliminates color biases, and addresses issues such as low contrast and blurry details in stereoscopic endoscopic 3D images, which may affect accurate lesion identification and assessment by physicians. It improves the visual quality and discernibility of the images. However, the method has a higher computational complexity and slightly larger computational cost. Sato et al. introduced a texture and color enhancement imaging technique to enhance the visual quality and discernibility of endoscopic images [33]. This method utilizes texture enhancement algorithms to enhance visual and structural information in the images, thereby making the lesion areas more clearly visible. In addition to noise caused by devices, uneven illumination can also affect the observation and diagnosis of lesions. Zhang et al. proposed an endoscopic image enhancement method based on an improved weighted guided filter [34]. By introducing parameters such as gradient threshold, luminance threshold, and blur coefficient, the method can enhance contrast in images containing lesions, thereby improving the detection rate of lesions. Wu et al. presented a synthesis algorithm based on Retinex and Pseudo-HDR [35]. The former corrects uneven illumination issues and improves contrast and brightness in images. The latter is used for synthesizing images with a wide dynamic range. This algorithm demonstrates good practicality and can be easily integrated and applied in actual endoscopic scenarios.

In the field of medical image processing, deep neural network technology has garnered significant interest from researchers due to its remarkable effectiveness. In recent years, researchers have focused on applying deep learning networks to enhance the quality of endoscopic images. To improve the visual quality and discernibility of endoscopic images, An et al. proposed a Retinex-Net network based on the Retinex theory, which employs image decomposition techniques to decompose the original endoscopic image into different frequency components, such as low-frequency and high-frequency components [36]. By enhancing the different components, the algorithm can enhance the contrast and details of the image and reduce the impact of image blur. Moreover, the reflection from the endoscope's mirror surface can also affect visual perception. Shen et al. proposed a content-aware mirror reflection suppression approach based on adaptive image restoration and neural networks, which effectively mitigates the influence of mirror reflections on the images [37]. Gomez et al. introduced a method for low-light image enhancement of high-speed endoscopic videos using CNNs [38]. In clinical examinations, inadequate illumination is often encountered in endoscopic imaging due to anatomical restrictions of the throat and technical limitations of recording devices. This method helps clinicians and researchers deal with images that frequently suffer from insufficient lighting, making clinical analysis more manageable. The lack of medical ground truth images for training has been a major bottleneck in deep learning-based medical imaging processing, mainly due to the difficulty in collecting original datasets. Unsupervised learning methods eliminate the need for ground truth medical images during training. Huang et al. studied a deep unsupervised endoscopic image enhancement method based on multi-image fusion [39]. By employing unsupervised mapping and deep learning networks, high-quality endoscopic images can be obtained from images with poor lighting conditions, low contrast, and color deviations without the need for real data, thus reducing the workload of data collection. Li et al. introduced a novel physics-based semi-supervised learning framework for endoscopic image enhancement [40]. They integrated a previous physical imaging defect model with the CycleGAN framework to address issues such as image haze, uneven lighting, and color deviations. This approach facilitates detail preservation and color restoration, achieving outstanding performance. Notably, the paper proposed a transfer learning network for generating datasets, which significantly improves network performance on small training datasets. **Table 5** provides a summary of some common image enhancement methods.

Image segmentation

Endoscopic image segmentation is one of the key tasks in the field of medical image processing. It plays a crucial role in endoscopic diagnosis and treatment. The purpose of image segmentation is to accurately separate different tissue structures, lesion areas, or regions of interest within the endoscopic images. Accurate image segmentation can assist physicians in precisely locating and identifying abnormalities, as well as facilitating accurate diagnosis, treatment planning, and surgical guidance. Due to factors such as lighting variations, noise, and diverse morphological appearances commonly present in endoscopic images, researchers have proposed numerous methods over the past few decades to address these challenges.

Early endoscopic image segmentation methods

Table 5. Common image enhancement methods

Method	Keyword	Advantage	Disadvantage	Effect comparison
Histogram equalization	Histogram, contrast enhancement	Enhance contrast by redistributing image pixel values	May cause excessive global contrast enhancement or distortion	Can enhance the contrast and details of an image, but may produce excessive enhancement or distortion
Fourier transform	Fourier spectrum, filtering	Enhance the edges and details of images by frequency domain filtering, capable of filtering out noise and blur	May cause spectral distortion or ringing phenomena, and may have limited effect on complex images and noise	Can enhance image edges and details, but may produce spectral distortion and ringing
Spatial domain filtering	Filtering, spatial domain processing	Specific image features can be processed by filters that can enhance image details and textures, and suppress noise	Parameters need to be adjusted for different image types and noise types, which may result in blurring or distortion of image details	Filtering and enhancement can be performed for different features, but the effect is limited in more complex cases.
Based on GANs	GAN, generators, discriminators	Can generate realistic images and maintain authenticity; can learn image features adaptively to provide better images	Requires large amount of training data and computational resources, with long training time and possible pattern collapse or unstable generation	Provides high-level image enhancement and restoration effects to produce realistic images
Based on CNN	CNN, super resolution	Capable of reconstructing low-resolution images into high-resolution images, can restore details and clarity for a wide range of image types and resolutions	Longer training time, requires large amount of training data, may have limited effect for complex images	Ability to reconstruct low-resolution images into high-resolution images and restore image details

Note: GAN, generative adversarial network; CNN, convolutional neural network.

primarily relied on traditional image processing techniques such as thresholding, edge detection, and morphological operations. The datasets used for traditional segmentation tasks were manually annotated by physicians. Liu et al. proposed a hue-texture embedded region model for narrow-band imaging-enhanced endoscopic image segmentation, which adjusts the hue component of the image to highlight the characteristic colors of structures such as vessels and lesions [41]. By combining color information and texture features, this approach achieves better segmentation of structures and lesion areas within the image. In the field of gastroenterology, segmentation of endoscopic images for detecting digestive ulcers has emerged as a novel domain in medical image processing. Rajivegandhi et al. introduced a collaborative and efficient algorithm for digestive ulcer detection based on watershed transformation, thresholding, and morphological operators [42]. This algorithm successfully detects ulcers, opening a new avenue for advancing gastroscopic image processing techniques and clinical applications.

With the rapid development of computer vision and machine learning, significant progress has been made in endoscopic segmentation. Machine learning and deep learning-based methods are gradually being proposed for handling complex endoscopic images. Endoscopic segmentation is primarily applied to disease detection and lesion segmentation. Jha et al. proposed a real-time polyp segmentation method based on NanoNet for both capsule endoscopy videos and colonoscopy videos, greatly improving detection efficiency [43]. Laves et al. presented a CNN-based semantic segmentation method and dataset for laryngoscopic images, utilizing four methods (SegNet, UNet, ENet, and ErfNet) and evaluating their accuracy

Table 6. Common image segmentation methods

Method	Keywords	Advantages	Disadvantages	Effect comparison
Segmentation based on thresholds	Threshold, pixel classification	Simple, intuitive, and easy to implement for situations where there is an obvious difference in pixel values between the apparent target and the background	Sensitive to light changes, noise and other factors, requiring the pre-setting of set suitable thresholds	Suitable for image segmentation where there is an obvious difference in pixel values between the apparent target and the background
Segmentation based on regional growth	Regional growth	Able to automatically identify continuous regions, good segmentation for regions with high similarity	Poor segmentation for regions with blurred target boundaries or low similarity, sensitive to light changes and noise	Suitable for region segmentation tasks with a high degree of similarity
Segmentation based on edge detection	Edge detection, contour extraction	Ability to accurately extract the outline of the target, good for images with clear edges	Poor image segmentation for blurred or complex backgrounds, sensitive to noise	Suitable for image segmentation where accurate target contours need to be extracted
FCN	CNNs	Ability to learn semantic information of images, better for targets of different scales	May be less effective in the case of fine targets and blurred edges	Provide better semantic segmentation results. Applicable to overall target segmentation
U-net	CNN, encoder, decoder	With encoding and decoding structure, capable of capturing multi-scale contextual information, good re-edge positioning and detail retention	Possible problems for datasets with unbalanced categories	Provide better target boundary segmentation and detail retention, suitable for medical image segmentation
Mask R-CNN	Target detection, instance segmentation	Combines target detection and segmentation tasks to accurately locate and segment multiple target instances, works well for large variations in target shape and size	High computational complexity, requiring more computational resources, may be less effective for complex backgrounds and overlapping targets	Provides accurate target instance segmentation results for multi-target localization and segmentation

Note: FCN, fully convolutional network; CNN, convolutional neural network.

using intersection over the union [44]. Lwasa et al. proposed a deep learning-based method for automatic segmentation of pancreatic tumors in contrast-enhanced endoscopic ultrasound image videos, which has the potential to become a powerful tool for early diagnosis and treatment of pancreatic tumors [45]. However, these methods require manual annotation of datasets, which is time-consuming and labor-intensive. Subsequently, unsupervised learning has gained attention, particularly in the context of endoscopic surgery. Sasmal et al. proposed an unsupervised image segmentation method for segmenting polyps in endoscopic images [46]. Mahmood et al. introduced an adversarial training-based reverse domain adaptation method, which uses unlabeled synthetic data to transform real data into a synthetically similar representation while preserving clinically relevant diagnostic features through regularization [47]. They generated a large dataset consisting of synthetically generated endoscopic images with annotated ground truth from normal colonoscopy images. **Table 6** summarizes some common segmentation methods.

Discussions and challenges

Currently, the integration of endoscopy and image processing technology has become a hot research topic in the medical field. An increasing number of researchers are exploring how to apply AI image processing techniques to the processing and analysis of endoscopic images. In existing studies, endoscopy combined with AI is mainly applied to lesion identification and classification, surgical assistance, training and education, pathology prediction, intelligent diagnosis, and therapy.

Although deep learning-based models have continued to dominate medical image processing, there are still numerous challenges associated with deep modeling. These challenges

limit the application and implementation of new methods in clinical practice, but also provide researchers with new opportunities. The following challenges are proposed:

Data scarcity and annotation: Creating annotated datasets is a difficult and time-consuming task. Therefore, it is crucial to design deep learning models that can effectively utilize both labeled and unlabeled data to generate training datasets. Additionally, due to privacy and ethical concerns, it is challenging to collect large-scale medical data. Hence, developing data augmentation models that extract key information from limited samples to form extensive "realistic" datasets is essential.

Real-time requirements: In clinical practice, real-time processing and analysis of endoscopic images are critical for prompt decision-making and treatment. However, deep learning methods often require long training and inference times, which cannot meet the real-time processing demands of clinical endoscopy. Therefore, a challenge lies in how to improve the speed of deep learning models while ensuring the accuracy of the analysis.

Data security: Endoscopic images contain sensitive patient information, making data privacy and security crucial considerations during model training.

Perspectives

This paper primarily presents the clinical application of image processing techniques in endoscopic imaging. Tracheal intubation is a primary method for airway management during general anesthesia and is also one of the emergency measures for critically ill patients. Direct laryngoscopy or video laryngoscopy is commonly used for oral/nasal tracheal intubation, with the latter offering a clearer field of view and higher intubation efficiency compared to the former. However, in certain special cases such as patients undergoing oral and maxillofacial surgery or emergency intubation, the presence of saliva, blood, or sputum in the oral pharynx can contaminate the video laryngoscope lens during the intubation process, obstructing the view of the glottis and posing safety risks during anesthesia. In this study, we propose to utilize deep learning-based image denoising techniques to address the issue of image blurring. By capturing video images of patients undergoing video laryngoscopy for tracheal intubation and generating a dataset of software-simulated noisy images, the aim is to develop a deep learning algorithm for denoising these images. The effectiveness of the program should be validated using real blurry images, with the ultimate goal of assisting anesthesiologists in tracheal intubation procedures, improving intubation efficiency, and reducing complications. The deep learning model will be built based on the Transformer network to restore the blur caused by blood, secretions, and other contaminants in endoscopic images. Additionally, a novel network is also being explored to address the problem of laryngeal structure recognition. Due to the complexity of the laryngeal structure, it is crucial to employ a segmentation approach to accurately delineate the major laryngeal regions during the intubation process. This approach aims to enhance the accuracy and speed of intubation by facilitating the identification of laryngeal structures, particularly for less experienced clinicians.

References

[1] Talo M, Yildirim O, Baloglu UB, et al. Convolutional neural networks for multi-class brain disease detection using MRI images. Comput Med Imaging Graph 2019;78:101673.

[2] Gupta N, Gupta D, Khanna A, et al. Evolutionary algorithms for automatic lung disease detection. Measurement 2019;140:590-608.

[3] Xue Y, Xu T, Zhang H, et al. SegAN: Adversarial Network with Multi-scale L(1) Loss for Medical Image Segmentation. Neuroinformatics 2018;16(3-4):383-392.

[4] Schlegl T, Seeböck P, Waldstein SM, et al. Unsupervised Anomaly Detection with Generative Adversarial Networks to Guide Marker Discovery. Inf Process Med Imaging 2017;146-157.

[5] Hu K, Jin J, Zheng F, et al. Overview of behavior recognition based on deep learning. Artif Intell Rev 2023;56(3):1833-1865.

[6] Keysers D, Deselaers T, Gollan C, et al. Deformation models for image recognition. IEEE Trans Pattern Anal Mach Intell 2007;29(8):1422-1435.

[7] Liu J, Sun J, Wang S. Pattern Recognition: An overview. Int J Comput Sci Network Secur 2006;6(6):57-61.

[8] Neumann M, King D, Beltagy I, et al. ScispaCy: Fast and Robust Models for Biomedical Natural Language Processing. ArXiv 2019;abs/1902.07669.

[9] Otter DW, Medina JR, Kalita JK. A Survey of the Usages of Deep Learning for Natural Language Processing. IEEE Trans Neural Netw Learn Syst 2021;32(2):604-624.

[10] Qiu X, Sun T, Xu Y, et al. Pre-trained models for natural language processing: A survey. Sci China Technol Sci 2020;63(10):1872-1897.

[11] Afouras T, Chung JS, Senior A, et al. Deep

Audio-Visual Speech Recognition. IEEE Trans Pattern Anal Mach Intell 2022;44(12):8717-8727.

[12] Han W, Zhang Z, Zhang Y, et al. ContextNet: Improving Convolutional Neural Networks for Automatic Speech Recognition with Global Context. ArXiv 2020;abs/2005.03191.

[13] Li Z, Liu F, Yang W, et al. A Survey of Convolutional Neural Networks: Analysis, Applications, and Prospects. IEEE Trans Neural Netw Learn Syst 2022;33(12):6999-7019.

[14] Gopi VP, Palanisamy P, Niwas SI. Capsule Endoscopic Colour Image Denoising Using Complex Wavelet Transform. Wireless Networks and Computational Intelligence 2012;220-229.

[15] Patil R, Bhosale S. Medical Image Denoising using Wavelet Transform and Singular Value Decomposition. Comput Sci 2021.

[16] Qu J, Jin K, Wang M, et al. Real-Time Stripe Noise Removal Method for Endoscope Image. 2021 IEEE 4th International Conference on Electronics Technology (ICET) 2021;865-870.

[17] Ning Cy, Liu Sf, Qu M. Research on removing noise in medical image based on median filter method. 2009 IEEE International Symposium on IT in Medicine & Education 2009;384-388.

[18] Magdalena R, Rahim T, Pratama IPAE, et al. RGB-Based Compressed Medical Imaging Using Sparsity Averaging Reweighted Analysis for Wireless Capsule Endoscopy Images. IEEE Access 2021;9:147091-147101.

[19] Zhang K, Zuo W, Chen Y, et al. Beyond a Gaussian Denoiser: Residual Learning of Deep CNN for Image Denoising. IEEE Trans Image Process 2017;26(7):3142-3155.

[20] Izadi S, Mirikharaji Z, Zhao M, et al. WhiteNNer-Blind Image Denoising via Noise Whiteness Priors. 2019 IEEE/CVF International Conference on Computer Vision Workshop (ICCVW) 2019;476-484.

[21] Zou S, Long M, Wang X, et al. A CNN-Based Blind Denoising Method for Endoscopic Images. 2019 IEEE Biomedical Circuits and Systems Conference (BioCAS) 2019;1-4.

[22] Ulyanov D, Vedaldi A, Lempitsky V. Deep Image Prior. International Journal of Comput Vision 2020;128(7):1867-1888.

[23] Ahmed A. Classification of Gastrointestinal Images Based on Transfer Learning and Denoising Convolutional Neural Networks. Proceedings of International Conference on Data Science and Applications 2022;631-639.

[24] Cho S, Wang J, Lee S. Video deblurring for hand-held cameras using patch-based synthesis. ACM Trans Graph 2012;31(4):Article 64.

[25] Peng L, Liu S, Xie D, et al. Endoscopic video deblurring via synthesis. 2017 IEEE Visual Communications and Image Processing (VCIP) 2017;1-4.

[26] Tchaka K, Pawar VM, Stoyanov D. Chromaticity based smoke removal in endoscopic images. Med Imaging 2017.

[27] Wang Q, Pan N, Xiong W, et al. Reduction of bubble-like frames using a RSS filter in wireless capsule endoscopy video. Opt Laser Technol 2019;110:152-157.

[28] Nah S, Kim TH, Lee KM. Deep Multi-scale Convolutional Neural Network for Dynamic Scene Deblurring. 2017 IEEE Conference on Computer Vision and Pattern Recognition (CVPR) 2017;257-265.

[29] Huang Z, Shi Z. Image Caption Combined with GAN Training Method. Intelligent Information Processing X 2020;310-316.

[30] Lin J, Jiang M, Pang Y, et al. A desmoking algorithm for endoscopic images based on improved U-Net model. Concurr Comput 2021;33(22):e6320.

[31] Yang X, Chen Y, Tao R, et al. Endoscopic Image Deblurring and Super-Resolution Reconstruction Based on Deep Learning. 2020 International Conference on Artificial Intelligence and Computer Engineering (ICAICE) 2020;168-172.

[32] Hai Y, Li L, Gu J. Image enhancement based on contrast limited adaptive histogram equalization for 3D images of stereoscopic endoscopy. 2015 IEEE International Conference on Information and Automation 2015;668-672.

[33] Sato T. TXI: Texture and Color Enhancement Imaging for Endoscopic Image Enhancement. J Healthc Eng 2021;2021:5518948.

[34] Zhang G, Lin J, Cao E-H, et al. A Medical Endoscope Image Enhancement Method Based on Improved Weighted Guided Filtering. Mathematics 2022.

[35] Wu JCH, Lin GS, Hsu HT, et al. Quality enhancement based on retinex and pseudo-HDR synthesis algorithms for endoscopic images. 2013 Visual Communications and Image Processing (VCIP) 2013;1-5.

[36] An Z, Xu C, Qian K, et al. EIEN: Endoscopic Image Enhancement Network Based on Retinex Theory. Sensors (Basel, Switzerland) 2022;22(14):5464.

[37] Shen DF, Guo JJ, Lin GS, et al. Content-aware specular reflection suppression based on adaptive image inpainting and neural network for endoscopic images. Comput Methods Programs Biomed 2020;192:105414.

[38] Gómez P, Semmler M, Schützenberger A, et al. Low-light image enhancement of high-speed endoscopic videos using a convolutional neural network. Med Biol Eng Comput 2019;57(7):1451-1463.

[39] Huang D, Liu J, Zhou S, et al. Deep unsupervised endoscopic image enhancement based

on multi-image fusion. Comput Methods Programs Biomed 2022;221:106800.

[40] Li W, Fan J, Li Y, et al. Endoscopy image enhancement method by generalized imaging defect models based adversarial training. Phys Med Biol 2022;67(9):095016.

[41] Liu X, Wang C, Bai J, et al. Hue-texture-embedded region-based model for magnifying endoscopy with narrow-band imaging image segmentation based on visual features. Comput Methods Programs Biomed 2017;145:53-66.

[42] Rajivegandhi C, Shree NSD, Khan S, et al. Detection of peptic ulcers based on thresholding and watershed segmentation. 2015 3rd International Conference on Signal Processing, Communication and Networking (ICSCN) 2015;1-5.

[43] Jha D, Tomar NK, Ali S, et al. NanoNet: Real-Time Polyp Segmentation in Video Capsule Endoscopy and Colonoscopy. 2021 IEEE 34th International Symposium on Computer-Based Medical Systems (CBMS) 2021;37-43.

[44] Laves MH, Bicker J, Kahrs LA, et al. A dataset of laryngeal endoscopic images with comparative study on convolution neural network-based semantic segmentation. Int J Comput Assist Radiol Surg 2019;14(3):483-492.

[45] Iwasa Y, Iwashita T, Takeuchi Y, et al. Automatic Segmentation of Pancreatic Tumors Using Deep Learning on a Video Image of Contrast-Enhanced Endoscopic Ultrasound. J Clin Med 2021;10(16).

[46] Sasmal P, Bhuyan MK, Dutta S, et al. An unsupervised approach of colonic polyp segmentation using adaptive markov random fields. Pattern Recognit Lett 2022;154:7-15.

[47] Mahmood F, Chen R, Durr NJ. Unsupervised Reverse Domain Adaptation for Synthetic Medical Images via Adversarial Training. IEEE Trans Med Imaging 2018;37(12):2572-2581.

Perioperative Precision Medicine
eISSN: 2957-5443

Zentime

Review Article https://doi.org/10.61189/803479emewvv

Medical image processing using graph convolutional networks: A review

Long Liu[1], Xiaobo Zhu[3], Jinjing Wu[1], Qianyuan Hu[1], Haipo Cui[1], Zhanheng Chen[2], Tianying Xu[2]

[1]School of Health Science and Engineering, University of Shanghai for Science and Technology, Shanghai 200093, China. [2]School of Anesthesiology, Second Military Medical University/Naval Medical University, Shanghai 200433, China. [3]College of Electronic and Information Engineering, Tongji University, Shanghai 201804, China.

Acknowledgments: This work was supported by the National Natural Science Foundation of China (62002297, 62073225, 61836005), the Science and Technology Commission of Shanghai Municipality (20XD1434400), the Talent Development Fund of Shanghai (2020075), the Medical-Engineering Cross Fund of Shanghai Jiao Tong University (YG2022QN043), and the Guangxi Science and Technology Base and Talent Special Project (2021AC19394). The authors would like to thank all the guest editors and anonymous reviewers for their constructive comments.

Declaration of conflicts of interests: None.

Received July 19, 2023; Accepted September 7, 2023; Published September 30, 2023

Highlights

- The development history of convolutional neural networks and the transition to graph convolutional networks are introduced, as well as the evolution of network layers.
- Graph convolutional networks have been widely demonstrated to be applicable in various perioperative medical image processing scenarios.
- This is the first comprehensive review of the applications of graph convolutional networks in image segmentation, image reconstruction, disease prediction, lesion detection and localization, disease classification and diagnosis, and surgical interventions.

Abstract

Deep learning, especially graph convolutional networks (GCNs), has been widely applied in various scenarios. Particularly in the field of medical image processing, the research on GCNs have continued to make breakthroughs and has been successfully applied to various tasks, such as medical image segmentation, as well as disease detection, localization, classification and diagnosis. GCNs have demonstrated the capacity to autonomously learn latent disease features from vast medical image datasets. Their potential value and enhanced capabilities in prediction, analysis, and decision-making in perioperative medical imaging have become evident. In recent years, GCNs have rapidly emerged as a research focus in the realm of medical image analysis. First, this review provides a concise overview of the development from convolutional neural networks to GCNs, delineating their algorithmic foundations and network structures. Subsequently, the diverse applications of GCNs in perioperative medical image processing are extensively reviewed, including medical image segmentation, image reconstruction, disease prediction, lesion detection and localization, disease classification and diagnosis, and surgical intervention. Finally, this review discusses the prevailing challenges and offers insights into future research directions for the utilization of GCN methods in the medical field.

Keywords: Deep learning, graph convolutional networks, medical image processing, perioperative medical applications

Introduction

In recent years, the rapid development of the big data has led to the swift emergence of artificial intelligence technologies. Specifically, machine learning and deep learning have made significant strides in various fields, such as speech, image, computer vision, and natural language processing. In the field of medical image mining, the traditional approach reliant on manual feature extraction by experienced experts has been gradually replaced by end-to-

Address correspondence to: Haipo Cui, School of Health Science and Engineering, University of Shanghai for Science and Technology, NO.334, Jungong Road, Shanghai 200093, China. Tel: +86-21-55271290, E-mail: h_b_cui@163.com; **Zhanheng Chen**, School of Anesthesiology, Second Military Medical University/Naval Medical University, No.800 Xiangyin Road, Shanghai 200433, China. Tel: +86 21 81872034, E-mail: chenzhanheng17@mails. ucas.ac.cn; **Tianying Xu**, School of Anesthesiology, Second Military Medical University/Naval Medical University, No.800 Xiangyin Road, Shanghai 200433, China. Tel: +86 21 81872029, E-mail: xty7910@163.com.

end deep learning technologies, represented by convolutional neural networks (CNNs). A series of groundbreaking research achievements have been made in areas like image classification, object detection,and image segmentation, showcasing the powerful feature learning and classification capabilities of CNNs [1-3]. These achievements have garnered widespread attention and pose significant values for research analysis.

The origins of graph convolutional networks (GCNs) can be traced back to 1943 when the renowned psychologist McCulloch and the mathematician Warren proposed the concept of neurons [4]. They realized that a simplified neuron model could be represented using simple addition and threshold processing. Inspired by this, in 1958, psychologist Rosenblatt constructed the first device, called the "perceptron" which truly applied these principles [5]. At that time, the perceptron was simulated on computers and demonstrated the ability to classify simple graphic data, marking the first successful experiment after the proposal of neurons. In 1985, Rumelhart proposed the error backpropagation algorithm, which facilitated the exchange of weights among multiple hidden layers and addressed the issue of network parameterization between these layers [6]. However, this algorithm suffered from slow computation speed. In 1989, LeCun introduced the term "convolution" in the early version of LeNet, and subsequently, LeCun et al. introduced the classic LeNet-5 model in 1998, which was the first successful application of a CNN to handwritten digit recognition [7].

As research progressed, although CNNs have advantages such as parameter sharing and automatic feature extraction, they have clear limitations when dealing with graph-rich data. This often leads to the loss of critical structural information, and their results are heavily depending on the preprocessing of the graph data. To address these challenges, the introduction of graph neural networks (GNNs) allows the data processing process to be directly built on graph data. This not only extends existing neural network models but also improves the accuracy of graph data processing. In 2009, Scarselli established the theoretical foundation for GNNs [8]. Scarselli and Micheli further inherited and developed GNNs algorithms, making certain improvements. In the early stages, GNNs primarily relied on recurrent neural networks as the main framework, generating vector representations for each node through simple feature mapping and node aggregation, but they could not effectively handle real-world complex and diverse graph data. To address this, Bruna et al. proposed applying CNNs to graphs and, through clever transformations of the convolution operator, introduced frequency-based and spatial-based GCNs [9]. In 2015, Defferrard et al. proposed using Chebyshev polynomials to approximate graph convolutions, enabling efficient computation of convolutions in the frequency domain [10]. They also introduced regularization techniques to improve the model performance, which is a critical milestone in the development of GCNs. In 2016, Kipf et al. proposed the first-generation GCN, which utilized the graph Laplacian matrix and learned node representations through convolutional operations [11]. This model has good performance and interpretability in handing single-layer graph data. With the introduction of GCNs, researchers continuously attempted to improve the performance of the networks and proposed various variants, including GraphSAGE, graph attention network, and others. These variants can handle multi-layer and multi-type graph data, offering better performance and flexibility [12, 13].

With the continuous advancement of GCNs, they have been synergistically integrated into the perioperative medical domain. Promising outcomes have been achieved in perioperative medical image processing realms, encompassing medical image segmentation, lesion detection and localization, medical image classification and diagnosis, as well as disease prognosis. Since 2000, research related to GCNs has been experiencing a significant surge in the Web of Science database. A total of 5,183 papers on this topic have been published during this period. The number of papers published in 2016 was 78, which increased to 1,825 in 2022. Among these papers, 1,121 papers report the application of GCNs in the field of medicine, demonstrating that research on medical applications based on GCNs has become another research hotspot following the usage of CNNs. This review will commence its narrative with the structural process outlined in **Figure 1**.

Fundamentals of GCN algorithm

Concepts and definitions

Graph symbols and definitions

A graph is made up of nodes and the edges connecting them, usually denoted as *G= (V, E)*, where $V = \{v_1, v_1, \ldots v_n\}$ represents the set of

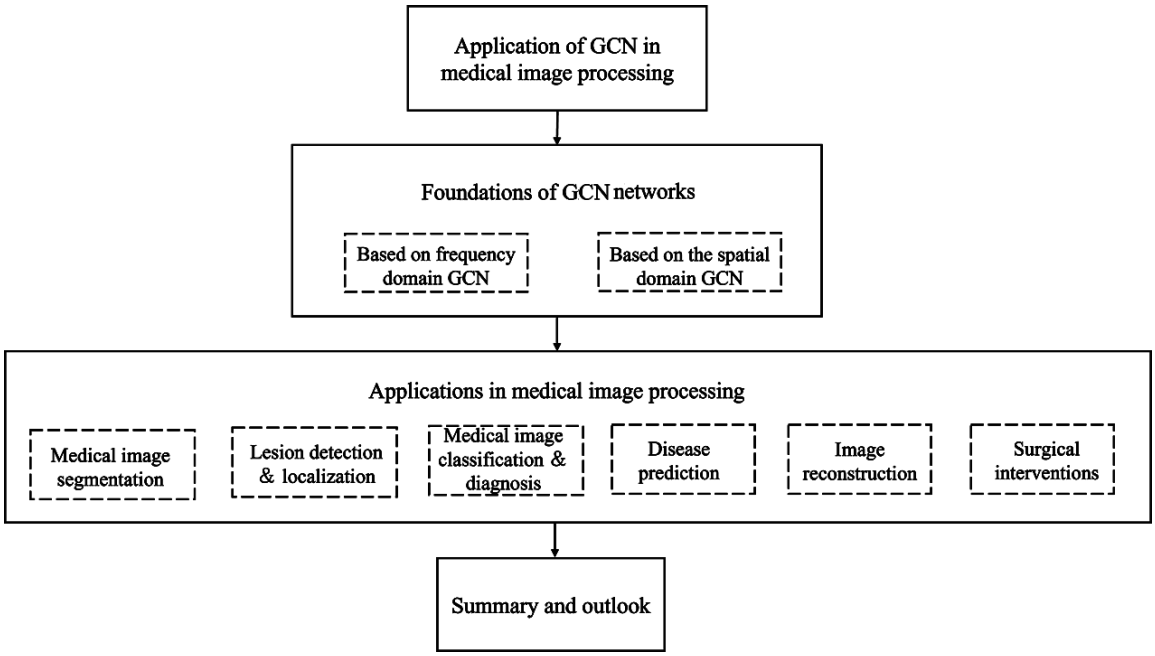

Figure 1. Structure of review. GCN, graph convolutional network.

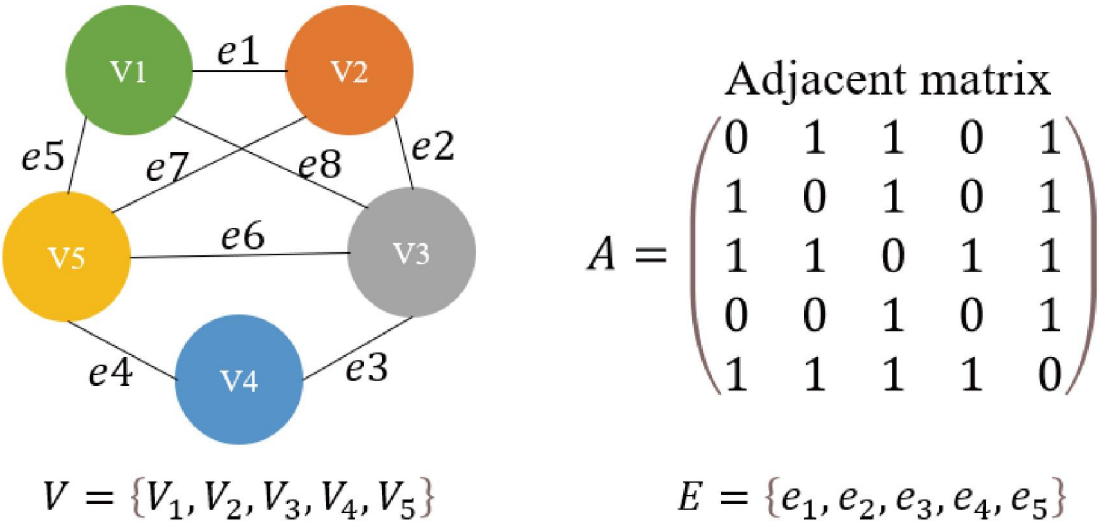

Figure 2. Undirected graphs and adjacency matrices.

nodes. The generic representation of a graph is a five-tuple *G (V, E, A, X, D)*, where *A* is the adjacency matrix, represented as a square matrix of $A^{N\times N}$. $X^{N\times F}$denotes the feature matrix of the nodes, and $D^{N\times N}$ represents the degree matrix. *N* and *F* represent the number of nodes and the feature dimension of the nodes, respectively. An undirected graph structure containing 5 nodes and 8 edges as well as its adjacency matrix are shown in **Figure 2**.

A combined Laplace matrix, which includes both a diagonal matrix and an adjacency matrix, is represented as shown in equation (1):

$$L = D - A$$

where D is the diagonal matrix, and A is the adjacency matrix, which contains non-zero elements only at the central node and the nodes connected at first order, while the rest are 0.

Types of graphs

The types of graphs have different classifications and interpretations in various fields. Graphs can be classified into directed graphs and undirected graphs based on the directionality of their edges. A weighted graph or an unweighted graph is determined by whether the edges of a graph have weights. A connected graph or a disconnected graph is determined by the existence of a path between any two nodes in a graph. They can also be classified as a labeled graph or an unlabeled graph according

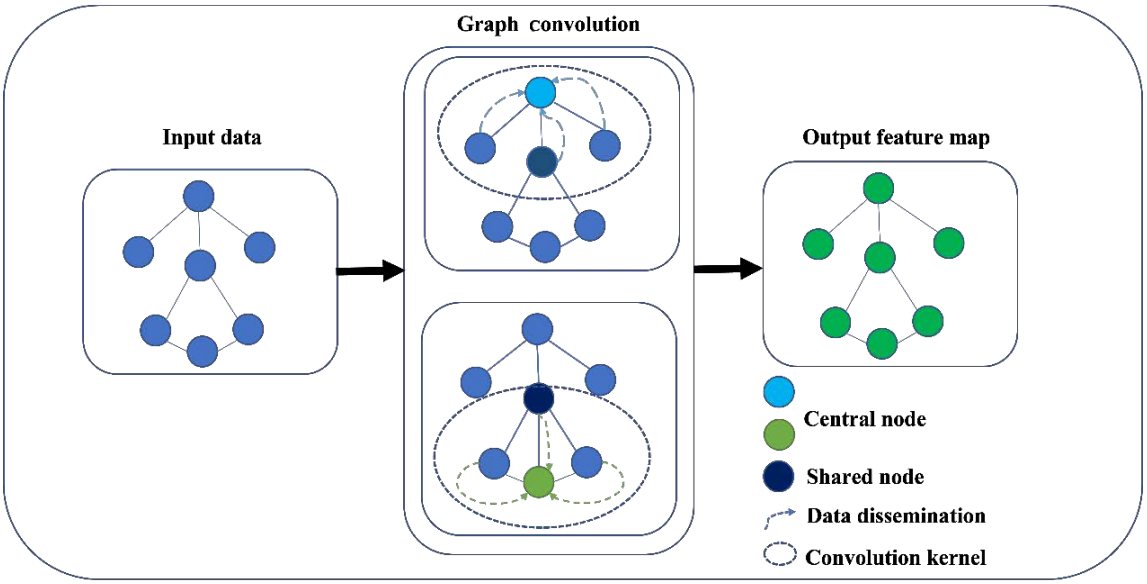

Figure 3. Graph convolutional network structure diagram.

to whether the nodes or edges of a graph have attributes.

GCNs

Framework for information diffusion

Information diffusion involves iteratively updating and training the parameters of graph convolutional layers. This mainly includes initializing node features, aggregating neighbors, transforming features, updating node features, and outputting prediction results. The GCN architecture for information diffusion is illustrated in **Figure 3**, while the information diffusion framework is represented by Equation (2):

$$H^{l+1} = f(H^l, A)$$

where A is the adjacency matrix, and H^l is the feature information output of the $(l+1)$th layer of the GCN. By normalizing and applying an activation function to A, the forward propagation of graph feature information can be achieved. The basic process of message propagation is shown in Equation (3):

$$f(H^l, A) = \sigma(\widetilde{D}^{-\frac{1}{2}}\widetilde{A}\widetilde{D}^{-\frac{1}{2}}H^l W^l)$$

where $\widetilde{A} = A + I$ (I is the unit matrix), $\widetilde{A}$ in $\widetilde{D} = \sum_j \widetilde{A}_{i,j}$ is the normalized degree matrix, W^l is the matrix of parameters to be trained in the model, σ is the activation function.

Based on the aforementioned diffusion framework, following the operational paradigm of GCNs, there are two types of graph convolutions: spectral-based and spatial-based.

Graph convolution

The purpose of the graph convolutional layer is to extract features from the input information. The convolutional layer consists of multiple convolutional units, and the parameters of each unit are optimized through the backpropagation algorithm. Based on the message propagation framework described in Section Framework for information diffusion, there are two types of data processing methods for graph convolution: spectral-based graph convolution and spatial-based graph convolution.

Spectral-based graph convolution is a commonly used method, which utilizes the eigenvalues and eigenvectors of the graph Laplacian matrix for signal propagation and transformation in the graph. It addresses the issue of lacking translational invariance in node domain data, preventing conventional convolutions. Common graph filters include low-pass filters and high-pass filters. Low-pass filters preserve low-frequency signals while suppressing high-frequency noise and details, making them suitable for smoothing and capturing global structural information. High-pass filters enhance high-frequency signals, highlighting details and edge information, making them suitable for edge detection and local structures. As spectral-based graph convolution methods have gained wide applications in graph signal processing and GNNs, there has been an increasing number of improvements and variants in the spectral domain. **Table 1** summarizes the spectral-based

Table 1. Spectral-based convolution methods and their variants

Presenters	Year	Model	Salient points or key elements
Bruna et al. [9]	2013	Spectral CNN	The first spectral-based graph convolution method
Defferrard et al. [10]	2016	ChebNet	Convolution kernel with locality
Kipf et al. [11]	2016	First-order ChebNet	Small parameter count
Li et al. [14]	2017	AGCN	Parameterizing the Laplacian matrix, introducing an adaptive spectral graph convolution algorithm
Xu et al. [15]	2019	GWNN	Model interpretability
Chiang et al. [16]	2019	Cluster-GWCN	Handling large-scale data
Jiang et al. [17]	2019	GLCN	Adaptive Learning
Derr et al. [18]	2020	DS-SGS-GCN	Semi-supervised graph convolution integrated with symbolic theory
Wang et al. [19]	2020	AM-GCN	Enhanced feature extraction capability
Fu et al. [20]	2021	GpLCN	Applying the Laplacian matrix to spectral graph filters
Zhu et al. [21]	2021	S2GCN	Effectively addressing the over-smoothing issue
Bo et al. [22]	2021	FAGCN	Effectively addressing the over-smoothing issue
Wang et al. [23]	2021	Bi-GCN	Reducing the number of parameters
Bo et al. [24]	2023	Specformer	Trainable convolutional kernel

Note: CNN, convolutional neural network; GCN, graph convolutional network; AGCN, adaptive graph convolutional neural network; GWNN, graph wavelet neural network; GWCN, gate way core network; GLCN, graph learning-convolutional network; FAGCN, frequency adaptation graph convolutional network; AM-GCN: adaptive multi-channel graph convolutional; GpLCN: graph p-Laplacian convolutional network.

Table 2. Spatial-based convolution methods and their variants

Presenters	Year	Model	Salient points or key elements
Hamilton et al. [12]	2018	GraphSAGE	Three types of message aggregation functions, and selecting a subset of neighboring nodes for information aggregation
Veličković et al. [13]	2018	GAT	Constructing an attention mechanism for aggregating information from neighboring nodes
Zhang et al. [25]	2009	NN4G	Fast computation speed
Niepert et al. [26]	2016	PATCHY-SAN	The node sequence transitions from ordered to unordered
Atwood et al. [27]	2016	DCNN	Simple computation
Chen et al. [28]	2018	FastGCN	Smaller sampled adjacency matrix
Cui et al. [29]	2019	KGCN	Implementing aggregation of three types of messages
Xu et al. [30]	2019	GIN	Introducing graph isomorphism into graph convolutional networks
Cai et al. [31]	2020	Graph Transformer	Not limited by the distance between nodes
Yang et al. [32]	2021	Graph -CTA	Capable of comprehensive modeling of relationships between nodes

Note: GAT, graph attention network; CTA, computed tomography angiography; GraphSAGE, graph sample and aggregate; DCNN, dynamic convolution neural network; KGCN, knowledge graph convolutional network; GIN, graph isomorphism network.

convolution methods and their variants.

Spatial-based graph convolution, in the context of GNNs, propagates information by clustering node features within the neighborhood of a graph. This approach primarily relies on the adjacency matrix and node connectivity, enabling aggregation and propagation within the neighborhood to facilitate the interaction and fusion of local and global information. Compared to spectral-based graph convolution, spatial-based methods are more intuitive and easier to understand as they do not require explicit computation of graph spectral decomposition. They are particularly suitable for handling sparse or large-scale graph data. **Table 2** provides an overview of spatial-based convolution methods and their variants.

Graph pooling

Similar to CNNs, the graph pooling layer in GCNs is primarily used to reduce the spatial dimension of feature maps, decrease the number of model parameters, and extract key features. Common pooling operations include max pooling and average pooling. Max pooling selects the maximum value within a local region as

Table 3. Development or improvement of graph convolutional networks pooling

Presenters	Year	Model	Application scenarios
Ying et al. [33]	2018	Diff Pooling	Graph classification
Zhang et al. [34]	2018	Sort Pooling	
Bianchi et al. [35]	2019	Mincut Pooling	Graph classification& Node clustering
Ma et al. [36]	2019	Eigen Pooling	Graph classification
Lee et al. [37]	2019	SAG Pooling	
Gao et al. [38]	2021	IPooling	

Note: SAG, self-attention graph.

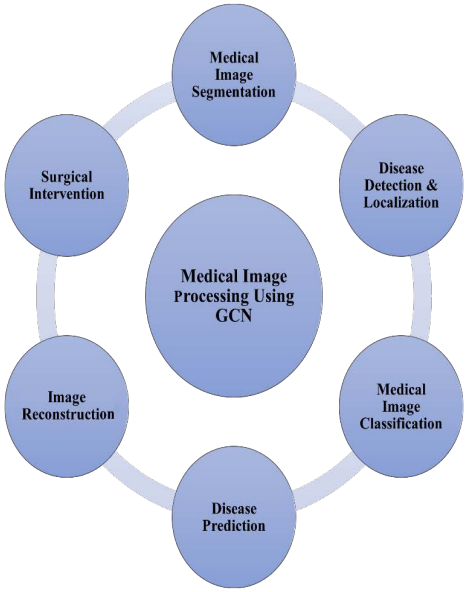

Figure 4. Applications of GCNs in medical image processing. GCN, graph convolutional network.

the pooled result, aiming to capture the salient features. On the other hand, average pooling computes the average value of the local region, aiming to preserve more detailed information. Current research on GCNs mainly focuses on adapting convolutional operators to graph-structured data and designing effective aggregation functions to achieve efficient representation of central node features. Therefore, the role of pooling operations in graph convolution is significant. **Table 3** summarizes the development or improvements of pooling layers in relevant GCNs.

Applications of GCNs in medical image processing

As depicted in **Figure 4**, this section provides an overview of the relevant applications of GCNs in medical image processing.

Medical image segmentation

Medical image segmentation is to segment medical images based on medical features, such as grayscale, texture, frequency domain features. Compared to general segmentation tasks, medical image segmentation exhibits a certain level of complexity and diversity. In the realm of perioperative medical image segmentation, the segmentation process exhibits enhanced celerity and precision, accompanied by heightened maneuverability. Its salient attributes endow it with substantial academic significance and research value in medical investigation, clinical diagnosis, pathological analysis, as well as related research and practical undertakings. This section provides a comprehensive overview of pertinent applications utilizing GCNs for perioperative medical image segmentation.

Vessel segmentation is an important task in medical image processing, aiming to extract vascular structures from medical images to assist in disease diagnosis and treatment. Zhou et al. proposed a hybrid method that utilizes GCN to enhance the propagation of feature information [39]. They constructed graph data by depicting the structural configuration of vessels, where in vascular segments in the arterial tree were designated as nodes, with physiological features of vessels as node features. This approach achieved segmentation of arterial vessels in CT images. However, a limitation of this method is the inability to perform end-to-end training. Wolterink et al. proposed a GCN-based method for coronary artery segmentation in cardiac CT images [40]. They constructed graph data by considering the vertices on the arterial lumen surface mesh as nodes, using the K-nearest neighbor approach. The optimization of information propagation among nodes was achieved through the combination of GCN. This method enables vessel segmentation in CT images without relying on mesh interactions. Shin et al. were the first to combine CNN with GCN, jointly learning the overall structure and local appearance of vessels [41]. They employed CNN for feature extraction and used GCN to establish graph connectivity among vessels. By learning this connectivity, they effectively captured the relationships

Table 4. Application of graph convolutional networks in medical image segmentation

Presenters	Segmentation targets	Data modalities	Model	Results	Limitations
Zhou et al. [39]	Coronary artery	CT	GCN	A segmentation accuracy of 82.5% and an F1 score of 95.4%	End-to-end training is not feasible in this case
Wolterink et al. [40]	Coronary artery	CT	KNN+ GCN	Dice similarity coefficient range from 0.73 to 0.75	The segmentation performance is dependent on the location of the vascular centerline
Shin et al. [41]	Retina	CT	CNN+ GCN	mAP and ROC better than or comparable to current state-of-the-art methods	Further validation is necessary to ascertain its generalizability
Zhai et al. [42]	Pulmonary arteries and veins	CT	CNN+ GCN	Effective single separation of arteries and veins can be achieved	Over-fitting may occur during training
Yang et al. [43]	Coronary artery	CT	CNN+ GCN	The average recall, average precision, and average F1 score all exceeded 95%.	May lead to the loss of some subtle features, resulting in model instability
Zhang et al. [44]	Brain tissue	MRI	KNN+ GCN	The average DSC on the two datasets was 91.6% and 79.3%, respectively	High model complexity
Wu et al. [45]	Cerebral cortex	MRI	CNN+ GCN	The average overlap between the segmentation results and the labels reached 94%±3	High model complexity
Tian et al. [46]	Prostate	MRI	CNN+ GCN	The segmentation results achieved 93.8 ± 1.2% and 94.4 ± 1.0%, respectively	Limited by the amount of MRI data
Zhao et al. [47]	Pancreatic diseases	CT	GCN	Promising in terms of segmentation quality and detection accuracy	High model complexity

Note: GCN, graph convolutional network; KNN, K-nearest neighbor; CNN, convolutional neural network; ROC, receiver operating characteristic; DSC, dice similarity coefficient.

between vascular structures. Inspired by this, Zhai et al. performed vessel segmentation on chest CT images by preprocessing them using vessel segmentation and skeletonization [42]. They constructed feature maps using CNN and directly inputted the extracted feature maps into GCN to predict each vessel segment, thereby achieving the segmentation of arteries and veins. Yang et al. proposed a conditional partial residual GCN for automatic labeling of coronary arteries [43]. This network utilized GCN to process the structural information of coronary arteries and employed conditional partial residual to capture the local appearance information. By inputting coronary artery CT angiography images and initial labels, more accurate coronary artery labels were generated as output.

Tissue segmentation involves dividing pixels in an image into tissue regions to facilitate the identification of pathological structures and the analysis of disease progression. GCNs can improve the performance of tissue segmentation by learning the surrounding pixel features of each pixel, thereby enhancing the accuracy of pathological analysis. Zhang et al. proposed a method that departs from voxel-based segmentation and employs GCN to extract feature maps from superpixels [44]. The feature maps are then fused and classified using ChebNet, and the labels are projected back onto voxels to achieve segmentation of brain tissues in MRI images. Wu et al. utilized the powerful learning capability of GCNs to directly segment regions of interest (ROIs) within the cerebral cortex without the need for spherical mapping and registration [45]. GCNs not only demonstrate excellent results in brain tissue segmentation

Table 5. Application of graph convolutional networks in lesion detection and localization

Presenters	Analytical objectives	Model	Results
Wu et al. [48]	Basal cell carcinoma	GCN	The method does not rely on pixel segmentation labels and achieves results with mAP and AUC of 0.9556 and 0.9502, respectively, in basal cell carcinoma recognition
Du et al. [49]	Breast cancer	CNN+GCN+GAT	Efficiently accomplished breast cancer detection
Liang et al. [50]	Musculoskeletal abnormalities	MSCNN+GCN	High accuracy and robustness in the identification of skeletal muscle abnormalities
Luo et al. [51]	Diabetic retinopathy	CNN+GCN	Automatic identification of the location and severity of diabetic retinopathy lesions

Note: GCN, graph convolutional network; CNN, convolutional neural network; GAT, graph attention network; MSCNN, multiscale convolutional neural network.

but also exhibit promising performance in feature extraction and fusion of other organ tissues. In the context of pancreatic tissue segmentation, Tian et al. introduced a multi-layer GCN model that leverages residual modules to obtain spatial features of multi-scale ROIs, achieving segmentation of the prostate edge contour in MRI images [46]. Zhao et al. employed GCN for multi-dimensional and multi-angle feature extraction [47]. This approach effectively utilizes the geometric and positional information of ROIs, enabling the segmentation of different pancreatic diseases. **Table 4** provides a comprehensive summary of the applications of GCNs in medical image segmentation, including segmentation targets, data modalities, models, results, and limitations.

Lesion detection and localization

The detection and localization of lesions hold paramount significance in the context of perioperative clinical diagnosis and treatment. Utilizing automated detection and localization techniques can realize rapid and precise identification of lesions, helping clinicians to obtain faster and more accurate diagnoses and formulate treatment plans. Moreover, this approach can effectively improve the efficiency of medical image processing, reduce the workload of physicians, and minimize manual diagnostic errors. Currently, GCNs have made notable advancements in various perioperative medical imaging domains, including pathological images, radiographic images, and retinal images. **Table 5** presents a summarized overview of the applications of GCNs in lesion detection and localization.

In cancer diagnosis, representing pathological structures allow GCNs to capture the spatial relationships and size of tumors through convolutional operations, assisting clinicians in further disease analysis and treatment. Wu et al. proposed a method called weakly-and semi-supervised graph CNN for identifying basal cell carcinoma in pathological images, demonstrating its potential in enabling faster and more accurate cancer diagnosis, which indirectly improves patient outcomes [48]. GCNs are also effective in anomaly detection in radiographic images. Du et al. combined the concepts of CNN and GCN for breast cancer detection in mammograms [49]. By employing graph attention network to discriminate the indicative features of lesions, they efficiently emulated radiologists' focal scrutiny of the lesion areas, culminating with the successful detection of breast cancer in X-ray images via graph attention network. Liang et al. constructed a novel multi-network architecture consisting of a multiscale CNN and a fully connected GCN for abnormality detection in musculoskeletal X-ray images [50]. Experimental results demonstrated the model's high accuracy and robustness in musculoskeletal X-ray images. In the field of retinal imaging, retinal lesions are a common ocular disease that, if severe, can lead to blindness. Therefore, the detection of lesions in retinal images is of great importance. Luo et al. fused the correlation information of lesions learned by GCNs with the retinal image features obtained by a CNN model to achieve automated detection and severity grading of diabetic retinopathy lesions [51].

Medical image classification and diagnosis

During the perioperative period, GCNs adeptly capture the spatial characteristics delineating inter-tissue relationships within histopathological imagery. Consequently, within the domain of computer-aided diagnosis rooted in histopathological images, GCNs inherently exhibit commendable adaptive capabilities, thereby affording a high degree of feasibility. Gao et al. proposed a novel computer-aided diagnosis classification framework for breast tissue histopathological images, aiming to learn and extract spatially related features from the images [52]. The framework utilizes CNNs to extract high-level features from the histopathological images and inputs the generated graphs into

Table 6. Application of graph convolutional networks in medical image classification and diagnosis

Presenters	Analytical objectives	Model	Results
Gao et al. [52]	Breast cancer	GCN+GCN	Experimental results on two public breast histopathology datasets outperform other algorithms
Shi et al. [53]	Cervical cell classification	GCN+GCN	The model substantially improved the classification of cervical cells
Marzullo et al. [54]	Classification of multiple sclerosis	GCN	Through clinical validation on MS patients, the results indicate that the proposed method can effectively perform clinical classification of MS-related categories
Zhou et al. [55]	Colorectal Cancer Grading	GCN	The results demonstrate that the proposed colorectal cancer -Net can achieve an optimal classification performance on colorectal cancer

Note: GCN, graph convolutional network.

GCN to learn the spatial features of the histopathological images, thereby accomplishing the classification task. Shi et al., in their study on cervical cell classification, introduced a method that effectively enhanced the representation capability of CNN features by propagating node relationships through GCN, resulting in improved classification performance [53]. This approach has significant implications for cervical cell classification and can be well applied in automated cervical cytology screening systems.

In addition to capturing spatial feature expressions between pathological tissues, GCNs can also be applied to other medical image analyses, such as disease grading. Marzullo et al., in their study on automatic classification of clinical features in multiple sclerosis, proposed the use of GCN models to describe the topological structures of brain network [54]. By leveraging the information between graph structures, multiple sclerosis patients were classified into four clinical features: Clinically Isolated Syndrome, Relapsing Remitting, Secondary Progressive, Primary Progressive. Compared to classical convolutional network models, the proposed GCN architecture achieved good results with relatively fewer parameters. Zhou et al., in their research on colorectal cancer grading, introduced a novel cell-graph convolutional network [55]. This method employs cell graph convolutional layers and pooling layers to process cell graphs, capturing the relationships and interactions between different cells. It was tested on multiple datasets, demonstrating more accurate grading of colorectal histopathological images compared to other existing methods. This approach holds the potential to facilitate early diagnosis and treatment of colorectal cancer. **Table 6** summarizes the applications of GCNs in medical image classification and diagnosis based on analysis objectives, utilized models, and analysis results.

Disease prediction

GCNs find extensive application in disease prediction, encompassing the entirety of the perioperative continuum. Leveraging the inherent graph structure of data, GCNs facilitate enhanced capture of intricate disease relationships and interaction patterns. This capability enables medical practitioners to more accurately prognosticate patients' disease conditions and recovery trajectories preoperatively, intraoperatively, and postoperatively. By furnishing heightened precision in prognostic and diagnostic outcomes, GCNs have gained widespread adoption in diverse domains, including gene expression prediction, disease diagnosis and treatment, and drug response forecasting. **Table 7** provides a comprehensive summary of the applications of GCNs in disease prediction.

Gene prediction is a critical task in bioinformatics, aiming to predict the interactions and regulatory relationships among genes to better understand the functionality and regulatory mechanisms of the genome. By utilizing GCNs to learn the interactions between genes, more accurate gene classification and prediction can be achieved. Mudiyanselage et al. proposed two circRNA-disease association prediction models, namely GCNs for Node Classification and GCNs for Link Prediction, to address the limited quantity of circRNA-disease associations and the constraints of scalability, time, and labor costs [56]. The effectiveness of the proposed models was further demonstrated through a case study on colorectal cancer. Li et al. proposed a novel approach called neural inductive matrix completion GCN for predicting microRNA-disease associations [57]. Through the verification on breast cancer cases, the proposed method achieved a prediction accuracy of 100%. Xuan et al. proposed a GCN and CNN-based method for inferring disease-related lncRNA candidate genes in a study of lncRNA -disease associa-

Table 7. Application of graph convolutional networks in disease prediction

Presenters	Predict Targets	Model	Results
Mudiyanselage et al. [56]	Colorectal cancer	GCN	The two models achieved AUC values of 97% and 98%, respectively, in predicting colorectal cancer
Li et al. [57]	Breast cancer	GCN	The accuracy rate of breast cancer prediction reached 100%
Xuan et al. [58]	Tumors and cancers	CNN+GCN	The proposed model effectively discovered potential lncRNA-disease associations, as confirmed by case studies in gastric cancer, osteosarcoma, and lung cancer
Wang et al. [59]	Cancer	SNF+GCN	Combining SNF and GCN algorithms and fusing multi-gene data for cancer survival prediction
Wang et al. [60]	Breast cancer	GCN	It contributes to the accurate prediction of breast tumor malignancy or benignity, thereby improving the accuracy of cancer diagnosis in breast X-ray examinations
Song et al. [61]	Memory and cognitive impairment	GCN	The model showed an average increase of 8.64% in accuracy, 9.93% in sensitivity, and 7.91% in specificity across six multimodal tasks, demonstrating its applicability for predicting disease progression
Yao et al. [62]	Brain diseases	GCN	MMTGCN demonstrates high performance in identifying brain disorders

Note: GCN, graph convolutional network; AUC, area under the curve; CNN, convolutional neural network; lncRNA, long noncoding RNA; SNF, similarity network fusion; MMTGCN, mutual multi-scale triplet GCN.

tions [58]. Through case studies on gastric cancer, osteosarcoma, and lung cancer, GCNLDA effectively discovered potential lncRNA -disease associations and demonstrated superior performance compared to other methods. Wang et al. proposed a GCN-based fusion of multiple genomic data for cancer survival prediction [59]. Building upon the similarity network fusion algorithm, they integrated multiple genomic data and clinical data, selected features from cancer samples, and utilized GCN for semi-supervised training on these two matrices, resulting in a GCN-based fusion approach for cancer survival prediction.

In addition to gene expression prediction, GCNs can also utilize clinical data and imaging data to construct disease networks and predict/diagnose diseases by learning the features of nodes and edges in the network. Wang et al. proposed a decoupling autoencoder with GCN that learns disease-related image features and explicitly separates them from other features [60]. This method shows excellent performance in predicting benign or malignant outcome in breast X-ray examinations, contributing to improved accuracy in cancer diagnosis. In cognitive impairment scenarios, GCNs play a vital role by automatically localizing, segmenting, and classifying brain structures for early diagnosis and treatment of neurological diseases, preventing further deterioration. Song et al. proposed a similarity-aware adaptive calibrated GCN (SAC-GCN), which combines functional and structural information for predicting disease-induced deteriorations [61]. Similar to the former, Yao et al. introduced a multi-scale triplet GCN for analyzing functional and structural connections in brain disease diagnosis [62]. Multiple GCN modules were used to extract features from brain multi-scale templates, and these features were input into a fusion module for multi-scale information integration. Experimental results demonstrated that multi-scale triplet GCN achieved high performance in identifying and predicting brain diseases.

Image reconstruction

The application of GCNs in the field of image reconstruction involves the task of image restoration or reconstruction using local structural information of the image. Traditional image reconstruction methods typically rely on pixel-level processing, while GCNs, by leveraging both global and local structural information of the image, can provide better image reconstruction results. In recent years, an increasing number of researchers have begun exploring the application of GCNs in the field of medical image reconstruction and have achieved a series of advancements. Lang et al. proposed an automatic key point localization method based on the local attention GCN, which can be applied in craniofacial and oral maxillofacial surgery, with the potential to improve the success rate and efficiency of the surgery [63]. Tang et al. introduced a neighborhood feature reconstruction algorithm to extract the underlying relationships between obtained features and reconstructed them as graph-structured data [64]. Based on this, they proposed a deep GCN model called

node self-convolution GCN, which can effectively diagnose COVID-19 using graph-structured data. Wang et al. presented an instantiation network that utilizes Dynamic Convolution Neural Network to extract features from 2D images and employs GCNs to reconstruct 3D meshes [65]. This method enables the reconstruction of the target's 3D mesh from a single 2D image, bridging the gap between the 2D image acquisition in current minimally invasive surgery and the 3D navigation requirements.

Surgical interventions

Surgical intervention refers to a medical procedure performed inside the body using interventional devices such as catheters and stents. In recent years, GCNs have been increasingly utilized in research related to surgical interventions. For instance, in the perioperative context, GCNs find applications in surgical planning, navigation, postoperative assessment, and monitoring. Wang et al. proposed a GCN-based method for detecting the presence and location of surgical instruments [66]. Compared to traditional CNN and recurrent neural network methods, this approach achieves more accurate detection of surgical instruments, demonstrating the potential of GCNs in tool detection tasks in surgical videos. Xi et al. introduced a Feedback Graph Convolutional Network-based method that can be used for multiple tasks in endoscopic videos, such as surgical action recognition, surgical step detection, and surgical process monitoring [67]. This method effectively improves surgical efficiency and quality, thereby enhancing patient treatment outcomes.

Discussion

GCNs are deep learning models based on graph-structured data, which have been widely applied in the medical field in recent years. By reviewing the research progress of GCNs in the medical domain, it is evident that with continuous algorithmic updates and iterations, GCNs will achieve greater success in the medical field. This section summarizes the future research directions of GCNs in medical applications.

Deep network structures

Traditional deep learning models have yielded substantial outcomes in numerous challenges by utilizing extensive network structures. However, some GCNs can achieve feature extraction and desired outcomes with fewer network structures. Increasing the stack of convolutional layers may lead to over-smoothing of features between nodes, resulting in deteriorated performance. In clinical applications, precise identification and localization are pursued. Therefore, designing deeper network structures that can avoid feature loss is an urgent problem to be addressed.

Large-scale data

Obtaining and annotating medical data often requires specialized medical knowledge and experience, which is not only limited in quantity but also consumes substantial human and material resources. However, deep learning typically requires a large amount of data to train models. Therefore, future research can focus on developing efficient GCN algorithms and optimization techniques to enhance the processing capability and scalability of large-scale graph data.

Dynamic graph data

Currently, most GCN models are designed for static graph data. However, in clinical applications, most medical features are dynamic. Consequently, a prospective research direction for GCNs involves expanding their applicability to model dynamic graphs and temporal graphs, thereby enabling the capturing of changes in graph data over time.

Interpretability

In the future, it is crucial to improve the generalization capability of models in clinical applications and reduce the difficulty of understanding results for medical professionals. Aligning the research focus with clinical requirements is a key aspect to address when further investigating the application of GCNs in the medical field.

Conclusion

This review initially elucidates the developmental trajectory of CNNs and GCNs, introducing the algorithmic foundations of the latter, including the concept of graphs, types of graphs, and the propagation framework of GCNs. Extensive discourse is dedicated to the pertinent applications of GCNs in the domain of perioperative medicine, encompassing medical image segmentation, lesion detection and localization, and medical image classification. While GCNs have made groundbreaking strides in several facets of perioperative medical scenarios, certain knowledge gaps persist, warranting further in-depth investigation. One such avenue pertains to the application of GCNs in the fusion of multimodal data. Perioperative medical images

typically involve diverse modalities, such as MRI and CT images. Future exploration could entail devising GCN-based strategies for processing multimodal medical image data to enhance the efficacy of medical image analysis and diagnosis. Additionally, there is potential in the realms of intraoperative monitoring and feedback. During surgical procedures, GCNs can real-time analyze intraoperative image data, assisting physicians in monitoring surgical progress and furnishing instantaneous feedback, thereby facilitating timely decision-making and adjustment of surgical strategies. Finally, intraoperative planning and navigation represent another prospect. GCNs can preoperatively analyze patients' medical image data to aid surgeons in devising more precise surgical plans, thereby ensuring the accuracy and safety of surgical procedures.

In conclusion, although there are still many directions that require further research and exploration in the field of GCNs and their application in medicine, this does not impede their future development and application in domains such as artificial intelligence. GCNs will continue to be a prominent area of research for a significant period of time, serving as a focal point for scholars and researchers.

References

[1] Gupta D, Anand RS. A hybrid edge-based segmentation approach for ultrasound medical images. Biomed Signal Process Control 2017;31:116-126.

[2] Hong J, Cheng H, Zhang Y-D, et al. Detecting cerebral microbleeds with transfer learning. Mach Vis Appl 2019;30(7):1123-1133.

[3] Chen L-C, Barron JT, Papandreou G, et al. Semantic Image Segmentation with Task-Specific Edge Detection Using CNNs and a Discriminatively Trained Domain Transform. 2016 IEEE Conference on Computer Vision and Pattern Recognition (CVPR) 2015:4545-4554.

[4] McCulloch WS, Pitts W. A logical calculus of the ideas immanent in nervous activity. Bull Math Biophys 1943;5(4):115-133.

[5] Rosenblatt F. The perceptron: a probabilistic model for information storage and organization in the brain. Psychol Rev 1958;65(6):386-408.

[6] Rumelhart DE, Hinton GE, Williams RJ. Learning representations by back-propagating errors. Nature 1986;323(6088):533-536.

[7] Lecun Y, Bottou L, Bengio Y, et al. Gradient-based learning applied to document recognition. Proceedings of the IEEE 1998;86(11):2278-2324.

[8] Scarselli F, Gori M, Tsoi AC, et al. The Graph Neural Network Model. IEEE Trans Neural Netw 2009;20(1):61-80.

[9] Bruna J, Zaremba W, Szlam A, et al. Spectral Networks and Locally Connected Networks on Graphs. CoRR 2013;abs/1312.6203.

[10] Defferrard M, Bresson X, Vandergheynst P. Convolutional neural networks on graphs with fast localized spectral filtering. Proceedings of the 30th International Conference on Neural Information Processing Systems 2016;3844–3852.

[11] Kipf T, Welling M. Semi-Supervised Classification with Graph Convolutional Networks. ArXiv 2016;abs/1609.02907.

[12] Hamilton WL, Ying R, Leskovec J. Inductive representation learning on large graphs. Proceedings of the 31st International Conference on Neural Information Processing Systems 2017;1025–1035.

[13] Veličković P, Cucurull G, Casanova A, et al. Graph attention networks. International Conference on Learning Representations 2017;1-12.

[14] Li R, Wang S, Zhu F, et al. Adaptive graph convolutional neural networks. Proceedings of the Thirty-Second AAAI Conference on Artificial Intelligence and Thirtieth Innovative Applications of Artificial Intelligence Conference and Eighth AAAI Symposium on Educational Advances in Artificial Intelligence 2018;Article 434.

[15] Xu B, Shen H, Cao Q, et al. Graph Wavelet Neural Network. ArXiv 2019;abs/1904.07785.

[16] Chiang W-L, Liu X, Si S, et al. Cluster-GCN: An Efficient Algorithm for Training Deep and Large Graph Convolutional Networks. Proceedings of the 25th ACM SIGKDD International Conference on Knowledge Discovery & Data Mining 2019.

[17] Jiang B, Zhang Z, Lin D, et al. Semi-Supervised Learning With Graph Learning-Convolutional Networks. 2019 IEEE/CVF Conference on Computer Vision and Pattern Recognition (CVPR) 2019;11305-11312.

[18] Derr T, Ma Y, Tang J. Signed Graph Convolutional Networks. 2018 IEEE International Conference on Data Mining (ICDM) 2018;929-934.

[19] Wang X, Zhu M, Bo D, et al. AM-GCN: Adaptive Multi-channel Graph Convolutional Networks. Proceedings of the 26th ACM SIGKDD International Conference on Knowledge Discovery & Data Mining 2020;1243–1253.

[20] Fu S, Liu W, Zhang K, et al. Semi-supervised classification by graph p-Laplacian convolutional networks. Inf Sci 2021;560:92-106.

[21] Zhu H, Koniusz P. Simple Spectral Graph

Convolution. International Conference on Learning Representations 2021;1-15.
[22] Bo D, Wang X, Shi C, et al. Beyond Low-frequency Information in Graph Convolutional Networks. AAAI Conference on Artificial Intelligence 2021.
[23] Wang J, Wang Y, Yang Z, et al. Bi-GCN: Binary Graph Convolutional Network. 2021 IEEE/CVF Conference on Computer Vision and Pattern Recognition (CVPR) 2021;1561-1570.
[24] Bo D, Shi C, Wang L, et al. Specformer: Spectral Graph Neural Networks Meet Transformers 2023.
[25] Zhang Z, Bu J, Ester M, et al. Hierarchical Graph Pooling with Structure Learning. ArXiv 2019;abs/1911.05954.
[26] Niepert M, Ahmed M, Kutzkov K. Learning convolutional neural networks for graphs. Proceedings of the 33rd International Conference on International Conference on Machine Learning 2016;2014–2023.
[27] Atwood J, Towsley D. Diffusion-convolutional neural networks. Proceedings of the 30th International Conference on Neural Information Processing Systems 2016;2001–2009.
[28] Chen J, Ma T, Xiao C. FastGCN: Fast Learning with Graph Convolutional Networks via Importance Sampling 2018.
[29] Cui J, Zhuang H, Liu T, et al. Semi-Supervised Gated Spectral Convolution on a Directed Signed Network. IEEE Access 2020;8:49705-49716.
[30] Xu K, Hu W, Leskovec J, et al. How Powerful are Graph Neural Networks? ArXiv 2018;abs/1810.00826.
[31] Cai D, Lam W. Graph Transformer for Graph-to-Sequence Learning. Proceedings of the AAAI Conference on Artificial Intelligence 2020;34:7464-7471.
[32] Yang L, Li W, Guo Y, et al. Graph-CAT: Graph Co-Attention Networks via local and global attribute augmentations. Future Gener Comput Syst 2021;118:170-179.
[33] Ying R, You J, Morris C, et al. Hierarchical graph representation learning with differentiable pooling. Proceedings of the 32nd International Conference on Neural Information Processing Systems 2018;4805–4815.
[34] Zhang M, Cui Z, Neumann M, et al. An end-to-end deep learning architecture for graph classification. Proceedings of the Thirty-Second AAAI Conference on Artificial Intelligence and Thirtieth Innovative Applications of Artificial Intelligence Conference and Eighth AAAI Symposium on Educational Advances in Artificial Intelligence 2018;Article 544.
[35] Bianchi FM, Grattarola D, Alippi C. Mincut pooling in Graph Neural Networks. ArXiv 2019;abs/1907.00481.
[36] Ma Y, Wang S, Aggarwal CC, et al. Graph Convolutional Networks with EigenPooling. Proceedings of the 25th ACM SIGKDD International Conference on Knowledge Discovery & Data Mining 2019;723–731.
[37] Lee J, Lee I, Kang J. Self-Attention Graph Pooling 2019.
[38] Gao X, Dai W, Li C, et al. iPool—Information-Based Pooling in Hierarchical Graph Neural Networks. IEEE Trans Neural Netw Learn Syst 2022;33(9):5032-5044.
[39] Zhou C. A Hybrid Approach for Coronary Artery Anatomical Labeling in Cardiac CT Angiography. J Phys Condens Matter 2020;1642(1):012020.
[40] Wolterink JM, Leiner T, Išgum I. Graph Convolutional Networks for Coronary Artery Segmentation in Cardiac CT Angiography. Graph Learn Med Imaging 2019;62-69.
[41] Shin SY, Lee S, Yun ID, et al. Deep vessel segmentation by learning graphical connectivity. Med Image Anal 2019;58:101556.
[42] Zhai Z, Staring M, Zhou X, et al. Linking Convolutional Neural Networks with Graph Convolutional Networks: Application in Pulmonary Artery-Vein Separation. Graph Learn Med Imaging 2019;36-43.
[43] Yang H, Zhen X, Chi Y, et al. CPR-GCN: Conditional Partial-Residual Graph Convolutional Network in Automated Anatomical Labeling of Coronary Arteries. 2020 IEEE/CVF Conference on Computer Vision and Pattern Recognition (CVPR) 2020;3802-3810.
[44] Zhang Y, Li Y, Kong Y, et al. GSCFN: A graph self-construction and fusion network for semi-supervised brain tissue segmentation in MRI. Neurocomputing 2021;455:23-37.
[45] Wu Z, Zhao F, Xia J, et al. Intrinsic Patch-Based Cortical Anatomical Parcellation Using Graph Convolutional Neural Network on Surface Manifold. Med Image Comput Comput Assist Interv 2019 2019;492-500.
[46] Tian Z, Li X, Zheng Y, et al. Graph-convolutional-network-based interactive prostate segmentation in MR images. Med Phys 2020;47(9):4164-4176.
[47] Zhao T, Cao K, Yao J, et al. 3D Graph Anatomy Geometry-Integrated Network for Pancreatic Mass Segmentation, Diagnosis, and Quantitative Patient Management. 2021 IEEE/CVF Conference on Computer Vision and Pattern Recognition (CVPR) 2021;13738-13747.
[48] Wu J, Zhong J-X, Chen EZ, et al. Weakly- and Semi-supervised Graph CNN for Identifying Basal Cell Carcinoma on Pathological Images.

Graph Learn Med Imaging 2019;112-119.
[49] Du H, Feng J, Feng M. Zoom in to where it matters: a hierarchical graph based model for mammogram analysis. ArXiv 2019;abs/1912.07517.
[50] Liang S, Gu Y. Towards Robust and Accurate Detection of Abnormalities in Musculoskeletal Radiographs with a Multi-Network Model. Sensors (Basel) 2020;20(11).
[51] Luo D, Kamata SI. Diabetic retinopathy grading based on Lesion correlation graph. 2020 Joint 9th International Conference on Informatics, Electronics & Vision (ICIEV) and 2020 4th International Conference on Imaging, Vision & Pattern Recognition (icIVPR) 2020;1-7.
[52] Gao Z, Lu Z, Wang J, et al. A Convolutional Neural Network and Graph Convolutional Network Based Framework for Classification of Breast Histopathological Images. IEEE J Biomed Health Inform 2022;26(7):3163-3173.
[53] Shi J, Wang R, Zheng Y, et al. Cervical cell classification with graph convolutional network. Comput Methods Programs Biomed 2021;198:105807.
[54] Marzullo A, Kocevar G, Stamile C, et al. Classification of Multiple Sclerosis Clinical Profiles via Graph Convolutional Neural Networks. Front Neurosci 2019;13:594.
[55] Zhou Y, Graham S, Koohbanani NA, et al. CGC-Net: Cell Graph Convolutional Network for Grading of Colorectal Cancer Histology Images. 2019 IEEE/CVF International Conference on Computer Vision Workshop (ICCVW) 2019;388-398.
[56] Bamunu Mudiyanselage T, Lei X, Senanayake N, et al. Predicting CircRNA disease associations using novel node classification and link prediction models on Graph Convolutional Networks. Methods 2022;198:32-44.
[57] Li J, Zhang S, Liu T, et al. Neural inductive matrix completion with graph convolutional networks for miRNA-disease association prediction. Bioinformatics 2020;36(8):2538-2546.
[58] Xuan P, Pan S, Zhang T, et al. Graph Convolutional Network and Convolutional Neural Network Based Method for Predicting lncRNA-Disease Associations. Cells 2019;8(9).
[59] Wang S, Xu F, Li Y, et al. KG4SL: knowledge graph neural network for synthetic lethality prediction in human cancers. Bioinformatics 2021;37(Suppl_1):i418-i425.
[60] Wang C, Sun X, Zhang F, et al. DAE-GCN: Identifying Disease-Related Features for Disease Prediction. Med Image Comput Comput Assist Interv 2021;43-52.
[61] Song X, Frangi A, Xiao X, et al. Integrating Similarity Awareness and Adaptive Calibration in Graph Convolution Network to Predict Disease. Med Image Comput Comput Assist Interv 2020;124-133.
[62] Yao D, Sui J, Wang M, et al. A Mutual Multi-Scale Triplet Graph Convolutional Network for Classification of Brain Disorders Using Functional or Structural Connectivity. IEEE Trans Med Imaging 2021;40(4):1279-1289.
[63] Lang Y, Lian C, Xiao D, et al. Automatic Localization of Landmarks in Craniomaxillofacial CBCT Images Using a Local Attention-Based Graph Convolution Network. Med Image Comput Comput Assist Interv 2020;817-826.
[64] Tang C, Hu C, Sun J, et al. NSCGCN: A novel deep GCN model to diagnosis COVID-19. Comput Biol Med 2022;150:106151.
[65] Wang S, Xu Z, Yan C, et al. Graph Convolutional Nets for Tool Presence Detection in Surgical Videos. Inf Process Med Imaging 2019;467-478.
[66] Wang Z-Y, Zhou X-Y, Li P, et al. Instantiation-Net: 3D Mesh Reconstruction from Single 2D Image for Right Ventricle. Med Image Comput Comput Assist Interv 2020 2020;680-691.
[67] Xi N, Meng J, Yuan J. Forest Graph Convolutional Network for Surgical Action Triplet Recognition in Endoscopic Videos. IEEE Trans Circuits Syst Video Technol 2022;32(12):8550-8561.

Perioperative Precision Medicine
eISSN: 2957-5443

Zentime

Research Article https://doi.org/10.61189/377184mkfywu

Impact of central venous pressure measurement on the prognosis of patients with septic shock: A retrospective analysis of the MIMIC- IV database

Yanchen Lin[1], Jing Huang[2], Ying Zhang[1], Houfeng Li[1], Huixiu Hu[1], Li Tan[3]

[1]Graduate School, Hebei North University, Zhangjiakou 075000, Hebei, China. [2]Graduate School, Wannan Medical College, Wuhu 241002, Anhui, China. [3]Department of Anesthesiology, Chongqing University Cancer Hospital, Chongqing 400030, China.

Declaration of conflict of interest: None.

Received August 24, 2023; Accepted September 7, 2023; Published September 30, 2023

Highlights

- The measurement of central venous pressure in patients diagnosed with septic shock does not yield prognostic improvements.
- Central venous pressure measurement in patients with septic shock is associated with prolonged ICU stay.
- Central venous pressure measurement is not advised for patients diagnosed with septic shock.

Abstract

Objective: To assess the impact of measuring central venous pressure (CVP) on the prognosis of patients with septic shock. **Methods:** Septic shock patients with and without CVP measurements were identified in the Medical Information Mart for Intensive Care IV database. The primary outcome was 28-day mortality, and a multivariate logistic regression model was used to analyze the association between CVP measurement and 28-day mortality in patients with septic shock. The results were validated using logistic regression after propensity score matching. Secondary outcomes were in-hospital mortality, 1-year mortality, incidence of acute kidney injury within the first 7 days in the intensive care unit (ICU), and length of stay in the ICU. After propensity score matching, logistic regression analysis was conducted to analyze the correlation between CVP measurements and secondary outcomes in patients with septic shock. **Results:** A total of 2966 patients were included, including 1219 patients whose CVP was measured within 24h after admission to the ICU. CVP measurement was found to be not correlated with 28-day mortality (odds ratio=0.978, 95% Confidence Interval 0.798-1.200, P=0.835). Analyzing the cohort after propensity score matching, CVP measurement was found to be associated with prolonged ICU stay (4.9 vs. 3.2 days; P<0.001). No statistical differences were found in the primary outcome and other secondary outcomes between those with CVP measurement and those not. **Conclusion:** CVP measurement is associated with prolonged ICU stay in patients with septic shock but not associated with mortality and incidence of acute kidney injury within 7 days.

Keywords: Septic shock, central venous pressure, 28-day mortality, length of intensive care unit stay

Introduction

Septic shock is a distinct subset within the spectrum of sepsis, a pathological condition characterized by a potentially fatal dysregulated immune response to infection, resulting in impaired organ function [1]. Septic shock is diagnosed if patients exhibit confirmed or suspected infection, and a Sequential Organ Failure Assessment score of ≥2, which necessitate the administration of vasopressor medications to sustain a mean arterial pressure of 65 mmHg, accompanied by a blood lactate level exceeding 2 mmol/L [2]. Various factors, such as trauma, fungal infection, and bacterial infection, can inflict harm upon the vascular endothelial cells of patients, resulting in interstitial fluid leakage, compromised microvascular blood flow, and insufficient tissue and organ perfusion, ultimately precipitating septic shock [3]. Septic shock is closely linked to a substantial incidence of complications, with a mortality rate exceeding 40% among affected individuals. This condition poses a severe threat to human life and impos-

Address correspondence to: Li Tan, Department of Anesthesiology, Chongqing University Cancer Hospital, No.181 Hanyu Road, Chongqing 400030, China. E-mail: tanlihh@163.com.

es a significant economic burden on both patients and society [4, 5]. Despite the significant advancements in pharmacologic therapy witnessed in recent years, septic shock continues to pose a substantial challenge for healthcare systems globally.

The implementation of the "sepsis bundle" has been a fundamental approach in managing septic shock since the initial release of the Surviving Sepsis Campaign (SSC) in 2004. In the 2018 guideline update, the 3-hour and 6-hour management bundles were consolidated into a 1-hour management bundle, emphasizing the urgency of initiating resuscitation and treatment upon sepsis diagnosis [6]. The assessment of fluid status in septic shock patients and subsequent implementation of personalized fluid therapy are crucial determinants of patient survival and prognosis. Central venous pressure (CVP) represents the pressure at the juncture of upper and lower veins as they enter the right atrium, and its value is influenced by a multitude of factors including right ventricular preload, afterload, contractility, compliance, venous tone, and volume status, among others [7].

In the 2012 SSC publication, CVP was recognized as an initial objective in resuscitation, and existing literature has indicated that elevated CVP levels are linked to both acute kidney injury (AKI) and mortality [8-11]. However, the 2021 SSC release asserted that CVP is an inadequate indicator of a patient's fluid status [12]. Consequently, there is ongoing debate regarding the early monitoring of CVP in fluid management for septic shock patients. This study aimed to assess the effects of early monitoring of CVP on the survival and prognosis of patients diagnosed with septic shock. This was achieved by analyzing the clinical characteristics of patients with septic shock in the Medical Information Mart for Intensive Care IV (MIMIC-IV) database.

Materials and Methods

Study design

This study utilized the freely accessible clinical database known as the MIMIC-IV [13]. The MIMIC-IV (v2.0) database encompasses clinical data from the year 2008 to 2019, comprising information of over 40,000 patients admitted to the intensive care unit (ICU). To ensure patient privacy protection, the database automatically removes patient identifiers in accordance with the Health Insurance Portability and Accountability Act security regulations. Consequently, this study does not involve any ethical concerns, and no ethics review is required. The researcher obtained access to the database and was responsible for data extraction (certification number 50199917).

Selection of participants

Patients diagnosed with septic shock were included in the study. The determination of septic shock was based on sepsis 3.0 criteria as well as International Classification of Diseases-9 (ICD-9) and ICD-10 codes in the MIMIC-IV database. Patients who were admitted to the ICU for less than 24 hours or had their initial CVP measurement taken after 24 hours of ICU admission were excluded from the analysis. Furthermore, patients with multiple admissions to the ICU were only considered for analysis based on their first admission. Patients who underwent their initial CVP measurement within 24 hours of ICU admission were categorized into a CVP group, while those who did not were classified into a no CVP group.

Variable extraction

Variables were obtained from the MIMIC-IV-2.0 database, and those with missing indicators ≥ 30% were excluded. The remaining variables were imputed for missing values using multiple imputation. The variables included demographic characteristics, vital signs, and laboratory indices measured within the initial 24 hours of ICU admission. In cases where a variable was recorded multiple times during this period, the value corresponding to the highest severity of disease was utilized. The primary outcome was 28-day mortality, while secondary outcomes included in-hospital mortality, 1-year mortality, the incidence of AKI within 7 days after ICU admission, and length of ICU stay. Data extraction for this study was conducted using STATA and Structured Query Language in Postgre STATA and Structured Query Language (v15.0).

Statistical analysis

Variables that adhered to a normal distribution were presented as mean (standard deviation), and intergroup comparisons were conducted using the t-test. Variables that did not adhere to a normal distribution were presented as median (interquartile range), and intergroup comparisons were conducted using the Wilcoxon rank-sum test. Categorical variables were presented as percentages, and intergroup comparisons were conducted using the chi-square test. Baseline variables that showed a correlation with prognosis through univariate analysis

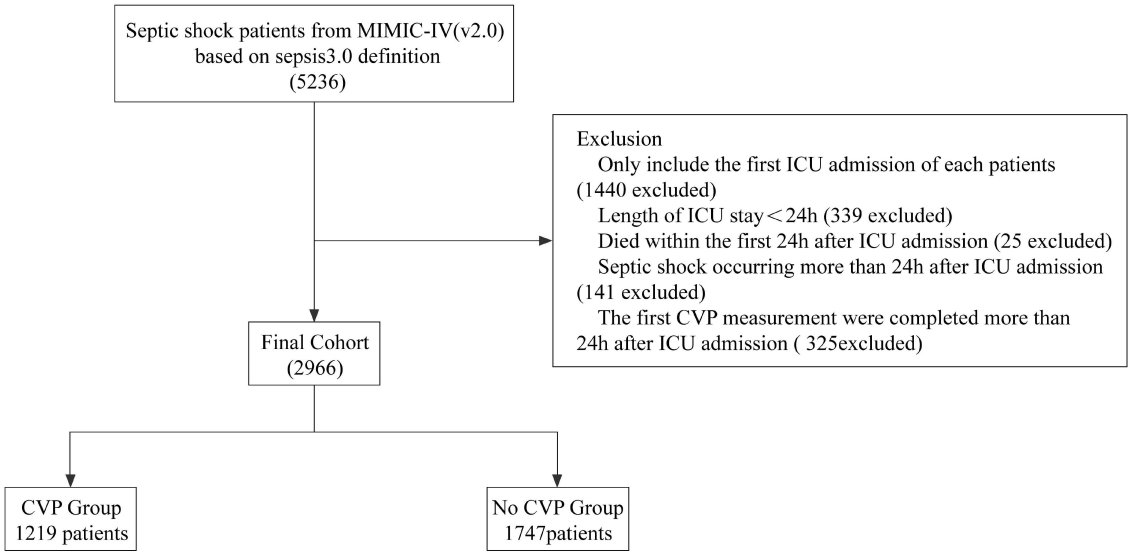

Figure 1. The flow chart of this study. MMIC-IV, Medical Information Mart for Intensive Care IV; ICU, intensive care unit; CVP, central venous pressure.

(P < 0.10) were included as covariates in the multivariate logistic regression model. These variables included age, body weight, sequential organ failure assessment score, Glasgow coma scale score, Charlson Comorbidity Index score, use of vasoactive medications, congestive heart failure, chronic lung disease, mild liver disease, diabetes mellitus, nephropathy, heart rate, mean blood pressure, body temperature, S partial pressure of oxygen, urea nitrogen, creatinine, lactate, partial pressure of oxygen, partial pressure of carbon dioxide, urine output, and incidence of acute kidney injury. The relationship between CVP measurement and the 28-day mortality of patients was then analyzed. Propensity score matching was employed to equalize the distribution of baseline indicators across groups, with a caliper value of 0.4 utilized to match CVP/no CVP in a 1:1 ratio. Subsequently, logistic regression analysis was conducted on the matched datasets using the R software. A statistical significance level of P < 0.05 was adopted to determine the observed differences between the two groups.

Results

Baseline characteristics

A total of 5236 patients diagnosed with septic shock were identified in this study. Among these patients, 1440 patients were admitted to the ICU on multiple occasions, 339 patients had an ICU stay of less than 24 hours, 25 patients died within 24 hours of ICU admission, 141 patients were diagnosed with septic shock more than 24 hours after ICU admission, and 325 patients received their initial CVP measurement after 24 hours of ICU admission. After applying the final inclusion criteria, 1219 included patients (41.10%) received their initial CVP measurement within 24 hours of admission (CVP group), while 1747 patients (58.90%) did not undergo CVP monitoring (no CVP group). The selection flowchart can be seen in **Figure 1**. The baseline characteristics of the patients in the CVP and no CVP groups are presented in **Table 1**. The CVP group exhibited significantly higher Sequential Organ Failure Assessment score (10 (IQR 7 - 13) vs. 8 (IQR 8 - 9)), simplified acute physiology score (SAPS II) (48 (IQR 37-59) vs. 44 (IQR 36-55)), and lactate level (2.8 mmol/L (IQR 1.7-5.0 mmol/L) vs. 2.6 mmol/L (IQR, 1.7-4.3 mmol/L)) compared to the no CVP group. There were no significant differences in baseline characteristics between the two groups following propensity score matching (PSM) (**Table 2**).

Primary outcome

Multivariate logistic regression analysis was conducted on the original cohort to assess the odds ratio (OR) of 28-day mortality in patients with septic shock based on CVP measurement. The analysis revealed an OR of 0.837 (95% CI 0.690-1.016), indicating no statistical difference between the CVP and no CVP groups. After PSM, the 28-day mortality rate was 33.9% in the CVP group and 33.4% in the no CVP group. The logistic regression analysis yielded an OR of 0.978 (95% CI 0.798-1.200), suggesting no significant difference between the two groups (**Figure 2**).

Secondary outcomes

Table 1. Baseline characteristics of the original cohort

Covariates	Original cohort		
	No CVP	CVP	P values
Age	69 (58-80)	69 (56-80)	0.163
Male (%)	941/1747 (53.9)	688/1219 (56.4)	0.165
Weight (kg)	77.0 (63.6-94.4)	80.0 (37.5-96.8)	0.001
Severity of illness			
SOFA score	8 (6-12)	10 (7-13)	<0.001
SAPSII score	44 (36-55)	48 (37-59)	<0.001
GCS score	13 (9-15)	12 (7-14)	<0.001
CCI score	6 (5-9)	3(4-8)	<0.001
Interventions, n (%)			
RRT use	176/1747 (10.1)	105/1219 (8.6)	0.181
MV use	1251/1747 (71.6)	924/1219 (75.8)	0.011
Vasopressor use	1266/1747 (72.5)	1116/1219 (91.6)	<0.001
Comorbidities			
Myocardial infarction	307/1747 (17.6)	234/1219 (19.2)	0.260
Congestive heart failure	512/1747 (29.3)	428/1219 (35.1)	0.001
Chronic lung disease	456/1747 (26.1)	364/1219 (29.9)	0.024
Diabetes mellitus	588/1747 (33.7)	377/1219 (30.9)	0.118
Kidney disease	448/1747 (25.6)	285/1219 (23.4)	0.160
Malignant cancer	415/1747 (23.8)	196/1219 (16.1)	<0.001
Severe liver disease	394/1747 (22.6)	301/1219 (24.7)	0.176
Vital signs			
Heart rate (bpm)	111 (97-125)	114 (98-129)	0.001
MAP (mmHg)	54 (48-60)	53 (45-58)	<0.001
Respiratory rate (bpm)	30 (26-34)	30 (26-34)	0.406
Temperature (℃)	37.4 (37.0-38.11)	37.6 (37.1-38.3)	0.001
Laboratory tests			
SpO_2	92 (89-94)	92 (89-94)	0.514
WBC (× 109/L)	16.3 (11.0-23.2)	17.2 (11.6-24.3)	0.019
Hemoglobin (× 1012/L)	9.3 (7.8-10.7)	9.7 (8.5-11.1)	<0.001
Platelet (× 109/L)	147 (93-213)	157 (100-229)	0.010
Bicarbonate (mmol/L)	19 (15-22)	18 (15-21)	0.001
Bun (mg/dL)	32 (20-53)	35 (22-54)	0.003
Creatinine (mg/dL)	1.5 (1.0-2.5)	1.7 (1.2-2.8)	<0.001
Lactate (mmol/L)	2.6 (1.7-4.3)	2.8 (1.7-5.0)	0.015
PH	7.30 (7.22-7.37)	7.26 (7.18-7.34)	<0.001
pO_2	43 (34-66)	49 (38-76)	<0.001
pCO_2	44 (38-53)	45 (38-54)	0.024
Urine volume (ml/24h)	1250 (640-2050)	1180 (594-2135)	0.617
AKI, n (%)	1037/1747 (59.4)	820/1219 (67.3)	<0.001

Note: CVP, central venous pressure; SOFA, Sequential Organ Failure Assessment; SAPS II, Simplified Acute Physiology Score II; GCS, glasgow coma scale; CCI, Charlson Comorbidity Index; RRT, renal replacement therapy; MV, mechanical ventilation; MAP, mean arterial pressure; WBC, white blood cell; Bun, blood urea nitrogen; pO_2, partial pressure of oxygen; pCO_2, partial pressure of carbon dioxide; AKI, acute kidney injury.

Table 2. Baseline characteristics of the matched cohort

Covariates	Matched cohort No CVP	CVP	P values
Age	68 (57-80)	69 (57-81)	0.261
Male (%)	439/823 (53.3)	432/823 (52.5)	0.730
Weight (kg)	78.5 (64-97)	79 (67-97)	0.331
Severity of illness			
SOFA score	10 (7-13)	10 (7-13)	0.273
SAPSII score	46 (36-56)	47 (36-58)	0.317
GCS score	13 (8-14)	13 (8-14)	0.715
CCI score	6 (4-8)	6 (4-8)	0.825
Interventions, n (%)			
RRT use	76/823 (9.2)	73/823 (8.9)	0.797
MV use	618/823 (75.1)	618/823 (75.1)	1.000
Vasopressor use	731/823 (88.8)	735/823 (89.3)	0.752
Comorbidities			
Myocardial infarction	152/823 (18.5)	155/823 (18.8)	0.849
Congestive heart failure	264/823 (32.1)	280/823 (34.0)	0.402
Chronic lung disease	235/823 (28.6)	234/823 (28.4)	0.956
Diabetes mellitus	253/823 (30.7)	261/823 (31.7)	0.671
Kidney disease	184/823 (22.4)	200/823 (24.3)	0.351
Malignant cancer	160/823 (19.4)	136/823 (16.5)	0.124
Severe liver disease	191/823 (23.2)	188/823 (22.8)	0.861
Vital signs			
Heart rate (bpm)	113 (97-127)	112 (98-127)	0.735
MAP (mmHg)	53 (47-59)	53 (46-58)	0.080
Respiratory rate (bpm)	29 (26-34)	30 (26-34)	0.946
Temperature (℃)	37.4 (37.1-38.2)	37.4 (37.0-38.3)	0.852
Laboratory tests			
SpO_2	92 (88-94)	92 (89-94)	0.762
WBC (× 109/L)	17.5 (11.8-24.4)	17.0 (11.6-23.7)	0.228
Hemoglobin (× 1012/L)	9.5 (8.1-11.0)	9.6 (8.3-11.0)	0.202
Platelet (× 109/L)	153 (95-218)	154 (99-223)	0.715
Bicarbonate (mmol/L)	18 (15-21)	18 (15-21)	0.322
Bun (mg/dL)	33 (21-56)	34 (23-54)	0.309
Creatinine (mg/dL)	1.7 (1.1-2.7)	1.7 (1.2-2.7)	0.140
Lactate (mmol/L)	2.5 (1.7-4.3)	2.7 (1.7-4.8)	0.194
PH	7.28 (7.20-7.35)	7.27 (7.19-7.34)	0.122
pO_2	44 (36-61)	44 (36-61)	1.000
pCO_2	45 (38-54)	46 (38-54)	0.960
Urine volume (ml/24h)	1200 (595-2120)	1190 (580-2135)	0.888
AKI, n (%)	530/823 (64.4)	534/823 (64.9)	0.837

Note: CVP, central venous pressure; SOFA, Sequential Organ Failure Assessment; SAPS II, Simplified Acute Physiology Score II; GCS, glasgow coma scale; CCI, Charlson Comorbidity Index; RRT, renal replacement therapy; MV, mechanical ventilation; MAP, mean arterial pressure; WBC, white blood cell; Bun, blood urea nitrogen; pO_2, partial pressure of oxygen; pCO_2, partial pressure of carbon dioxide; AKI, acute kidney injury.

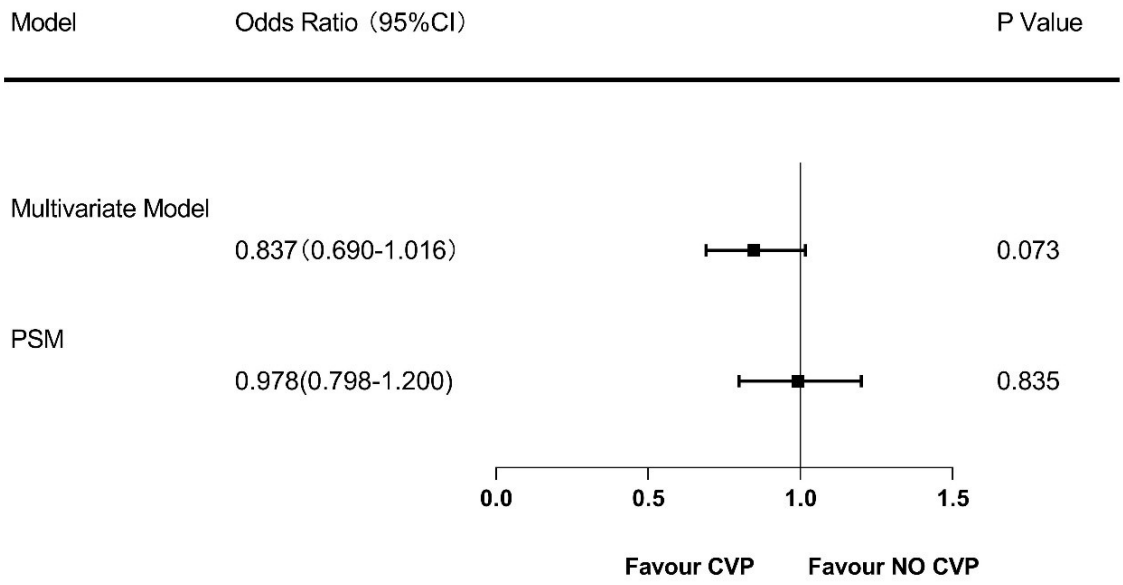

Figure 2. Association between CVP measurement and 28-day mortality. The odds ratios and 95% confidence intervals, represented by error bars, were computed in both cohorts based on the method of covariate adjustment. PSM, propensity score matching; CVP, central venous pressure.

After PSM, CVP measurement was also not associated with the in-hospital mortality (OR 0.994(95% CI 0.807-1.225), P=0.958), ICU mortality (OR 1.125(95% CI 0.893-1.416), P=0.318), 1-year mortality (OR 0.925(95% CI 0.763-1.122), P=0.430) and incidence of AKI within 7 days after ICU admission (OR1.242 (95% CI 0.977-1.579), P=0.077). However, it is worth noting that the CVP group displayed a significantly prolonged ICU stay when compared to the no CVP group (4.4(2.7-9.2) vs. 3.6(2.1-7.5), p<0.001) (**Figure 3**, **Table 3**).

Discussion

The mortality rate associated with septic shock continues to be high, and prompt identification and resuscitation are crucial in mitigating patient mortality. Nevertheless, there has been a contentious debate on the necessity of CVP monitoring for patients with septic shock. In this investigation, employing PSM, we conducted an analysis which revealed that CVP monitoring significantly prolonged the ICU stay among septic shock patients. However, it did not exhibit any impact on 28-day mortality, ICU mortality, in-hospital mortality, 1-year mortality, or the incidence of AKI within 7 days after ICU admission.

Septic shock arises from diverse etiological factors that induce microvascular dilatation, extensive blood stasis within the microvessels, and subsequent plasma protein extravasation, leading to a reduction in plasma osmolality. This condition is further aggravated by plasma extravasation, ultimately resulting in inadequate effective circulating blood volume for the affected patients [14, 15]. In the management of septic shock, expeditious and efficacious fluid therapy assumes utmost importance and is closely linked to patient prognosis [16]. Inadequate fluid therapy can lead to inadequate maintenance of circulating blood volume, thereby exacerbating the patients' condition. Conversely, excessive fluid therapy poses a potential hazard of fluid accumulation or overload, which can induce vasodilation, damage cardiomyocytes, worsen glycocalyx injury, and prolong mechanical ventilation due to the formation of pulmonary edema [17, 18]. Conducting a meticulous evaluation of intravascular volume status and organ perfusion in order to guide fluid therapy is crucial to prevent both excessive and inadequate resuscitation. CVP serves as a frequently employed clinical monitor because it is easily accessible in clinical settings. Elevated CVP often signifies a heightened likelihood of organ impairment, thereby indicating the potential occurrence of peripheral edema [19, 20]. The extent of CVP elevation was found to demonstrate a correlation with mortality rates among septic patients [21].

However, it should be noted that CVP is a static measure that is influenced by numerous confounding variables, thus limiting its ability to fully and accurately depict a patient's volume status and responsiveness. As Hiroshi et al. elucidated, veins possess thinner walls compared to arteries, rendering them more compliant [22]. Consequently, CVP exhibits

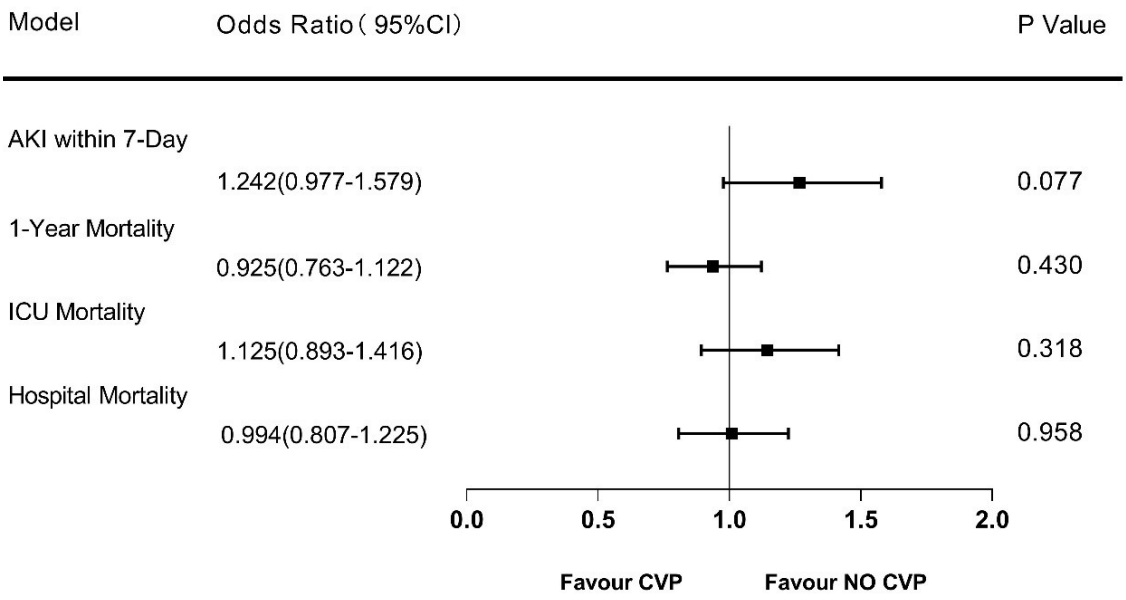

Figure 3. Association between CVP measurement and secondary outcomes. The logistic regression was utilized to calculate the odds ratios and 95% confidence intervals (error bars) in both cohorts. AKI, acute kidney injury; ICU, intensive care unit; CVP, central venous pressure.

Table 3. Clinical outcomes in PSM cohort

Outcomes	NO CVP	CVP	P value
Primary outcome			
28-day mortality	279/823 (33.9)	275/823 (33.4)	0.835
Secondary outcomes			
Hospital mortality	256/823 (31.1)	255/823 (31.0)	0.958
ICU mortality	179/823 (21.7)	196/823 (23.8)	0.318
1-year mortality	426/823 (51.8)	410/823 (49.8)	0.430
Incidence of AKI within 7 days, n (%)	640/823 (77.8)	669/823 (81.3)	0.077
Length of ICU stay	3.6 (2.1-7.5)	4.4 (2.7-9.2)	<0.001

Note: PSM, propensity score matching; CVP, central venous pressure; ICU, intensive care unit; AKI, acute kidney injury.

minimal fluctuations in response to alterations in blood volume [22]. The SSC 2021 guideline proposes the implementation of a dynamic monitoring approach to assess pertinent indicators in patients. This approach includes conducting the passive leg-raising test for cardiac output-related measurements, evaluating fluid challenge against output per beat, systolic blood pressure, pulse pressure, and observing the response of cardiac output per beat to alterations in intrathoracic pressure or positive end-expiratory pressure [12, 23, 24]. In clinical practice, CVP is typically measured through a central venous cannula, which carries the potential for complications such as infection and thrombosis, as well as the risk of unreliable CVP values due to different skill levels [25, 26]. When there is a lack of other dynamic indices to assess fluid status, it is important to consider the relationship between CVP and cardiac output. Only when there is a small change in CVP and an increase in cardiac output can it be inferred that the patient is responsive to fluid. CVP should not be considered as the primary target for fluid administration, but rather as a safety indicator. When CVP values are higher,-discontinuing fluid infusion is often beneficial as it indicates the risk of capillary fluid leakage and organ edema. However, there is no precise range for CVP values, and setting the CVP value too high can expose patients to the risk of fluid accumulation.

The most recent guidelines have discontinued the endorsement of CVP-guided fluid resuscitation for patients with septic shock. Our research findings revealed that the implementation of CVP monitoring not only failed to enhance the prognosis of septic shock patients, but also contributed to the extended length of ICU stays, which amplifies the economic burden on patients. Nevertheless, certain studies have validated that CVP measurement substantially diminishes mortality rates among septic shock

patients, contradicting our outcomes. There are several reasons for the observed disparities in this study compared to the study conducted by Chen et al. [27]. Firstly, Chen et al. utilized the MIMIC-III database encompassing patient data from 2001-2012, whereas this study employed the MIMIC-IV database containing patient information from 2008-2019 [27]. Additionally, the definition of septic shock has undergone multiple revisions over the past two decades, resulting in variations in the diagnosis criteria of septic shock. This study encompassed patients who met both the septic shock ICD codes and sepsis 3.0 criteria, resulting in variations in patient inclusion between the two studies.

This study is still subject to several limitations. Firstly, the utilization of a retrospective study design to examine the impact of early CVP monitoring on the survival of patients with septic shock inherently introduces limitations associated with the nature of retrospective studies and the selection bias of the target population. However, it is worth noting that patients with septic shock were identified according to the sepsis 3.0 criteria. Secondly, our study only included patients who underwent CVP monitoring within the first 24 hours of admission to the ICU, thereby excluding those who received CVP monitoring beyond this time frame. Lastly, the inclusion of patients solely from the MIMIC-IV database introduces potential bias, necessitating the need for multicenter validation, such as a prospective study or a retrospective analysis of electronic medical record systems from multiple centers.

Conclusion

In conclusion, the utilization of CVP measurement in patients diagnosed with septic shock does not result in improved prognosis. Moreover, CVP monitoring in these patients is correlated with prolonged ICU stay. Consequently, it is not recommended to administer CVP measurement for patients diagnosed with septic shock.

References

[1] Singer M, Deutschman CS, Seymour CW, et al. The Third International Consensus Definitions for Sepsis and Septic Shock (Sepsis-3). JAMA 2016;315(8):801-810.

[2] Shankar-Hari M, Phillips GS, Levy ML, et al. Developing a New Definition and Assessing New Clinical Criteria for Septic Shock: For the Third International Consensus Definitions for Sepsis and Septic Shock (Sepsis-3). JAMA 2016;315(8):775-787.

[3] Joffre J, Hellman J, Ince C, et al. Endothelial Responses in Sepsis. Am J Respir Crit Care Med 2020;202(3):361-370.

[4] Quenot JP, Binquet C, Kara F, et al. The epidemiology of septic shock in French intensive care units: the prospective multicenter cohort EPISS study. Crit Care 2013;17(2):R65.

[5] Rudd KE, Johnson SC, Agesa KM, et al. Global, regional, and national sepsis incidence and mortality, 1990-2017: analysis for the Global Burden of Disease Study. Lancet 2020;395(10219):200-211.

[6] Levy MM, Evans LE, Rhodes A. The Surviving Sepsis Campaign Bundle: 2018 update. Intensive Care Med 2018;44(6):925-928.

[7] Gelman S. Venous function and central venous pressure: a physiologic story. Anesthesiology 2008;108(4):735-748.

[8] Dellinger RP, Levy MM, Carlet JM, et al. Surviving Sepsis Campaign: international guidelines for management of severe sepsis and septic shock: 2008. Crit Care Med 2008;36(1):296-327.

[9] Legrand M, Dupuis C, Simon C, et al. Association between systemic hemodynamics and septic acute kidney injury in critically ill patients: a retrospective observational study. Crit Care 2013;17(6):R278.

[10] Chen CY, Zhou Y, Wang P, et al. Elevated central venous pressure is associated with increased mortality and acute kidney injury in critically ill patients: a meta-analysis. Crit Care 2020;24(1):80.

[11] Boyd JH, Forbes J, Nakada TA, et al. Fluid resuscitation in septic shock: a positive fluid balance and elevated central venous pressure are associated with increased mortality. Crit Care Med 2011;39(2):259-265.

[12] Evans L, Rhodes A, Alhazzani W, et al. Surviving sepsis campaign: international guidelines for management of sepsis and septic shock 2021. Intensive Care Med 2021;47(11):1181-1247.

[13] Johnson A, Bulgarelli L, Pollard T, et al. MIMIC-IV (version 2.0). PhysioNet 2022. Available at: https://doi.org/10.13026/6mm1-ek67.

[14] Leone M, Einav S, Antonucci E, et al. Multimodal strategy to counteract vasodilation in septic shock. Anaesth Crit Care Pain Med. 2023;42(3):101193.

[15] Wei JX, Jiang HL, Chen XH. Endothelial cell metabolism in sepsis. World J Emerg Med 2023;14(1):10-16.

[16] Zheng R, Jin X, Liao W, et al. Association between the volume of fluid resuscitation and mortality modified by disease severity in patients with sepsis in ICU: a retrospective cohort study. BMJ Open 2023;13(4):e066056.

[17] Du W, Sun J, Chen H. Effects of excess fluid administration and dehydration treatment on venous return in canine model of septic shock. Chin Med J (Engl) 2022;135(23):2872-2874.

[18] Marik PE, Byrne L, van Haren F. Fluid resuscitation in sepsis: the great 30 mL per kg hoax. J Thorac Dis 2020;12(Suppl 1):S37-s47.

[19] Chen KP, Cavender S, Lee J, et al. Peripheral Edema, Central Venous Pressure, and Risk of AKI in Critical Illness. Clin J Am Soc Nephrol 2016;11(4):602-608.

[20] De Backer D, Vincent JL. Should we measure the central venous pressure to guide fluid management? Ten answers to 10 questions. Crit Care 2018;22(1):43.

[21] Chen H, Gong SR, Shang XL, et al. The magnitude, but not the duration of elevated central venous pressure is associated with mortality in sepsis patients: An analysis of the MIMIC-IV database. PLoS One 2023;18(2):e0281549.

[22] Ueyama H, Kiyonaka S. Predicting the Need for Fluid Therapy-Does Fluid Responsiveness Work? J Intensive Care 2017;5:34.

[23] Lai C, Shi R, Beurton A, et al. The increase in cardiac output induced by a decrease in positive end-expiratory pressure reliably detects volume responsiveness: the PEEP-test study. Crit Care 2023;27(1):136.

[24] Osman D, Ridel C, Ray P, et al. Cardiac filling pressures are not appropriate to predict hemodynamic response to volume challenge. Crit Care Med 2007;35(1):64-68.

[25] Wu C, Zhang M, Gu W, et al. Daily point-of-care ultrasound-assessment of central venous catheter-related thrombosis in critically ill patients: a prospective multicenter study. Intensive Care Med 2023;49(4):401-410.

[26] Tatsuno K, Ikeda M, Wakabayashi Y, et al. Clinical Features of Bloodstream Infections Associated with Peripheral Versus Central Venous Catheters. Infect Dis Ther 2019;8(3):343-352.

[27] Chen H, Zhu Z, Zhao C, et al. Central venous pressure measurement is associated with improved outcomes in septic patients: an analysis of the MIMIC-III database. Crit Care 2020;24(1):433.